NAS9–14521–T–114–5–MA–527T
FR–2689–101

FINAL REPORT

NONINTRUSIVE FLOWMETER

September 1976

National Aeronautics and Space Administration
Lyndon B. Johnson Space Center
Houston, Texas   77058

Beckman® INSTRUMENTS, INC.

ADVANCED TECHNOLOGY OPERATIONS
ANAHEIM, CALIFORNIA 92806

FINAL REPORT

NONINTRUSIVE FLOWMETER

September 1976

National Aeronautics and Space Administration
Lyndon B. Johnson Space Center
Houston, Texas   77058

Beckman® INSTRUMENTS, INC.

ADVANCED TECHNOLOGY OPERATIONS
ANAHEIM, CALIFORNIA 92806

Beckman® INSTRUMENTS, INC.

ADVANCED TECHNOLOGY OPERATIONS

1630 SOUTH STATE COLLEGE
ANAHEIM, CALIFORNIA 92806
TELEPHONE 714/997-0730

TITLE: NONINTRUSIVE FLOWMETER

PREPARED FOR: National Aeronautics and Space Administration
Lyndon B. Johnson Space Center
Houston, Texas 77058

	Date
Prepared by _M W Breene_	_Sept 3, 1976_
Approved by _M W Breene_	_Sept 3, 1976_
Approved by ____	____
Approved by ____	____
Approved by ____	____
Approved by ____	____

DISTRIBUTION LIST

Copies	Name
1	NASA Lyndon B. Johnson Space Center R&T Procurement Branch Attn: Connie S. Parks, Mail Code BC73(40) Houston, TX 77058
4	NASA Lyndon B. Johnson Space Center Technical Library Branch Attn: Retha Shirkey, Mail Code JM6 Houston, TX 77058
1	NASA Lyndon B. Johnson Space Center Technology Utilization Office Attn: John T. Wheeler, Mail Code AT3 Houston, TX 77058
38	NASA Lyndon B. Johnson Space Center Propulsion and Power Division Attn: M. Buchanan, Mail Code EP2 Houston, TX 77058
1	Melvyn Savage Director, Advanced Development, MTG NASA Headquarters Washington, DC 20546
1	Paul E. Fitzgerald, Jr. Technical Assistant, Technical Planning Office, AT Lyndon B. Johnson Space Center Houston, TX 77058
1	NASA Lyndon B. Johnson Space Center Public Affairs Office Attn: Mail Code AP3 Houston, TX 77058

ABSTRACT

This report contains the results of analytical and experimental
work performed in the design, fabrication, and test of a Proto-
type Nonintrusive Gaging System (NIGS) for use in monitoring the
consumption of earth-storable fuels and oxidants in either a
one-g or a zero-g environment. The design specifications were
those applicable to the Reaction Control System (RCS) and to
the Orbital Maneuvering System (OMS) fuel and oxidant on the
space shuttle while in orbit. The major requirement was for
the measurement of flow pulses with sufficient accuracy to
provide a continuous knowledge of the fuel (and oxidant) re-
maining in the OMS system to within 1% or better. The approach
chosen was an ultrasonic frequency "chirp" technique having a
high inherent rejection for signals traversing stray paths, and
for random noise generated by the flowing liquid.

The final report contains a detailed analysis of the frequency
chirp approach for two modes of operation (period and phase
changes), including an error analysis. Experimental results for
tests of preliminary and final designs are presented in detail.
Transducer impedance matching and backloading theory, design,
and test results are also discussed, as well as tables, graphs,
and reproductions of oscillograph charts showing significant
final test results.

CONTENTS

CONTENTS (Continued)

SUMMARY

The first objective of this contract was to select an optimum measurement approach for monitoring the consumption of fuel (hydrazine, MMH, UDMH, or 50/50 hydrazine/UDMH), and oxidant (N_2O_4) by the reaction control system (RCS) of the space shuttle. The Nonintrusive Gaging System (NIGS) principle selected was an ultrasonic flowmeter utilizing a sweep frequency ("chirp") technique, with compensation for density variations with temperature to provide a mass flow rate output. (See paragraph 5D for details of the density compensation scheme.)

The second objective of the contract was to perform a comprehensive Design Study, resulting in optimization of the design parameters with regard to the specific requirements of the RCS application. The major unusual requirement is for the measurement of very short flow pulses (40 ms), by which up to 10% of the tank capacity may be consumed. The contract specified that the selected NIGS approach was to be capable of providing a knowledge of the fuel (or oxidant) remaining in the system to within "1% or better." The combined requirement is, therefore, that the mass transferred by 40 ms flow pulses (10% of total capacity) be measured within 10% or better to ensure that the cumulative error is less than 1% of capacity, and that the accuracy improve rapidly with flow pulse duration to 1% or better at full-scale flow rate (occurring for relatively long flow pulses).

The third major objective of this contract was to fabricate, test, and deliver a prototype NIGS for Design Feasibility Testing. The prototype design was, of course, to be based on the results of the Design Study phase of the contract.

The initial Design Study effort resulted in equations describing the performance of an idealized (simplified) system. These functional relationships characterized the signal-to-noise ratio (SNR) in terms of all design and performance requirement parameters. The frequency chirp ultrasonic principle offers an advantage over other ultrasonic flowmeter implementations with regard to noise suppression.

All ultrasonic flowmeters measure the difference in up- and down-stream sonic transit times, but various approaches to the measurement are possible. Briefly, two transducers that are mounted diagonally across the pipe are alternately interchanged electronically as transmitter and receiver by transmit/receive (T/R) switches. The transit times are equal for two successive T/R half cycles in the absence of flow, and are different when there is flow since the flow velocity increases the speed of sound in one direction and decreases it in the other. In the frequency chirp approach, during each T/R half cycle the transmitter is driven by a voltage which is swept in frequency ("chirped") linearly with time. The receiver picks up the signal that was transmitted at an earlier time. However, the difference between transmitted and received frequencies at any time within the T/R half cycle (greater than the sonic transit time) is

constant, and proportional to the sonic transit time. A signal having a fre-
quency equal to the difference in transmitted and received frequencies, called
the intermediate frequency (IF), is obtained by multiplying (mixing) the two
radio frequency (RF) signals and filtering to retain only the "low sideband."
(This is a standard electronic technique, based on trigonometric identities,
for obtaining the difference of two high frequencies.) The IF signal may be
filtered to reject received signals (noise) that do not bear the proper transit
time relationship to the transmitted signal, which improves the SNR. The band-
pass of the filter must, of course, be wide enough to pass changes in IF fre-
quency as large as the combined effects of flow velocity and thermal density
changes.

The analysis demonstrated that both the phase and the frequency of the result-
ant IF signal are functions of the sonic transit time. Either the difference
in IF phase or in IF frequency (or period) for two successive IF half cycles
will, therefore, provide a measure of the flow velocity. Measurement of the
effect of flow on sonic transit time is, of course, the basis of all ultra-
sonic flowmeters, but the frequency chirp technique has unique advantages over
systems that measure the difference of sonic transit time directly. To illus-
trate the point, the nominal sonic transit time for the contraints of the NIGS
will be about 70 μs. The difference in transit times at full-scale flow rate
will be only about 1 μs. To obtain resolution of one-tenth percent of full-
scale flow directly would require resolution of the transit time difference to
within 1.0 ns (10^{-9} s), which requires very sophisticated circuitry with severe
weight and power penalties. In contrast, the frequency chirp technique provides
"multiplication" of the difference in transit times, making it possible to re-
solve one-tenth percent of full-scale time difference with a time resolution of
about 50 ns (5 x 10^{-8} s), which is within the capability of ordinary T^2L logic.
An additional advantage, as noted above, is that the IF signal may be bandpass
filtered to provide excellent rejection of flow-generated noise, signals that
are received through paths other than the flowing medium, and signals that are
due to multiple reflections between the transducers, all of which are major
problems for conventional acoustic flowmeters. The "penalty" is that the T/R
half-cycle time must be significantly longer than the direct transit time, in
proportion to the delay time "amplification" desired. However, the T/R cycling
can easily occur at a rate of 100 or more times per second, which is adequate
for almost any application, especially since the noise is suppressed.

The Design Study revealed that an idealized frequency chirp system was capable
of meeting all requirements of the NIGS provided that the simplifying assump-
tions made in the analysis were not too restrictive with regard to the
realities of an actual system. The Design Study was extended to include basic
transducer and signal-conditioning experiments to better define the actual per-
formance of such a system. The initial test results indicated the need for a
further Design Study effort. Specifically, a study was made of the potential
benefits of impedance-matching and transducer back-loading. New transducers
were then fabricated utilizing selected acoustic impedance-matching and crystal
back-loading techniques, and further preliminary tests were performed. This
cyclic process of analysis, test, refine, and retest culminated in a Bread-
board Nonintrusive Gaging System, ready for testing.

In the interests of economy the Flow Test capability at Beckman was limited to essentially the verification of response to flow. The NIGS was connected to the two-inch water main entering the plant. This system provided a maximum of 25% of full-scale flow--3.6 kg/s (8 lb/s). The flow rate varied randomly with water main pressure which was 80 psig maximum, and the only available reference flowmeter covered the zero-to-minimum specified flow rate range--zero to 1.0 kg/s (2.2 lb/s). Pulsed flows could not be obtained with the Beckman system.

The Final Design Feasibility Tests were conducted in two one-week cycles at the NASA-JSC Thermochemical Test Area (TTA). The first week of testing at the TTA, April 1976, provided the first opportunity to test the Nonintrusive Gaging System at full-scale flow rate at the required pressure (250 psig) and with rapidly pulsed flow rates. The Breadboard Nonintrusive Gaging System was revised and upgraded into the end-item Prototype Nonintrusive Gaging System. The prototype NIGS was subjected to further testing at the TTA in May, 1976.

DESIGN FEASIBILITY TEST OUTLINE AND RESULTS

The tests summarized below were planned (see Document No. TTA-TP-2P230), but time and equipment constraints restricted the tests actually performed, as noted in each case. The following summarize the desired tests and the extent to which the NIGS was tested:

- Accuracy of integrator for steady-state flow over a range of 0.09 to 15.8 kg/s (1.5 to 250 gal/min, or 0.22 to 35 lb/s). (See paragraphs 7E, 8B, and 9B.)

- Linearity of flow rate digital-to-analog (DAC) converter output over the range. (See paragraphs 7E, 8B, and 9B.)

- Pulsed flow integrator accuracy at 0.5, 1, 2, and 5 Hz. (See paragraph 9C.)

- The effect of passing a hot "slug" of water through the flow cell upon the accuracy of the measured mass transferred. (See paragraph 9E).

- Pulsed flow rate measurement accuracy at minimum flow rate for pulses as short as 40 ms. (This test was not accomplished due to equipment limitations.)

- Reversed flow effects. (Time constraints permitted only a reversal of the transducer leads, which reversed the output.)

- Upstream flow perturbation effects. (This test was not done due to test time constraints.)

The contract "optimum design goal requirements" and the degree to which the prototype gaging system complied are summarized in TABLE 2-1. Those requirements for which compliance was not tested are so indicated in the table. There were only two significant failures:

- Electronics. Thermal instability of both digital and analog prototype NIGS circuitry resulted in some totally erratic results. The required circuits are, however, well within the state of the art. (See paragraph A4 of the Appendix.)

- Pulsed Flows. The transducers tested in May were affected by 5-Hz pressure ringing of the TTA flow system. The same transducers, when stiffened with 0.17 cm (0.070 inch) thick magnesium and 0.07 cm (0.030 inch) thick Lucite impedance-matching facings, passed this test in April. This failure can be rectified by transducer modifications that will also be beneficial in other respects.

The basic NIGS integrator accuracy, linearity, and pulsed flow data obtained on four days of successful testing are summarized in TABLES 2-2 through 2-5. The "run numbers" in these tables coincide with those of the TTA rough log to facilitate direct comparison. The calculated mass transferred for the NIGS

TABLE 2-1. COMPLIANCE TO DESIGN REQUIREMENTS (SHEET 1 OF 3)

	Optimum Design Objectives	Extent to which Prototype NIGS Complied with Optimum Design Objectives
Application	Measure RCS and OMS usage to determine fuel and oxidant remaining in system to assure restart of OMS engines.	Complied (April test) Would prefer better accuracy at 0.9 kg/s (2 lb/s) flow rate, and must revise transducers to handle pressure ringing due to periodic flow pulses (May test). See paragraph A4 of Appendix.
Configuration	3.8 cm (1.5 inch) tubing, nonintrusive.	Complied, except used 3.8 cm (1.5 inch) pipe inlet and outlet instead of tubing.
Compatibility	N_2H_4, N_2O_4, MMH, UDMH 50/50 N_2H_4/UDMH. Test with water only.	Complied. Tested on water only. Would weld flight model transducers instead of using O-ring seals for complete compatibility.
Service Life	7 years shelf; 5 years use.	No Test. Believed to be feasible.
Thermal	Flow Cell: 4.4 to 37.7°C (40 to 100°F). Electronics: -1.1 to 65.4°C (30 to 150°F).	Complied, but results were not absolutely conclusive. Failed Commercial electronics were inadequate. See paragraph A4 of Appendix.
Flow Rate	0.9 kg/s (2 lb/s) for 40 ms to 15.8 kg/s (35 lb/s) for 5 min.	Complied. Capable of measuring from zero flow up. Must revise transducers to handle pressure ringing due to periodic flow pulses (May test). See paragraph A4 of Appendix.
Pressure	Operate: 200-275 psig. Pressure Drop: None Proof: 375 psig (min) Burst: 500 psig (min)	Complied. Complied. Complied. Active transducers not tested. No Test. Design calculations indicate compliance.

TABLE 2-1. COMPLIANCE TO DESIGN REQUIREMENTS (SHEET 2 OF 3)

	Optimum Design Objectives	Extent to which Prototype NIGS Complied with Optimum Design Objectives
Orientation	No dependence.	No Test. No reason to believe there is a dependence, except possibly with regard to bubble entrapment in 1 g.
Weight and Size	Minimum	No Attempt to comply for economic reasons. Estimate flight model will weigh less than five pounds.
Vibration	Design compatible with: ● OMS engine burn ● Orbiter engine burn ● Lift-off ● Transonic ● Max Q	No Test. General considerations indicate no problem. Vibration of flow cell due to water hammer and flow effects was very severe, but not measured.
Accuracy	Better than 1%, both dynamic and steady state.	Complied. Steady state, when electronics temperature was acceptable. Failed with 5-Hz flow pulses. Needs transducer modification.
Space Environment	Design to operate in both zero-g and one-g.	No Test. No problem anticipated.
Bi-directional Flow Capability	Highly desirable for use in filling tanks.	Complied. Limited testing due to test time constraints.
Flow Rate Signal-to-Noise Ratio	No separate specification.	Obtained 3% of scale peak noise in best configuration, with 20 ms output DAC updates. Anticipate equal performance with 6 ms updates.

TABLE 2-1. COMPLIANCE TO DESIGN REQUIREMENTS (SHEET 3 OF 3)

	Optimum Design Objectives	Extent to which Prototype NIGS Complied with Optimum Design Objectives
Units of Output	Pounds mass transferred.	Complied. Because of the difference in sensitivity expected for the different configurations to be evaluated, no attempt was made to scale output to read in pounds mass directly. Similarly, the expense of making a density correction for temperature was avoided since the effect was negligible for water (0.3% maximum).
Linearity	No separate specification.	Obtained better than 1% of full scale across range, based on integrator output for several hundred pounds of water at various flow rates.

TABLE 2-2. *SUMMARY OF ALL STEADY-STATE FLOW DATA OBTAINED ON 30 APRIL, USING PERIOD MODE AND WITH IMPEDANCE MATCHING FACINGS. AMBIENT TEMPERATURE WAS REASONABLY STABLE DURING THESE RUNS.*

Run No.	Calculated Average Flow Rate Catch-Weigh (gpm)	(lb/s)	Transferred Mass By Catch-Weigh System (lb)	By NIGS Integrator Output, Calculated (lb)	NIGS Integrator Voltage Change (volts dc)	Cumulative Mass Transferred (NIGS Mean SENS. = 19.311 lb/volt) Catch-Weigh System (lb)	NIGS Integrator Times Sensitivity (lb)	NIGS Integrator Error (lb)	NIGS Error, % of Total Mass
41	212	29.4	440.7	440.7	22.82	440.7	440.7	0	0
42	216	30.0	449.4	462.9	23.97	890.2	903.6	+13.5	+1.5
43	160	22.2	440.0	454.2	23.52	1334.2	1357.8	+23.6	+1.8
44	162	22.5	450.7	438.8	22.72	1784.9	1796.6	+11.7	+0.7
45	106	14.7	442.2	448.2	23.21	2227.1	2244.8	+17.7	+0.8
46	109	15.1	453.6	452.3	23.42	2680.7	2697.1	+16.4	+0.6
47	54	7.5	224.9	225.2	11.66	2905.6	2922.3	+16.7	+0.6
48	16	2.2	134.9	135.6	7.02	3040.5	3057.9	+17.4	+0.6
49	16	2.2	138.3	139.2	7.21	3178.8	3197.1	+16.3	+0.6
50	13	1.8	104.6	99.8	5.17	3283.4	3296.9	+13.5	+0.4

TABLE 2-3. SUMMARY OF ALL STEADY-STATE FLOW DATA OBTAINED ON 27 MAY, USING PERIOD MODE, OMITTING DATA FOR WHICH LARGE CIRCUIT THERMAL ERRORS WERE DEMONSTRATED

Run No.	Calculated Average Flow Rate Catch-Weigh		Transferred Mass By Catch-Weigh System	By NIGS Integrator Output, Calculated	NIGS Integrator Voltage Change	Cumulative Mass Transferred (NIGS Means SENS. = 18.584 lb/volt)			
						Catch-Weigh System	NIGS Integrator Times Sensitivity	NIGS Integrator Error	NIGS Error, % of Total Mass
	(gpm)	(lb/s)	(lb)	(lb)	(volts dc)	(lb)	(lb)	(lb)	
88	241	33.5	335	331	17.81	335	331	− 4	−1.2
89	182	25.3	379	374.7	20.16	714	706	− 8	−1.2
90	182	25.3	377	370	19.91	1091	1076	−15	−1.4
91	225	31.2	340	331.7	17.85	1431	1408	−23	−1.6
92	132	18.3	367	368.3	19.82	1798	1776	−22	−1.2
93	134	18.6	372	368.3	19.82	2170	2144	−26	−1.2
94	79	11.0	330	326.5	17.57	2500	2472	−28	−1.2
95	81	11.2	448	456.6	24.57	2948	2929	−19	−0.6
96	−	−	aborted	−	−	−	−	−	−
97	26	3.6	430	446.2	24.01	3378	3375	− 3	−0.1
98	16	2.2	407	419.4	22.57	3785	3794	+ 9	+0.2

TABLE 2-4. SUMMARY OF ALL STEADY-STATE FLOW DATA OBTAINED ON 28 MAY, USING THE PHASE MODE. These runs were completed before the ambient temperature increased to the point causing failure of the electronics.

2-7

Run No.	Calculated Average Flow Rate Catch-Weigh (gpm)	(lb/s)	Transferred Mass By Catch-Weigh System (lb)	By NIGS Integrator Output, Calculated (lb)	NIGS Integrator Voltage Chabge (volts dc)	Cumulative Mass Transferred (NIGS Means SENS. = 31.50 lb/volt) Catch-Weigh System (lb)	NIGS Integrator Times Sensitivity (lb)	NIGS Integrator Error (lb)	NIGS Error, % of Total Mass
116	16	2.2	399	427	13.56	399	427	+28	+7.0
117	16	2.2	398	428	13.60	797	855	+58	+7.3
126	16	2.2	399	411	13.04	1196	1266	+70	+5.9
127	14	1.9	358	343	10.90	1554	1609	+55	+3.5
128	11	1.5	278	265	8.42	1832	1874	+42	+2.3
129	51	7.1	427	412	13.08	2259	2286	+27	+1.2
130	52	7.2	431	427	13.54	2690	2713	+23	+0.9
131	123	17.1	342	338	10.74	3032	3051	+19	+0.6
132	123	17.1	428	427	13.56	3460	3478	+18	+0.5
133	108	15.0	452	459	14.57	3912	3937	+25	+0.6
134	70	9.7	327	327	10.37	4239	4264	+25	+0.6
135	80	11.1	223	219	6.95	4462	4483	+21	+0.5
136	12	1.7	308	306	9.73	4770	4789	+19	+0.4
137	154	21.4	536	530	16.83	5306	5319	+13	+0.2
138	157	21.8	436	440	13.98	5742	5759	+17	+0.3
139	206	28.6	418	409	12.99	6160	6168	+ 8	+0.1
140	203	28.2	423	415	13.18	6583	6583	0	0
141	240	33.3	499	497	15.79	7082	7080	- 2	-0.03
142	252	35.0	524	530	16.81	7606	7610	+ 4	-0.05
143	214	29.7	386	381	12.10	7992	7991	- 1	0
144	224	31.1	373	365	11.59	8365	8356	- 9	-0.1
145	71	9.9	392	384	12.20	8757	8740	-17	-0.2

TABLE 2-5. *SUMMARY OF ALL PULSED FLOW DATA (SHEET 1 OF 2)*

Run No.	Frequency of Flow Pulses, Hz	NIGS Integrator Sensitivity, lb/volt	Sensitivity Error, % of Mean for Steady Flow	Calculated Average Flow Rate at Peak gpm	lb/s	Remarks
22	0	18.25	Mean Sensitivity=	15.3	2.1	29 April Data
23	0	17.72	17.985 lb/volt	15.3	2.1	
24	1	18.55	+3.1%	15.0	2.1	Period mode, five IF
25	1	18.56	+3.2%	15.0	2.1	cycles. Impedance matched
26	0.5	17.95	−0.2%	14.3	2.0	for 0.75 MHz, operated at
27	0.5	17.71	−1.6%	14.3	2.0	0.75 MHz. Nonlinear above
28	0.5	18.85	+4.8%	14.3	2.0	about 150 lb/s.
29	5.0	17.13	−5.0%	6.8	0.9	(See paragraph 9C.)
30	5.0	16.74	−7.4%	6.8	0.9	
98	0	18.03	(used)	16.3	2.3	27 May Data.
99	5.0	33.00	+66.0%	15.8	2.2	
100	5.0	29.09	+46.0%	15.4	2.1	Period mode, five IF
101	0	20.23	(used)	16.2	2.2	cycles. No impedance
102	0	24.95	(not used)	16.1	2.2	matching layers. Oper-
103	0	22.22	(not used)	16.4	2.3	ating 0.75 MHz crystals
104	0	19.84	mean of six	16.3	2.3	at 0.38 MHz. Runs 102
105	0	19.75	data used =	16.2	2.2	and 103 not used in ob-
106	0	21.76	19.935	16.2	2.2	taining steady state mean
107	0	20.00	lb/volt	16.3	2.3	value because they dis-
108	5.0	27.59	+38.0%	15.4	2.1	played a thermal error
109	5.0	30.48	+53.0%	15.4	2.1	not applicable to pulsed
110	0.5	21.25	+6.6%	16.3	2.3	flow data.
111	0.5	20.96	+5.1%	16.1	2.2	(See paragraph 9C.)
112	1	20.00	+0.3%	16.3	2.3	
113	1	20.99	+5.3%	16.3	2.3	
114	2	23.33	+17.0%	16.8	2.3	

TABLE 2-5. SUMMARY OF ALL PULSED FLOW DATA (SHEET 2 OF 2)

Run No.	Frequency of Flow Pulses, Hz	NIGS Integrator Sensitivity, lb/volt	Sensitivity Error, % of Mean for Steady Flow	Calculated Average Flow Rate at Peak gpm	lb/s	Remarks
116	0	29.42	mean for three	16.0	2.2	28 May Data
117	0	29.26	data=29.76 lb/V	15.9	2.2	
118	0.5	35.00	+17.6%	11.2	1.6	Phase Mode, no impedance
119	0.5	33.13	+11.3%	11.1	1.6	matching layers. Oper-
120	1.0	42.22	+42.0%	11.4	1.6	ating 0.75 MHz crystals
121	1.0	39.24	+32.0%	11.3	1.6	at 0.38 MHz.
122	2.0	40.43	+36.0%	11.2	1.6	(See paragraph 9C.)
123	2.0	40.94	+36.0%	11.3	1.6	
124	5.0	46.70	+57.0%	10.6	1.5	
125	5.0	49.53	+66.0%	10.6	1.5	
126	0	30.6	(used)	16.0	2.2	

integrator output is based upon the mean sensitivity in pounds per volt for all data. Better agreement with the catch-weigh system would be obtained if the NIGS system mean sensitivity had been calculated by taking the ratio of total mass transferred to the total integrator voltage change. This would have the effect of applying a "weighting factor" to the sensitivity data obtained for small total masses transferred, at low flow rates. For example, in each of TABLES 2-2, 2-3, and 2-4 the "NIGS error, % of Total Mass" errors are predominantly of one sign, which is a clear indication that a better mean value of the NIGS sensitivity can be found for each table. The mean values used for TABLES 2-2, 2-3, and 2-4 have the merit of being simple, direct, and of requiring no justification.

Ambient temperature effects caused gross errors in some tests before the NIGS was properly aligned, and the data of TABLES 2-2, 2-3, and 2-4 were obtained during times when ambient temperature was relatively stable (probably about ±5°F). In particular, data obtained on 27 May that were proven to be of abnormal sensitivity due to circuit over-temperature were not included in TABLE 2-3, while data obtained after taking corrective action are included.

CONCLUSIONS

The following conclusions are made, based on the results of the Final Design Feasibility Tests:

- The frequency chirp ultrasonic flowmeter is capable of meeting all requirements for the RCS fuel and oxidant consumption application. This approach can probably be used to advantage for other NASA flow-monitoring requirements. (See Appendix, paragraph A4, for recommended revisions.)

- The inherent bi-directional capability of the approach permits use of the NIGS for monitoring the tank-filling operation, as well as for measuring usage while in orbit.

- Passage of large gas bubbles through the flow cell results in loss of the basic signal, causing large erroneous flow signals. The error in cumulative mass transferred can be minimized by not transferring data for apparent flow rates exceeding a preset threshold to the accumulator. The presence of such large apparent flow-rate transients can be utilized to warn of the presence of gas bubbles. Similarly, a "cloud" of small bubbles will attenuate the basic received signal (by scattering the sonic energy), and the resultant IF signal, but within limits the NIGS will indicate that mass is transferred (with some density error). Abnormal IF amplitude can be used to indicate the passage of such small bubbles. (See Section 8 and paragraph 9E for more detailed discussions.)

- Preferential orientation in mounting may be desirable to reduce bubble entrapment in a one-g environment.

- The NIGS should be located away from sources of abnormal heating. Specifically, asymmetrical thermal transients accompanying flow pulses can result in significant systematic errors if the asymmetry of temperature rise and fall rates exceeds about 10°C/s.

- The flow cells and transducers can be identical for N_2H_4, MMH, UDMH, and N_2O_4, but it will be necessary to use different "calibration modules" or the equivalent to provide a direct reading output in engineering units.

- Deviations from the nominal density of a given liquid would necessitate additional calibration factors to avoid proportional mass flow errors if the simple scheme analyzed (refer to Appendix) is employed. This is probably a justified "deficiency," in view of the added complexity and reduced reliability of adding a direct density measurement to the system. It is believed that this could only be a problem if there is an error in making the 50/50 mixture of hydrazines, and if the NIGS is used during tank filling the necessary correction factor will be available from these data and the known tank volume. (See paragraph 5D for details of the density correction scheme.)

- The flow cell should have a portion of the electronics mounted on or near it (within about one meter). The Prototype NIGS utilized one-meter (3-foot) coaxial cables for interconnection of the transducers to the Flow Cell Electronics. The balance of the NIGS circuitry may be located within the distance normally employed for T^2L logic signals. (The prototype used a four-meter (12-foot) cable for convenience.)

- The NIGS digital output data could be handled by an on-board computer, using time-sharing, to avoid additional circuitry. The scaling (cali-bration factors) and all computation might be controlled by a software program, if this approach is utilized.

RECOMMENDATIONS

It is recommended that additional revision, testing, and further analysis be performed as the initial phase of a program for development of a flight prototype. Several specific aspects of the NIGS require further testing to ensure that the major expense of a flight model design effort is not incurred prematurely. These factors are summarized as follows:

- A partial replacement of the Prototype NIGS electronics, with emphasis on thermal stability, and with elimination of much of the complexity. The Prototype NIGS included a number of switch-selectable and potentiometer-adjustable features which were essential to testing the effect of many design parameters and the two different modes of operation. A design dedicated to a specific mode of operation would simplify the circuitry and assist in reducing thermal coefficients.

- Further evaluation of transducer design, which may be accomplished using the prototype electronics with minimal improvements. In particular, it must be directly demonstrated that the effect of temperature on the transducers is negligible, as may be inferred from the Design Feasibility Test results and from the fact that other ultrasonic transducers have been used on liquid nitrogen. In addition, it would be desirable to directly confirm that the use of lower natural frequency crystals and rear potting of the transducers will generally improve performance and eliminate the observed effect of 5-Hz pressure ringing. Finally, a concept for an improved transducer (discussed in the Appendix) could be evaluated at relatively low cost and, if successful, this design concept should be incorporated in any future model.

- Design of closed-loop electronics for control of the two most critical parameters which are open-loop in the Prototype NIGS. These circuits should be flight-model compatible with regard to both the design approach and the components used. This effort should include further analytical--and possibly experimental--evaluation of the concept of varying the frequency ramp rate to hold the IF frequency constant as a potentially superior mode of operation.

After a further breadboarding effort such as that outlined above, the development of a flight prototype could proceed in an orderly manner with a low development risk.

INITIAL DESIGN PHASE AND RESULTS

5A   INTRODUCTION

The ultimate objective of this contract was to develop a Prototype Nonin-
trusive Gaging System (NIGS) for use with earth storable fuels and oxidant to
be used on the Space Shuttle Program for monitoring the useage from the
Orbital Maneuvering System (OMS) tanks by the Reaction Control System (RCS)
engines. The basic requirement is for a system suitable for both one-g and
zero-g operation, capable of measuring the mass of fuel (and oxidant) consumed
with sufficient accuracy to provide a knowledge of the amount of fuel (and ox-
idant) remaining in the acquisition system to within 1% or better. A signifi-
cant requirement for this application is an accurate measurement of flow
pulses of only 40 ms duration.

The program plan called for an initial study from which an optimum approach
was to be selected, followed by fabrication of breadboard hardware for prelim-
inary feasibility testing, design refinement, and further testing. Final
Design Feasibility Testing with water was performed at the NASA-JSC Thermo-
chemical Test Area (TTA). Testing at the contractor's facility was limited
to semi-quantitative demonstration of response to water flow, to avoid un-
necessary duplication of test facilities.

The approach selected as a result of the proposal effort was to develop an
ultrasonic flowmeter utilizing a "frequency chirp" technique to suppress spur-
ious signals and random noise effects. The study phase of the contract effort
resulted in a theoretical optimization of the approach, the accuracy of which
was recognized to be very dependent on the simplifying assumptions made in the
analysis (see Appendix). The study phase was extended to include several ex-
perimental verification and refinement cycles before incurring major design
and fabrication expenditures. The breadboard system that resulted from the
test, study, and refinement cycles was upgraded after initial testing at the
NASA-JSC TTA for delivery as the end-item NIGS.

The prototype delivered consists of the following four major components:

- Flow Cell — The cell design exposed only stainless steel to the flowing
  medium, except for two seal O-rings. The design can easily be made com-
  patible with N_2H_4, MMH (monomethylhydrazine), UDMH (unsymmetrical di-
  methylhydrazine), and N_2O_4 by welding the transducers into the flow cell.

- Flow Cell Electronics — This component was of a breadboard quality, and
  had many switch selectable and adjustable features to facilitate evalua-
  tion of all important parameters during the available TTA test time,
  and to permit operation in either of two modes of flow measurement.
  The basic data are also combined to provide a speed-of-sound output,
  which is used to compensate one operational mode (phase) output for a
  dependence on the speed of sound. The second mode of flow measure-
  ment is not dependent on the speed of sound.

- <u>Digital Conversion Assembly</u> — This prototype quality module contained
  a digital mini-computer that provided both digital and digital-to-
  analog converter (DAC) outputs of flow rate and total mass transferred.
- <u>Power Supply Module</u> — This prototype quality module contained all dc
  power supplies (commercial quality) required by the system.

The Digital Conversion Assembly (DCA) was available at no cost from the resid-
ual inventory of an in-house Beckman development of a bidirectional respiratory
flowmeter. The mini-computer limited the speed of response of the system, but
this was considered to be a cost-effective trade-off for an evaluation Proto-
type Gaging System. Similarly, a new program (using a PROM) could have been
generated to provide scaling for direct digital readout of the mass transferred,
in pounds, but this was not deemed to be essential for a demonstration proto-
type, particularly in view of the anticipated difference in flow sensitivity
for different selections of the various parameters, and for the two modes of
operation, to be evaluated in the Feasibility Demonstration Tests. Finally,
the use of the DCA and mini-computer program from the in-house Beckman program
provided bidirectional flow measurement capability at minimal cost to this
contract. The prototype gaging system, therefore, demonstrated the feasibil-
ity of measuring the fuel (or oxidant) during the tank filling operation, as
well as during the use cycle.

The Design Feasibility Test results demonstrated that a frequency chirp flow-
meter can meet all of the requirements for the RCA NIGS application. The
thermal stability of the electronics for a flight model will need to be at
least an order of magnitude better than that of the prototype tested. This
can be accomplished by using closed-loop control of the two most critical cir-
cuit parameters, an oscillator with 0.1% frequency stability, and digital cir-
cuit designs and components that are stable over the required thermal range.
Several minor changes in the transducer design will make them perform within
specifications under worst cast "water hammer" and pressure "ringing" con-
ditions, for which the one pair of prototype transducers tested was marginal.

5B   DESIGN STUDY RESULTS

The initial study consisted of a derivation of equations describing the per-
formance of an idealized frequency chirp-type ultrasonic flow measuring system,
plus an error analysis to identify error sources and to quantify the errors to
be expected for various operating parameters. The necessary trade-offs to
optimize the system for the RCS fuel (or oxidant) measurement requirements
followed from the error analysis. While it was recognized that a practical
system might not achieve the performance predicted for an idealized system,
this analysis provided an understanding of the best possible performance,
against which the performance of the prototype system could be judged.

The detailed derivations are given in the Appendix. Those results necessary
for a complete understanding of the discussion are summarized in this section
without detailed justification.
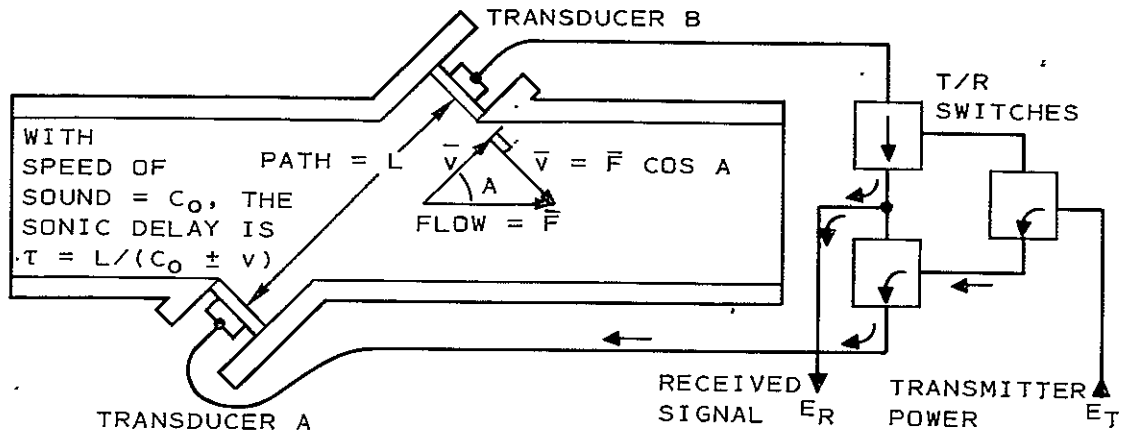
5B-1   Background of Ultrasonic Techniques

Numerous flowmeters utilizing the effect of flow on sound transmission have been developed in recent years. A number of different schemes for making the measurement have been developed. In the final analysis all such techniques measure the flow-induced change in sonic transit time between two (or more) transducers positioned along the flow axis. The angle between the sonic axis and the axis of flow must be less than 90 degrees, and is zero degrees (for maximum flow sensitivity) in some designs. The flow velocity adds (algebraically) its vector component along the sonic path to the inherent speed of sound in the medium. To minimize the effects of changes in the speed of sound, which are usually large compared to the range of flow velocities to be measured, it is necessary to measure the transit time in both directions and take the difference to obtain the change in transit time due to flow of the medium. In addition, most approaches provide an output that is dependent on either the speed of sound or the speed of sound squared, which requires compensation of the output.

Major problems in implementation of the measurement arise from flow-generated noise (received as spurious signals by the receiver) and from "stray sonic paths." The possible transit times for stray paths are dependent on a number of parameters. The stray paths include direct transmission through the flow conduit wall, multiple reflections within the flow cell wall and the interconnecting conduits, and multiple reflections between the transducers through the fluid medium itself. Typically, the received signal is the summation of a polygot of sound, only one component of which is effected predictably by the flow velocity to be measured. The art has advanced rapidly in recent years, primarily due to the rapidly expanding capability of integrated circuits. However, the random noise for all fully developed designs is so large as to necessitate integration of the signal for times long compared to the RCS requirement for accurately monitoring 40 ms flow pulses. As a result, the speed of response is not even mentioned in the published specifications for commercially available ultrasonic liquid flowmeters, even when an accuracy of 1% or better is claimed. In contrast, the recently developed Beckman respiratory flowmeter, which utilizes the frequency chirp technique to suppress noise and stray path signals, has a peak output noise of about ±0.25% of full scale at zero flow, and less than ±3% of full scale at full-scale flow when operating with a system rise time (10 to 90%) of 25 ms. These facts resulted in selection of the frequency chirp technique for further study and development for use on the RCS fuel and oxidant systems. It was anticipated that comparable performance could be obtained for liquid applications provided that the transmission of sound through an acceptable wall (305L stainless steel) was not too poor, and/or that the flow noise generated by liquids did not increase disproportionately compared to that for gases.
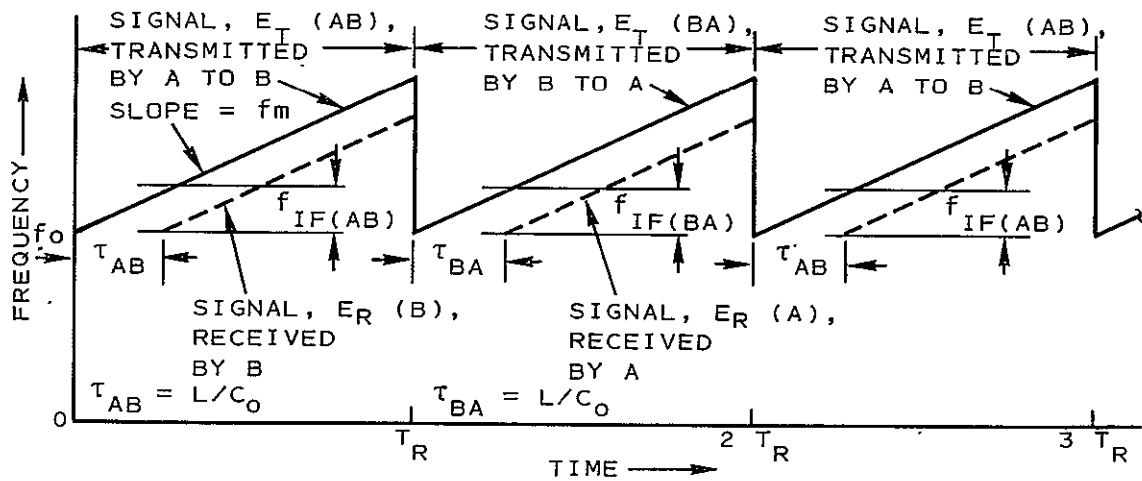
5B-2   Frequency Chirp Approach

The "frequency chirp" principal as illustrated in FIGURE 5-1 involves transmission of a sonic signal with frequency variable in time over a short time interval. The received signal is a time-delayed version of the transmitted

A. *Illustration of Ultrasonic Flow Meter Cell and T/R Switches for Alternate T/R Cycles*

TRANSDUCER B

T/R SWITCHES

WITH SPEED OF SOUND = C_O, THE SONIC DELAY IS $\tau = L/(C_O \pm v)$

PATH = L $\quad \bar{v}$ $\quad \bar{v} = \bar{F} \cos A$

FLOW = $\bar{F}$

RECEIVED SIGNAL E_R

TRANSMITTER POWER E_T

TRANSDUCER A

B. *Transmitted and Received Signals vs Time for Zero Flow*

SIGNAL, E_T (AB), TRANSMITTED BY A TO B SLOPE = fm

SIGNAL, E_T (BA), TRANSMITTED BY B TO A

SIGNAL, E_T (AB), TRANSMITTED BY A TO B

$f_{IF(AB)}$

$f_{IF(BA)}$

$f_{IF(AB)}$

FREQUENCY

fo

τ_{AB}

τ_{BA}

τ_{AB}

SIGNAL, E_R (B), RECEIVED BY B

SIGNAL, E_R (A), RECEIVED BY A

$\tau_{AB} = L/C_O$

$\tau_{BA} = L/C_O$

0 $\qquad T_R \qquad 2 T_R \qquad 3 T_R$

TIME

C. *Transmitted and Received Signals vs Time With Flow (Exaggerated) from A Toward B*

E_T (AB)

SLOPE = f_m

E_T (BA)

$f_{IF(AB)}$

$f_{IF(BA)}$

$f_{IF(AB)}$

τ_{AB}

τ_{BA}

τ_{AB}

E_R(B)

E_R(A)

$\tau_{AB} = \dfrac{L}{C_O + v}$

$\tau_{BA} = \dfrac{L}{C_O - v}$
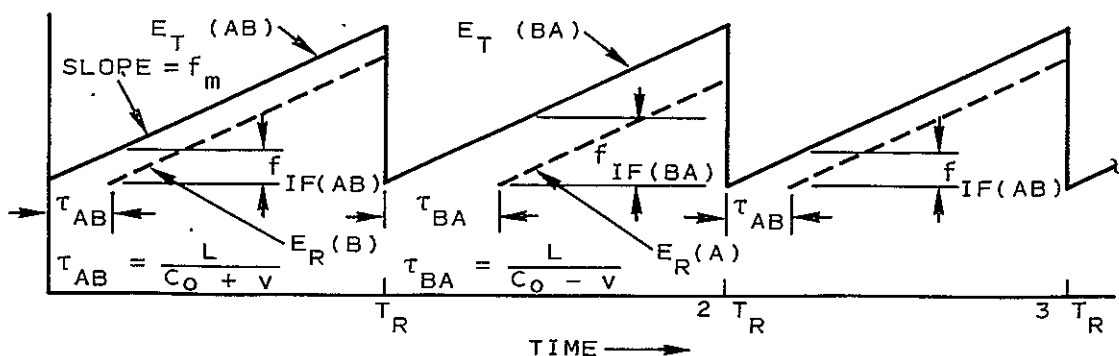
$T_R \qquad 2 T_R \qquad 3 T_R$

TIME

Figure 5-1. *Typical Flow Cell Design and Frequency versus Time Plots for the Frequency Chirp System.*

5-4

signal, where the time delay is the sonic transit time through the medium. The difference between the instantaneous transmitted and received frequencies is a function of the sonic delay time and of the rate of change of the transmitted frequency with time. If the difference frequency is obtained by mixing (multiplying) the transmitted and received signals and by using a band-pass filter for the low sideband only, an intermediate frequency (IF) signal is obtained. Both the frequency and the phase of the IF signal are functions of the sonic delay time. The sonic delay time, in turn, depends on the speed of sound in the medium and on the vector component of flow velocity along the sonic path between the two transducers. The IF filter band-pass can be tailored to provide immunity to all stray path signals having transit times differing from that of the desired signal by more than a few percent, the required band-width depending primarily on the anticipated variations in the speed of sound in the medium and upon the full-scale flow velocity which must be accommodated. An IF filter with a half-band-width of about 16 to 20% of the nominal IF frequency will meet the requirements of the RCS system. (A half-band-width of about 6% is adequate for water.) The attenuation at half the fundamental and at the second harmonic should be at least 60 dB.

The system briefly described above is illustrated schematically in FIGURE 5-1. The Gaging System flow cell and associated transmit/receive (T/R) switches are shown in FIGURE 1A. The switches are driven to transmit alternate frequency "ramps" from transducer A to B then from B to A. The second transducer is connected as the receiver in each case. The basic configuration of FIGURE 1A is used in most ultrasonic flowmeters. As indicated mathematically in the illustration, the sonic delay time is a function of path length, L. It is also a function of the vector sum of the speed of sound in the medium, C_o, and the component of the flow velocity, F, resolved along the sonic path, which is expressed as $v = F \cos A$. The flow velocity component adds to the speed of sound for one direction of transmission and subtracts from it for the other.

The frequency of the transmitted signal is shown by solid lines of slope f_m in the frequency versus time plots of FIGURES 5-1B and 5-1C. The received signal frequencies, shown by dashed lines, correspond to the frequencies transmitted at times τ, the sonic transit time, earlier in the frequency ramp. The frequencies of the transmitted and received signals during a given frequency ramp differ by an intermediate frequency, f_{if}. The IF frequency, for the linear frequency ramp shown, is equal to $f_m \tau$ in each case. FIGURE 5-1B illustrates the case for zero flow velocity, for which $\tau AB = \tau BA$ and $f_{if}(AB) = f_{if}(BA)$. FIGURE 5-1C provides an exaggerated illustration of the effect of flow upon the delay times and intermediate frequencies for the two directions of sound transmission. (The phase of the IF signal is also a function of delay time, but this cannot be shown in the frequency domain plots of FIGURES 5-1B and 5-1C.) The IF signal contains the flow information in a frequency chirp system. As noted above, band-pass filtering of the IF signal permits noise discrimination.

The IF signal for an idealized frequency chirp system may be written as:

$$e_m = E_m \cos 2\pi(f_m \tau t + f_o \tau) = E_m \cos 2\pi\left(\frac{f_m L}{C}t + \frac{f_o L}{C}\right) \qquad (1)$$

where

E_m	is (ideally) a constant IF amplitude. It is only assumed that E_m is constant for each pair of sonic T/R half-cycles. Start and stop transients are neglected;
f_m	is the time rate of change of transmitted frequency (constant);
$\tau = L/C$	is the sonic transit delay time;
f_o	is the starting frequency of the transmitted signal (constant for the present discussion);
t	is the time from the start of each frequency ramp, assumed to be greater than τ but less than or equal to the time of each frequency ramp, T_r;
$f_m \tau = f_m L/C$	is the "instantaneous frequency" of the IF signal;
$2\pi f_o \tau = 2\pi f_o L/C$	is the phase of the IF signal, neglecting a second order term, $\pi f_m \tau^2$;
C_o	is the speed of sound in the medium;
F	is the flow velocity;
$v = F \cos A$	is the vector flow velocity component along the sonic path, which is positive for one direction of transmission and negative for the opposite direction;
A	is the angle between the flow and sonic path vectors;
$C = C_o + v$	is the vector sound velocity including the flow velocity component;
L	is the sonic path length, assumed to consist of the flowing medium only for simplicity of discussion.

The simplifying assumptions are summarized, as follows:

- The transmitted and received signal amplitudes are both constant, making E_m constant for any given ramp pair.

- The transmitted frequency changes linearly with time during each T/R half-cycle (or "ramp"), making f_m constant.

- The starting frequency is the same for each ramp, making f_o constant.

- $f_o \gg f_m \tau^2/2$, making a component of the IF phase angle which is second order in τ negligible.

- The IF filter is "perfect" with regard to both the suppression of components having other frequencies and the freedom from introduction of phase, amplitude, and frequency distortions into the IF signal, making E_m constant and the frequency and phase of the signal free from distortion.

- Portions of the sonic delay due to transit through crystal mounts, and the sonic delay due to stagnant medium, are negligible compared to the delay in the flowing medium path.

- Phase shifts of the transmitted sonic signal relative to the drive voltage, and phase shifts of the receiver, are negligible.

- Transient effects of T/R switching, and from resetting the transmitter frequency ramp generator to f_0 at the end of one ramp for the beginning of the next, can be made negligible.

- The sonic transit time is negligible compared to the time of each T/R ramp, making the time lost due to this source of T/R transients negligible.

- $f_m\tau$=IF frequency is large enough to provide at least one cycle during each ramp, to give the concept of "instantaneous frequency" significance.

The above conditions are to a large degree interdependent. Furthermore, most of them should not be assumed to be necessary for a usable system. They were introduced primarily to simplify the initial analysis and to clarify the operational principles. Each deviation of a real system from these assumed conditions requires individual consideration.

5B-3   Summary of Equations Relating IF Signal Parameters to Flow Velocity and to the Speed of Sound

From Equation (1), it follows that a measurement of either the IF frequency or its phase will provide a measure of the sonic delay time. By algebraic manipulation the difference in IF periods (reciprocal of frequency) for successive T/R half-cycles provides a measurement of the flow velocity independent of the speed of sound. Specifically, the difference of IF periods for the two directions of sonic transmission (successive T/R ramps), ΔP, yields the flow velocity, F, in accordance with Equation (2).

$$F_P = \frac{f_m L}{2 \cos A} (\Delta P) \tag{2}$$

The difference of frequencies does not provide a measure of F which is independent of C_0.

The phase of the IF signal, $f_0\tau$ from Equation (1), also provides a means of measuring F, but the phase is dependent on the speed of sound squared. The flow velocity is related to the difference in phase of the IF signals for successive ramps, $\Delta\phi$, by Equation (3).

$$F = \frac{C_0^2}{4\pi f_0 L \cos A} (\Delta\phi) \tag{3}$$

The speed of sound in the medium can be obtained from the sum of the two IF periods, independent of the flow velocity. The sum of the IF periods may be used, therefore, to obtain a compensation signal for eliminating the speed-of-sound effect on the flow velocity measured by the phase difference approach.

The speed of sound is related to the sum of the periods, $(P_1 + P_2)$, by Equation (4).

$$C_0 = \frac{f_m L}{\cos A} \left(\frac{P_1 + P_2}{2} \right) = \frac{f_m L}{\cos A} \bar{P} \tag{4}$$

where $\bar{P}$ is the average period for successive T/R half cycles.

The time differences actually measured with the chirp technique (corresponding to $\Delta\phi$ and ΔP changes) may be larger than the direct variation in transit time due to flow. The flow rates and conduit sizes required for the RCS system dictate that the transit time will be about 60 μs, and that the full-scale flow will cause a difference in up- and down-stream transit time of only about 0.9 μs. To achieve 1% of full-scale digital resolution for a system directly measuring the transit time would require a clock period of about 9 ns (110 MHz). A 110 MHz clock is possible, but relatively sophisticated electronic components and specialized circuitry are required. The times that are measured with the chirp technique are related to the direct transit time delay, $\Delta\tau$, caused by flow, as shown in Equations (5A) and (5B):

$$t_p = \frac{-n}{f_m \tau^2} (\Delta\tau) = \frac{-n}{f_{if} \tau} (\Delta\tau), \text{ for the period mode} \tag{5A}$$

$$t_\phi = \frac{f_0}{f_m \tau} (\Delta\tau) = \frac{f_0}{f_{if}} (\Delta\tau), \text{ for the phase mode} \tag{5B}$$

In Equation (5A), n is the number of IF cycles for which the IF period is measured. The second order phase term, $-f_m \tau^2/2$, has been neglected compared to f_0 in Equation (5B). While τ and $\Delta\tau$ are essentially fixed by the geometrical constraints and the specified full-cycle flow rate of the RCS gaging system, f_m and f_0 are design parameters that may be varied to optimize the effective measurement time multiplier. In this way a 50 ns clock period (20 MHz) in the prototype system provided 0.2% of full-scale resolution. Ordinary T^2L circuitry operates satisfactorily at 20 MHz, making this a significant advantage for the frequency chirp approach compared to a system making a direct measurement of the sonic transit time changes, $\Delta\tau$.

5B-4   Digital Measurement Techniques Employed

The IF phase and frequency are conveniently measured by digital techniques. The basic approach is outlined here for clarity of the error analysis which follows. This approach, selected in the study phase, was used in the prototype system.

FIGURE 5-2 is a simplified block diagram of the Prototype Gaging System (period mode only), with dashed lines separating the analog and digital
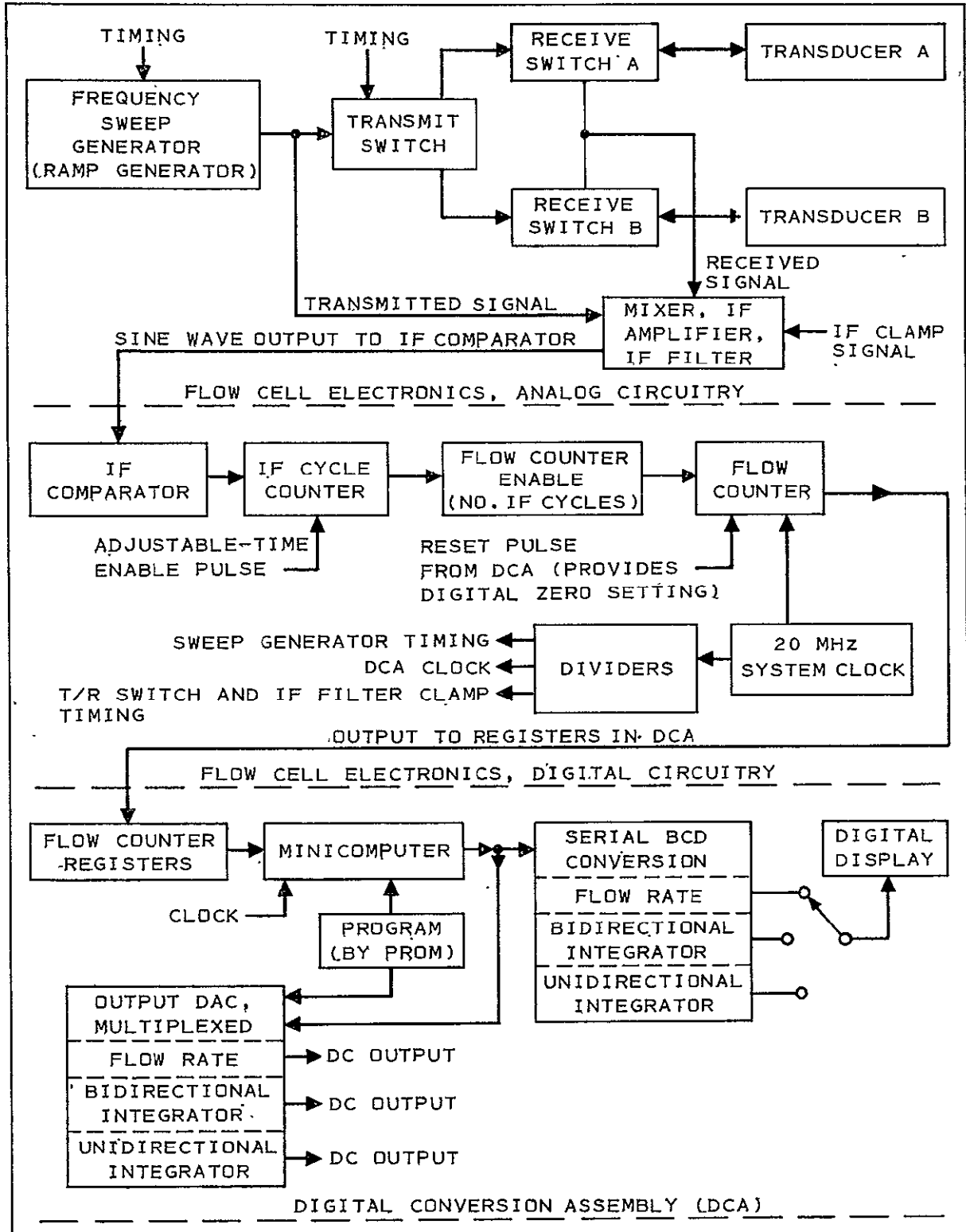
Figure 5-2. Simplified Gaging System Block Diagram (Flow by Period Mode Only)

portions of the flow cell electronics, and the DCA electronics. For clarity, this diagram is simplified to show only the period-mode flow output. The frequency ramp generator of the block diagram provides an output such as the frequency domain plot for the transmitted signal shown in FIGURE 5-1. The ramp and all other fixed-time signals are provided by division of the 20 MHz clock, as indicated in the Flow Cell Electronics Digital Circuitry section of FIGURE 5-2. The T/R switches are also controlled by signals derived from the 20 MHz system clock, as is the IF filter clamp signal. The T/R switches alternately interchange transducers A and B as transmitter/receiver, in synchronization with the ramp generator cycles.

FIGURE 5-3 illustrates the essential features of the signals at various points in the Flow Cell Electronics. Curve A of FIGURE 5-3 is a repeat of FIGURE 5-1B, illustrating the transmitted and received frequencies versus time for a ramp pair. The IF signal is obtained by use of an integrated circuit mixer which multiplies the received signal by an attenuated portion of the transmitted signal. By trigonometric identities, the mixer output is the sum of two signals--one having a frequency equal to the difference of the transmitted and received signals, and the other having a frequency equal to the sum of the two signal frequencies. After amplification, the IF signal is passed through an active filter having $f_m \tau_0$ (the nominal IF frequency) as its center frequency and a half-bandwidth of about 8%, which is adequate for water. The Q of the active filter is high enough to provide 60 to 80 dB attenuation for signals differing from $f_m \tau_0$ by a factor of two or more. The signal at the output of the IF filter is illustrated by curve B of FIGURE 5-3. In the preceding analysis it was assumed that the mixer and IF filter outputs were of constant amplitude, for simplicity of discussion. The waveform shown in curve B is typical of that actually obtained with an active filter. It indicates significant group delay and rise time delays that are introduced by the active filter. These waveforms also contain amplitude distortions that result from the fact that the two inputs to the mixer are not of constant amplitude. These deviations from the ideal model limit the number of IF cycles that can be measured for a given ramp time and IF frequency. The effect of this limitation is considered in the error analysis that follows.

The signal from the active IF filter is converted to a square wave IF signal, illustrated in curve C of FIGURE 5-3, using a comparator that switches state at each zero crossing of the sinusoidal IF signal. The comparator is shown as the first block of the Flow Cell Electronics Digital Circuitry in the simplified block diagram of FIGURE 5-2.

The period of a number (switch selectable) of IF cycles is measured by counting the number of 20 MHz clock pulses that occur between selected zero crossings of the IF signal, corresponding to positive- and negative-going transitions of the squared IF signal. To determine which cycles are measured, an IF Cycle Counter is enabled by a pulse, shown in curve D of FIGURE 5-3, formed by two "one-shot" circuits at a fixed time (but adjustable) after the start of a ramp cycle. The IF Cycle Counter and associated circuitry is preset to generate a Flow Counter Enable signal (curve E) lasting for a fixed (but switch-selectable) number of IF cycles, beginning at a predetermined zero crossing following the
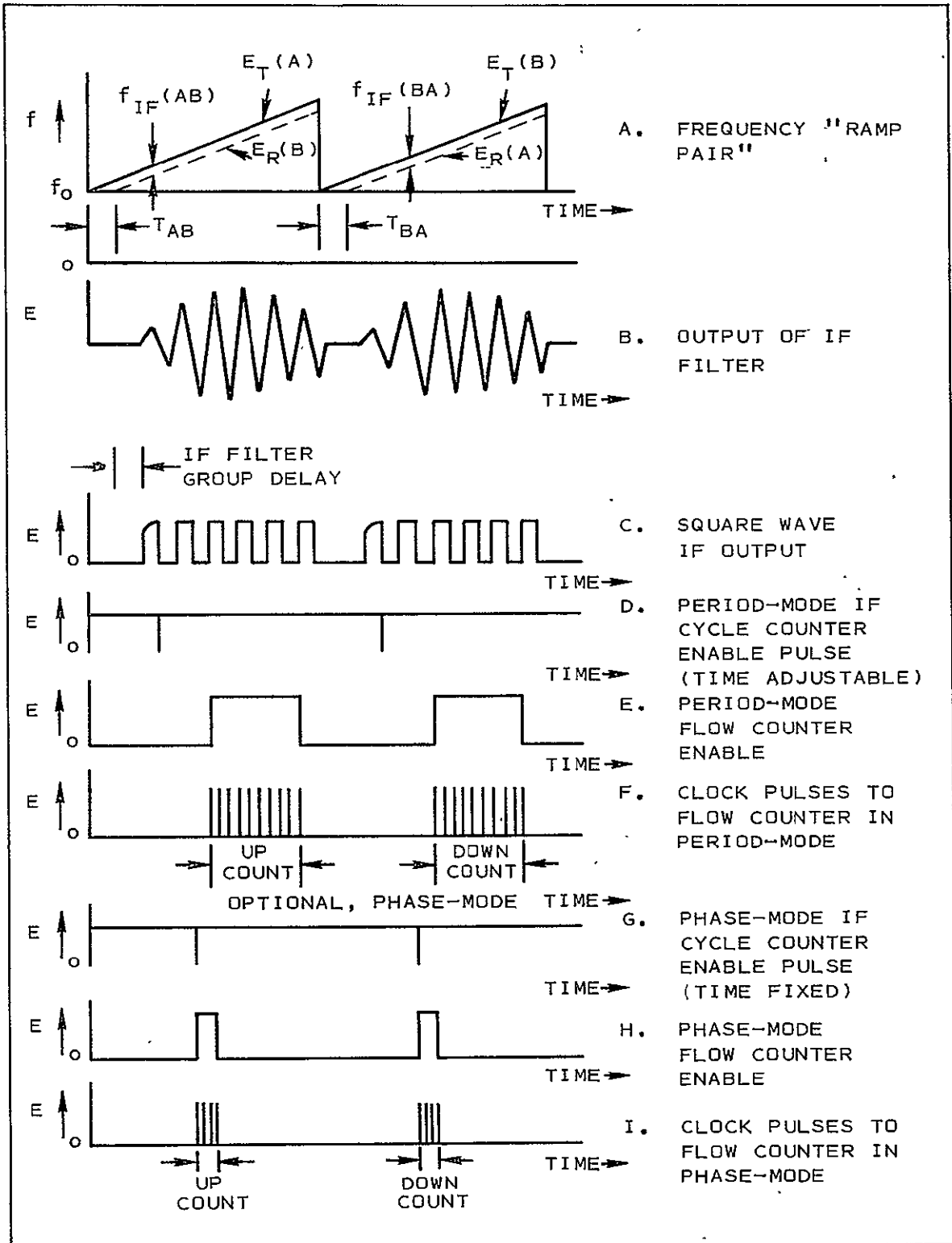
Figure 5-3.   Timing Diagram for Signals in Flow Cell Electronics

IF Cycle Counter Enable pulse. The Flow Counter is, therefore, enabled to count the 20 MHz clock pulses as illustrated in curve F of FIGURE 5-3. The clock is counted "up" for one ramp and "down" for the succeeding ramp, for a time period of each ramp determined by a preselected number of IF cycles. The number of up or down counts accumulated is proportional to the period of the corresponding IF signal and to the number of cycles counted. The difference in counts accumulated for two successive ramps provides the measure of flow velocity in the period mode of operation. (Actually, the mini-computer in the DCA receives the total counts for each T/R half-cycle, and performs the necessary arithmetic operations by PROM program.)

The block diagram (FIGURE 5-2) indicates blocks for the IF Cycle Counter and the Flow Counter Enable functions, which create the Flow Counter Enable signal. Actually, the Flow Counter starts counting the 20 MHz clock as soon as it is enabled, but a Reset Pulse from the DCA (indicated in FIGURE 5-2) resets the counter to zero shortly after the counter is enabled. The DCA provides a fixed time delay for the Reset Pulse following the start of the A-to-B ramp, and an adjustable time delay for the B-to-A ramp. This adjustment provides a means of setting the digital count difference to zero at zero flow rate. Minor differences in signal propagation times for the two T/R directions result in a digital count zero off-set which is compensated in this manner. This level of detail is omitted in FIGURES 5-2 and 5-3 in the interests of clarity. It is described here as an indication of the degree of simplification of the block diagram shown in FIGURE 5-2.

The Flow Counter is output to registers in the DCA, which contains a mini-computer programmed by a PROM. The block diagram of the DCA as shown in FIGURE 5-2 is simplified to illustrate only the basic functions of the DCA. It is a CMOS, bit-serial computer, and is inherently rather slow. The BCD conversion to drive a digital display, in particular, required more than 4.2 ms per T/R half-cycle for a meaningful digital display, even though the DAC outputs could operate at this speed. As delivered, the Prototype Gaging System could operate with either a 5-ms or 10-ms T/R ramp, with data output either every 10 ms or 20 ms, respectively. The final Feasibility Demonstration Tests were performed with the 10-ms ramp time to ensure that the mini-computer had adequate time to drive the digital display.

When operating in the phase mode, the IF signal phase is determined by generating a pulse which is fixed in time following the beginning of a ramp. The fixed time pulse is generated by counting down the system clock. This pulse is shown in curve G of FIGURE 5-3. It is used to initiate the Phase-Mode Flow Counter Enable signal shown in curve H, which is terminated by the next zero-crossing of the IF signal (positive transition of the squarewave IF). The Flow Counter is, therefore, enabled to count clock pulses beginning at a fixed time after the start of the T/R ramp and lasting until the next zero-crossing of the IF. The phase-mode clock pulses are illustrated in curve I of FIGURE 5-2. The number of counts accumulated for each ramp is proportional to the time to IF zero-crossing after the fixed point in time. The difference in clock counts for successive ramp cycles is the measure of phase shift due to flow. The Reset Pulse from the DCA provides zero control, as in the period

mode. In the final prototype system, the 20 MHz clock was divided down to
4 MHz for the phase-mode measurement to provide scaling. The phase-mode
sensitivity was greater than the period-mode sensitivity due to choice of f_O
and f_m. The operating mode was selected by three toggle switches, which
switched the clocks and the Flow Counter Enable signals to determine which
signal was measured by the Flow Counter.

Recalling that the phase of the IF signal is determined by $f_O\tau$ (neglecting
$-f_m\tau^2/2$) and that the frequency is determined by $f_m\tau$, further discussion of
curve B of FIGURE 5-3 will promote better understanding of the way in which the
IF signal varies. The IF filter output waveform (viewed on an oscilloscope)
will shift all cycles to the left or to the right as either f_O, L, or C_O is
varied. For changes in f_O, L, or C_O, the IF waveforms for the AB and BA T/R
half-cycles (or ramps) will shift phase identically. Simultaneously, there
will be a less noticeable change in IF frequency when L or C_O change, which
will increase or decrease the total number of IF cycles being viewed on the
oscilloscope pattern. Again, the IF patterns for the AB and BA T/R ramps will
be effected identically when L or C_O vary. Varying f_m will result in varying
the IF frequency only, which will effect the number of IF cycles in the pattern
but will not effect the position of the first zero-crossing (phase) of the IF
pattern. Both the AB and BA T/R ramp patterns are effected identically in the
absence of flow.

Only a change in flow velocity will result in opposite shifts of IF phase and
frequency for the two T/R ramp patterns. For practical values of the design
parameters, the phase shift is ten or more times as large as the frequency
change due to flow. It is, therefore, easier to visually discern the effect
of flow upon phase than upon frequency.

The speed of sound in the medium was also measured in the end-item Prototype
Gaging System by averaging the measured IF periods (counts accumulated) for
successive cycles at the output of a DAC, similar to that employed in the DCA,
to provide an analog signal only. This part of the system is omitted from
FIGURE 5-2 for clarity. A separate counter, similar to the Flow Counter, was
employed. It was enabled by the Period Mode Flow Counter Enable signal, but
counted a 1.25-MHz clock (20 MHz divided by 16) to provide convenient scaling
with adequate sensitivity. Although the prototype did make use of this signal
for open-loop (approximate) compensation of the phase mode output for the
effect of the speed of sound, this circuit was primarily employed to demon-
strate feasibility of making the correction precisely in a future flight model.

5B-5   Summary of Equations Describing Idealized System

In summary, the relevant equations relating difference in counts accumulated
for a pair of T/R half-cycles to flow velocity, the speed of sound, and to
other parameters for the period- and phase-modes of operation, and the average
number of counts, $\overline{N}_p$, for the speed-of-sound measurement, are as follows:

$$\Delta N_p = \frac{2vf_c n}{f_m L} \quad \text{for the period mode} \tag{6A}$$

$$\Delta N_\phi = \frac{2vf_c f_o}{f_m C_o} \quad \text{for the phase mode} \tag{6B}$$

$$\bar{N}_p = \frac{nC_o f_c}{f_m L} \quad \text{for the average IF period for } C_o \text{ measurement} \tag{6C}$$

By multiplying Equation (6B) by (6C), one obtains:

$$(\Delta N_\phi)(\bar{N}_p) = \frac{2vf_c f_o n}{f_m^2 L} \tag{6D}$$

In Equations (6A) through (6D),

n is the number of IF cycles measured,

f_c is the frequency of the clock being counted,

$v = F \cos A$ is the flow velocity component along the sonic path, and

$\frac{v}{C_o} \ll 1$ has been assumed in Equations (6B) and (6D).

5C   ERROR ANALYSIS AND OPTIMIZATION FOR PERIOD MODE

While the phase mode is more sensitive, only one data point is available per ramp pair. The period mode permits data taking for a major portion of the time. Further, the advantages of measuring flow velocity independent of the speed of sound made the period mode of operation particularly attractive. The error analysis and necessary trade-offs for optimization of the system for the period mode were an early major objective of the study phase of the contract.

Prior experience gained on Beckman's in-house Respiratory Flowmeter development had shown that the higher phase mode sensitivity provided a better signal-to-noise ratio (SNR) than did the period mode, as might be expected. In addition, the periods of successive IF waves were found to be very non-uniform, apparently due to the phase shift characteristics of the transmitting and receiving crystals, which were necessarily frequency swept in the region of their resonant frequencies to obtain significant received signal. The impedance match between gas and the crystals (lead metaniobate) is so poor that the received voltage signal is only about 10^{-5} times the transmitter drive voltage, even at resonance. The impedance match to water, MMH, and N_2O_4 can be 10^3 times as good, resulting in received signals of about 1% of that applied to the transmitter. It was anticipated that the improved coupling of sonic energy to a liquid medium would largely offset the need to work with a high-Q transducer with the attendant large phase shifts for a small frequency sweep, allowing an

acceptable SNR for the period mode of operation. The initial period mode analysis was performed, therefore, for an idealized system, assuming perfect uniformity of the IF cycles.

5C-1   Inherent Resolution of Period Mode

The error sources which may be easily treated analytically are as follows:

- Digital resolution limitations
- Sample rate (inactive time/active time) effects
- IF zero crossing "jitter" due to noise in IF amplitude

To the extent that these effects are random, they result in noise in flow rate and totalized flow outputs which may not result in significant errors in the total flow output for a statistically significant number of flow pulses. The analysis predicted that the peak relative errors (as % of full-scale flow) for a single flow pulse will be:

$$_p\bar{\varepsilon}_r = \sqrt{\frac{2}{T_r T_p}} \left(\frac{1}{k \; f_c}\right)\left(\frac{C_o}{v_m}\right) (100\%) \text{ for the digital resolution error} \qquad (7A)$$

$$_p\bar{\varepsilon}_s = \frac{T_r(1-k)}{T_p} \text{ (\% Flow) for the sampling rate error} \qquad (7B)$$

$$_p\bar{\varepsilon}_z = \sqrt{\frac{2}{T_r T_p}} \left(\frac{E_n}{E_m}\right)\left(\frac{C_o}{v_m}\right)\left(\frac{C_o}{2\pi f_m L}\right)(100\%) \text{ for the IF zero crossing} \qquad (7C)$$

$$\sum \bar{\varepsilon}_p = \frac{1}{T_p}\sqrt{\frac{2T_p}{T_r}} \left(\frac{1}{k}\right)\left(\frac{C_o}{v_m}\right)\left[\frac{1}{f_c} + \frac{C_o}{2\pi f_m L} \left(\frac{E_n}{E_m}\right)\right](100\%) + \frac{T_r}{T_p} (1-k)(\% \text{ Flow}) \qquad (7C)$$

for the sum of the errors of Equations (7A through 7C).

In the above equations,

T_r = time of a single frequency ramp (or T/r half cycle)

T_p = duration of a flow pulse, assumed to be rectangular

$k\leq 1$ = ratio of active measurement time to ramp time

$v_m = f_m \cos A$ = full-scale flow velocity component

$\dfrac{E_n}{E_m}$ = reciprocal of IF signal amplitude SNR

$\dfrac{T_p}{T_r} > T_r$ to provide five or more data points for the minimum
T_p to permit division of the errors ε_r and ε_z for each

data point by the square root of the number of data points obtained for each flow pulse. In accordance with applic-able statistical principles, this is valid for a large number of data points, and reasonably accurate for five or more.

% Flow = percentage of full-scale flow at peak for a flow pulse of duration T_p. The flow pulse is assumed to be rectangular.

It is also assumed that "jitter" in the IF period is adequately included in the "IF amplitude SNR." Noise in f_o, which directly causes jitter in the IF phase, is cancelled in the method of enabling the flow counter described above. Noise in f_m is a major source of IF-period jitter.

Examination of Equation (7D) reveals that some trade-offs must be made to achieve optimum total errors, as described below:

- Reducing T_r/T_p reduces the second term (sampling rate error) directly but increases the first-term error (combined digital resolution and zero-crossing errors) by the square root. For a given minimum flow pulse duration (40 ms for this program) there will be an optimum ramp time unless one of the two terms of Equation 7D can be made negligible. The ramp time is, therefore, an important design parameter.

- Increasing k (obtaining data during a larger percentage of the time) is of direct benefit in reducing all three errors. This factor is, therefore, an important design parameter.

- Increasing the clock frequency, f_c, can make the digital resolution error negligible compared to the zero-crossing error in the first term of Equation (7D). The clock frequency is, therefore, an important design parameter. Its choice is also completely independent of the other parameters.

- Noting that $f_m L/C_o$ is the nominal IF frequency, it is apparent that increasing the IF frequency will reduce the zero-crossing error component of the first term of Equation (7D) provided the IF SNR does not decrease proportionately. The important design goal is, therefore, to maximize the product of IF frequency and IF SNR.

- Increasing T_p reduces both terms of Equation (7D), but the minimum T_p (maximum error contribution) is a flight-system constraint. However, for the minimum pulse duration the flow cannot reach full scale. This is why the second-term error is multiplied by "% Flow," instead of by 100%.

- Decreasing C_o/v_m would reduce the first term, but C_o/v_m is fixed at about .130 for water by system constraints.

Equation (7D) may be evaluated using reasonable values for all quantities. The IF SNR is not easily preducted from theory alone, but prior experience indicated that SNR > 130 is possible. An estimate for a 20 MHz clock, 2 kHz IF, SNR = 130, T_p = 40 ms, T_r = 4 ms, k = 0.5, C_o/v_m = 130, and for a % Flow of 10% of scale (maximum) for T_p = 40 ms, is:

$$\Sigma\bar{\epsilon}_p = 0.0146\% \text{ (digital res.)} + 1.8\% \text{ (zero crossing)} + \qquad (7E)$$
0.5% (sampling rate)

2.3% of full scale, or about 23% of the approximate peak flow rate of 10% of scale for T_p = 40 ms.

It has been estimated by Space Shuttle Program personnel that up to 10% of the total RCS fuel (and oxidant) consumption might occur from such 40 ms flow pulses. Therefore, the error in the total tank capacity measurement should not exceed 2.3%, even if all 40 ms pulses had this peak error in the same direction. If the errors are all random, then from statistical considerations the net probable error for N similar pulses would be expected to be reduced by division by the square root of N. The error for the average of five or more such 40 ms pulses should be less than 1% of full scale.

The initial analysis of the idealized system indicated, therefore, that a period-mode system meeting the RCS application requirements was feasible provided that factors ignored in making the analysis did not introduce large errors. Potential sources of major error are "water hammer" pressure transients, pressure "ringing" of the system, and vibration of the system at critical frequencies. In addition, the allowable values of f_m, f_o, T_r, and k are quite interdependent, making optimization of these parameters more difficult than it might appear. The following paragraphs outline the balance of the period-mode analytical work performed in the Design Study Phase of the contract, before significant experimental data were obtained. In particular, the stability requirements for the "constants" were determined, as summarized in the following paragraphs. The detailed analysis is given in the Appendix.

5C-2   Period-Mode Errors due to Variations of L, f_m, and C_o

It follows from Equation (6A) and the techniques of the differential calculus that the relative error (or noise) in the flow indicated by the period-mode measurement will be equal to the sum of the relative errors (or noise) of the constants L, f_m, and C_o. There appears to be no problem with making both the frequency rate of change and the path length stable (for many years) to within 0.1% or better for a flight model. However, because the system obtains the signal expressed in Equation (6A) by measuring the small difference of large numbers of counts obtained for successive T/R half-cycles, any noise in L and f_m will cause relatively large noise in the output signal. In particular, modulation of f_m or L at 1/2, 3/2, 5/2, ...(2n + 1)/2 multiples of the fundamental ramp frequency, $1/T_r$, will result in systematic errors. In the case of random noise or such synchronous modulation of f_m and L, the relative error equation, derived from the root equations of Equation (6A), is:

$$\frac{dF_p}{F_p} = \left(\frac{dL}{L} + \frac{df_m}{f_m}\right)\frac{C_o}{vm}, \text{ for noise and/or modulation of L and } f_m \qquad (8A)$$

The relative errors (or noise) in L and f_m are amplified by C_o/vm. Since C_o/vm is about 130 for the case of interest, the sum of the percentage modulations of

L and f_m must be significantly less than 1/130 times the desired percentage error (or noise) in flow measurement. Random noise will average out, but systematic errors will be introduced by synchronous modulation at the critical frequencies.

While Equation (6A) indicates that the period mode of operation makes the system independent of C_0, any time rate of change of C_0 that is large enough to introduce a difference in the value of C_0 for successive T/R half-cycles will cause an amplified flow measurement error. An appropriate expression for the relative error due to this source is:

$$\left.\frac{dF_p}{F_p}\right|_c = -\frac{dC}{C} \text{ for changes in C that do not cancel for successive} \qquad (8B)$$
ramps

The principal cause of variations in C_0 will be variations of the liquid temperature. Slow variations will be cancelled by the difference technique, but fast changes will not. The flow error from this source will be:

$$\left.\frac{dF_p}{F_p}\right|_c = -\left(\frac{1}{C}\frac{dC_0}{dT}\right)\left(\frac{dT}{dt}\right) T_r\left(\frac{C_0}{vm}\right), \text{for errors due to rapid changes} \qquad (8C)$$
in C_0 due to rapid thermal transients

The speed of sound is not a strong function of temperature, and T_r will be of the order of 3×10^{-3} seconds. The magnitude of $(1/C)(dC/dT)$ is about $10^{-3}°C^{-1}$. Even if dT/dt reaches $100°C/s$ when C_0/vm is 130 (minimum value, occurring at full scale flow rate), the error in measured flow per ramp pair will only be about 13%. Furthermore, to the extent that the thermal transient of the flowing medium has a symmetrical rise and fall curve, the error in total mass transferred will cancel out as the slug passes through. (If the rate of temperature rise is systematically greater than the rate of fall, a positive error in the period-mode output will result.) Only small flow pulses, which leave the warm "slug" of fluid in the gaging system cell until it cools, would cause truly systematic errors. In this case, the value of dT/dt should not be as large as $100°C/s$, which would reduce the error. Finally, it should be easily possible to locate the gaging system cell and the lines supplying it in positions remote from sources of heat that might introduce such large thermal transients.

Variations in flow cell pressure will cause variations in L which might introduce significant errors. In particular, pulsed flow will result in large "water hammer" transient pressures, and will result in pressure "ringing" at the system resonant frequency. These pressure effects upon L will result in relative flow error (or noise) given by:

$$\left.\frac{dF_p}{F_p}\right|_L = \left(\frac{1}{L}\frac{dL}{dP}\right)\left(\frac{dP}{dt}\right) T_r\left(\frac{C_0}{vm}\right) \qquad (8D)$$

If the flow cell pressure systematically rises more rapidly than it falls, the system will provide low period mode readings. (The apparent sign reversal is due to having solved for F before differentiating to obtain the error relationship. The positive sign in Equation (8D) means that a flow increase is necessary to offset an increase in path length.)

In summary, the stability of f_m and L will be critical. In particular, modulation of either or of both at odd multiples of the ramp-pair frequency will result in systematic errors that will affect the total-mass-transferred output. Similarly, any non-random transient in C_o, such as that due to a warm slug of fluid passing through the gaging system each time an RCS engine fires, may result in systematic errors. The combined relative error function is:

$$\frac{dF_p}{F_p} = \left(\frac{1}{L}\frac{dL}{dP}\frac{dP}{dt}T_r + \frac{df_m}{f_m} - \frac{1}{C}\frac{dC}{dT}\frac{dT}{dt}T_r\right)\left(\frac{C_o}{vm}\right) \tag{8E}$$

The above discussion demonstrates that $(1/L)dL/dP$, f_m, and dT/dt are very important design parameters for a flight model operating in the period mode. Water hammer and pressure ringing effects can modulate L at the critical frequencies. Such pressure transients are capable of introducing systematic errors, which will not average out. Modulation of f_m by the line frequency and its harmonics can be a problem if the ramp frequency coincides. Even more important, because the basic data are output for each ramp, and the final data for each ramp pair, it will be necessary to guard against modulation of f_m by the resulting power supply and ground coupled transients, which will necessarily occur at the critical frequency. Any rapid and very large thermal transients that are systematic in nature will also result in systematic flow measurement errors.

5D   CORRECTION OF MASS FLOW FOR THERMAL EFFECT UPON DENSITY

For a future flight model, it will be necessary to apply a density-temperature correction to obtain mass flow data. It will be advantageous to obtain the thermal correction data from a measurement of the speed of sound by taking the average IF period for each ramp pair. This avoids the thermal lag problems that are inescapable with a direct temperature measurement, and provides a compensation signal derived from exactly the same set of data that are used for the flow measurement for each ramp pair.

The scheme for thermal compensation is best illustrated by the following derivation, which is based upon the simplifying assumption that deviations in both the density of the medium and the speed of sound are approximately linear functions of thermal variations about the nominal temperature. More complicated expressions (polynomials, which are second or higher-order in T) to obtain greater precision are possible, but the simple linear relationship illustrates the principle. The relevant equations are:

$$\rho = \rho_o(1 + \alpha\Delta T) \text{ for variations of density} \qquad (9A)$$

$$C = C_o(1 + \beta\Delta T) \text{ for variations of the nominal speed of sound} \qquad (9B)$$

$$\bar{P} = \frac{C}{f_m L} = \frac{C_o(1 + \beta\Delta T)}{f_m L} \text{ for variations of the average period, } \bar{P} \qquad (9C)$$

$$\Delta T = \left(\frac{\bar{P}f_m L}{C_o} - 1\right)\frac{1}{\beta} = \frac{\overline{\Delta P}}{\bar{P}_o}\frac{1}{\beta}, \text{ from (9C), where } \bar{P}_o \text{ is the nominal} \atop \text{IF period.} \qquad (9D)$$

Substituting (9D) in (9A),

$$\rho = \rho_o\left(1 + \frac{\alpha}{\beta}\frac{\overline{\Delta P}}{\bar{P}_o}\right) = \rho_o\left(1 + \frac{\alpha}{\beta}\frac{\overline{\Delta N}}{\bar{N}}\right), \text{ where } \overline{\Delta N} \text{ is the variation from} \atop \text{the constant digital count for} \atop \text{the nominal average period, } \bar{N}_o. \qquad (9E)$$

The mass flow rate, M, is the volumetric flow rate multiplied by the density. The volumetric flow rate is the measured average flow velocity, F, multiplied by the cross-sectional area of the flow cell, A. Using Equation (6A), the mass flow rate when using the period mode is:

$$M_p = F_p A\rho = \frac{f_m L}{2f_c n \cos B}(\Delta N_p)A\rho_o\left(1 + \frac{\alpha}{\beta}\frac{\overline{\Delta N}}{\bar{N}_o}\right) \qquad (9F)$$

where B is used for the angle to avoid confusion with the area, A;

ΔN_p = the difference in period mode counts for successive ramp cycles due to flow;

$\overline{\Delta N}$ = variation in counts for the average period from the nominal value due to variations in temperature;

$\bar{N}_o$ = the average period for the nominal temperature, which is a constant.

All terms of Equation (9F) are constants for a given liquid except the digital counts, ΔN_p and $\overline{\Delta N}$. The first is obtained as the difference of the digital counts representing the IF periods for successive T/R ramps. The second is the deviation of the sum of the same digital counts from a constant value. The conversion to mass flow rate can, therefore, be both precise and free from thermal transient errors.

While the phase mode of operation was not included in the original Design Study, this mode was tested. The analysis was performed late in the program, and is included in the Appendix. The equations for conversion of the phase mode measured flow velocity to mass flow rate with and without compensation for the speed of sound, are:

$$M_\phi = \frac{f_m C_O}{2f_c f_O \cos B} (\Delta N_\phi) A\rho_O \left(1 + \frac{\alpha}{\beta} \frac{\overline{\Delta N}}{N_O}\right), \text{ for the uncorrected phase} \quad (10A)$$

mode measurement; and

$$M_{\phi,\overline{p}} = \frac{f_m^2 L \overline{N}_p}{2f_c^2 f_O n \cos B} (\Delta N_\phi) A\rho_O \left(1 + \frac{\alpha}{\beta} \frac{\overline{\Delta N}}{\overline{N}_O}\right) \text{ for the phase measure-} \quad (10B)$$

ment corrected for the speed of sound.

There are only two digital count variables in Equation (10A), and three in (10B), for a given liquid. The average period count, $\overline{N}_p$, is the third variable in Equation (10B). The mass conversion temperature correction term is, of course, the same for all three modes of measurement.

Some of the relevant properties of the fuels and oxidants of interest are given in an Air Force Report, "Engineering Property Data on Rocket Propellants," Technical Report AFRPL-TR-68-100. The density of MMH is a linear function of temperature over a wide range, with $\alpha = -1.02 \times 10^{-3}/°C$ ($-5.65 \times 10^{-4}/°F$). The density of MMH changes, therefore, about 5.6% over a 56°C (100°F) range. The speed of sound variation with temperature for MMH is not given, but the more complete data for N_2O_4, discussed below, suggest that the speed of sound in MMH may vary up to 20% over a 56°C (100°F) range. The speed of sound in N_2O_4 is given as a linear function of the temperature in the referenced report, with $\beta = -4.05 \times 10^{-3}/°C$ ($-2.25 \times 10^{-3}/°F$). The Speed of sound of N_2O_4 changes, therefore, about 22.5% over a 56°C (100°F) range. The density of N_2O_4 varies with both temperature and pressure. The change with pressure will be less than 1%/1000 psia, or less than $\pm0.1\%$ for ±100 psia variations in the application of interest. The varying pressure effect may, therefore, be neglected. The density of N_2O_4 changes about 8% over a 56°C (100°F) range. Precise correction of N_2O_4 density for temperature (at fixed pressure) requires a polynominal which is second order in temperature, but the linear assumption used above with a $\alpha = -1.40 \times 10^{-3}/°C$ ($-7.78 \times 10^{-4}/°F$) will result in less than $\pm0.3\%$ error in density compensation for $\pm28°C$ ($\pm50°F$) variations about the nominal temperature. If desired, solving the second order polynominal will reduce this error to about $\pm0.03\%$. However, neglecting both the pressure effect (for ±100 psia variations) and the thermal effect (due to neglecting the second order term for $\pm28°C$ variations) will result in less than $\pm0.5\%$ error in the mass flow of N_2O_4 measured for worst-case conditions.

The density of water changes only about 0.018%/°C (0.01%/°F), which would intro-duce a mass flow error of $\pm0.3\%$ for the 21 $\pm17°C$ (70 $\pm30°F$) range required in this contract. The speed of sound changes about 0.25%/°C (0.14%/°F in the vicinity of room temperature, resulting in a change of about $\pm4.2\%$ for the re-quired 21 $\pm17°C$ (70 $\pm30°F$) range. It was decided that the cost effective approach for the prototype NIGS (for use with water only) was to avoid the cost of including compensation for density variations with temperature until test results more fully demonstrated the basic feasibility of the approach. An analog speed of sound (average period) output was provided to demonstrate the feasibility of obtaining the necessary compensation signal. This output

was used to make an approximate (open loop) compensation for the speed-of-sound effect on the phase mode flow measurement.

5E   ANTICIPATED EFFECTS OF FLOW PROFILE

The ultrasonic flowmeter inherently measures an average flow velocity, F, across the sonic path. For laminar flow, the velocity profile across a tube of circular cross section is parabolic, having essentially zero velocity at the wall, maximum velocity at the axis, and the average velocity at one-third of the tube radius from the axis. For turbulent flow, the velocity profile tends toward a square shape, with uniform velocity across the bore of the tube. Intuitively, one would expect the average flow velocity measured by sonic transit time to be dependent on the flow condition, resulting in non-linearity for ranges spanning the laminar to fully turbulent conditions. This potential problem was addressed during the Beckman proposal effort. For the minimum flow rate of interest and for the tube diameter specified, the Reynolds number is large enough to ensure turbulent flow. Consequently, it is not necessary to measure in the laminar and transition flow regions for the RCS application. Because the uniform velocity profile is the case treated in the analysis of the idealized system, it was anticipated that the linearity for turbulent flow would be excellent.

A detailed analysis of the sonic averaging mechanism for the entire flow range is a formidable task. The Beckman respiratory flowmeter is known to operate from zero to fully turbulent flow with no significant non-linearity being discernible in the laminar-to-turbulent transition region. This fact suggests that the sonic flow averaging mechanism is essentially independent of the flow profile, at least for tubes of about 1.5-inch diameter and for comparable transducer dimensions. In view of this prior experience and the fact that all required RCS measurements are in the turbulent region, it was elected to defer extensive theoretical consideration until (and unless) test results indicated that a problem might exist. The preliminary test and Design Feasibility Test results, discussed in Sections 8 and 9, verified that the gaging system has no discernible non-linearity from zero to full-scale flow. Consequently, it is not necessary that the flow pulses be rectangular to avoid errors in the zero-to two-pound-per-second (minimum specified flow rate) region. The assumption of rectangular flow pulses, therefore, merely simplifies the derivation, and provides the worst-case error.

6A   SELECTION OF PARAMETERS FOR PERIOD MODE MEASUREMENT

The initial design was based on the period mode of measurement. (The phase mode was treated analytically near the end of the program when the prototype was modified to provide phase-mode measurement capability. See Appendix for details of the analysis.) It was assumed that system noise due to noise in L, C_O, and f_m could be made acceptable in the integrated output (total mass transferred) and that systematic errors due to modulation of L and f_m at the T/R cycle frequency, $1/2\ T_r$ and its odd harmonics, could be made negligible by design. The errors of Equation (8A) were neglected, therefore, and the parameters k, f_O, f_m, and T_r were considered for optimization according to Equation (7D). Equation (7D) is rearranged and repeated here for convenience:

$$\sum \bar{\varepsilon}_p = \sqrt{\frac{2}{T_r T_p}} \left(\frac{1}{k}\right)\left(\frac{C}{v_m}\right)\left[\frac{1}{f_c} + \frac{1}{2\pi f_{IF} E_m/E_n}\right] (100\%) + \frac{T_r}{T_p}(1-k)(\% \text{ Flow}) \qquad (11A)$$

This equation gives the sum of the errors as a percentage of full scale. The following parameters were considered fixed at the values given by the NIGS requirements:

- T_p = 40 ms minimum, which causes maximum noise (or error)
- C/v_m = 100 for MMH and N_2O_4, and 130 for water. (v_m is the full-scale flow velocity component.)

Several parameters were considered to have practical limitations from the standpoint of the cost effective route to a realistic demonstration of feasibility. These are summarized as follows:

- T_r > 4 ms, due to the estimated limitations of the available (at no cost) DCA. (It was discovered in testing that $T_r \geq 8.4$ ms was necessary.) The smallest practical value of T_r was desired to achieve maximum data rate.

- f_c = 20 MHz, is a reasonable maximum (inexpensive) clock frequency for T^2L logic. The digital resolution for this clock should be adequate to make that source of error negligible compared to the anticipated zero-crossing noise.

- k > 0.5 if possible, to suppress all errors. Since k<1 by definition, achieving k=0.5 would provide optimization within a factor of two, except for the sampling rate error. (k is the fraction of the ramp time during which the measurement is made.)

It follows from the above discussion that maximizing the product of the IF frequency and its amplitude signal-to-noise ratio was the major goal. More correctly, k should be included in the product to be maximized, since k, f_O,

f_m, T_r, and the usable bandwidth of the transducers are all inter-related. This term of Equation (11A) accounts for the zero-crossing jitter of the IF signal. The SNR is difficult to predict analytically, but it is probable that the major source of noise is the noise in f_m. The period mode SNR due to f_m alone, from Equation (8A), would be:

$$SNR_p \big|_{f_m} = \left(\frac{v}{c}\right) \frac{f_m}{df_m} \qquad (11B)$$

Equating this SNR to E_m/E_n in Equation (11A) results in the following expression for the term of interest (zero-crossing uncertainty, including k):

$$\frac{1}{2\pi k f_{IF} E_m/E_n} = \left(\frac{c}{v}\right)\left(\frac{df_m}{f_m}\right) \frac{1}{2\pi k f_{IF}} \qquad (11C)$$

where all noise sources except df_m/f_m have been considered to be negligible.

If it is assumed that df_m/f_m will remain constant when the IF frequency is increased, and that it will not be necessary to reduce k if f_{IF} is increased, then increasing f_{IF} is the proper (and only feasible) way to reduce the zero-crossing uncertainty for the prototype NIGS. The assumption that k and df_m/f_m are not inverse functions of f_{IF} being reasonable, it was decided that the maximum IF frequency attainable with the transducers (still to be designed) was the preferred initial approach.

6B   TRANSDUCER DESIGN CONSIDERATIONS

During the in-house Beckman development of a respiratory flowmeter, it was necessary to operate the transducers in the region of resonance to receive usable signals. Presumably, this was a consequence of both the poor impedance match between the crystals and gas and of the absorption of sound by gases, which becomes significant above several hundred kilohertz. Among the piezo-ceramics, lead metaniobate has the broadest resonance (Q of about 15) and the most stable long-term properties available. It is especially resistant to degradation due to thermal cycling. In the gas flowmeter these crystals are exposed to the sample gas, and they are frequency chirped through a portion of the fundamental resonance at about 250 kHz. The output is derived from the phase mode of operation. The noise in the period mode is unacceptable, and the IF periods of successive cycles are non-uniform due to the phase shift associated with sweeping through the resonant frequency.

For the NIGS application, it was decided that an initial attempt should be made to operate off-resonance to obtain uniformity of the periods of successive IF cycles. It was also concluded that initial tests should be performed with lead metaniobate crystals, having 1.0 and 2.5 MHz fundamental resonances, each type with both 0.25- and 0.5-inch diameters, mounted to 0.005-inch-thick stainless steel. This thickness of the stainless steel would be approximately transparent according to applicable sonic coupling concepts. (The equations

describing sonic energy transmission and reflection at interfaces are essentially those employed in the transmission line and optical coating disciplines. See Section 7 for details.) The test plan also included comparison of the IF signal obtained with 0.005-inch-thick to that for 0.125-inch-thick stainless-steel crystal mounts, for the preferred type of crystal.

The choice of 1.0 and 2.5 MHz crystals for the RCS application was based on the desire to increase f_{IF}, as discussed above. Once T_r is selected (4 ms, or higher if necessary, for the minicomputer), then the maximum value of kf_{IF} will be determined by the allowable frequency sweep over which usable IF cycles can be obtained. The maximum value of f_m is simply $\Delta f/T_r$. Since τ is essentially fixed by RCS specifications, the maximum kf_{IF} is fixed by $\Delta f/T_r$. Such crystals have resonances at the fundamental and at the odd (only) harmonics of the fundamental resonance frequency. The Δf from zero to the fundamental frequency, f_o, can approach f_o. Also, the Δf between the fundamental, f_o, and the third harmonic, $3f_o$, is $2f_o$. In principle, at least, a larger Δf sweep without encountering serious distortions in the IF cycle uniformity can be realized with a crystal having a higher fundamental resonant frequency, if off-resonance operation is feasible. Even if off-resonance operation is not feasible, a larger Δf (across resonance) is available for the same type of crystals (having the same Q) for crystals having a higher fundamental resonant frequency.

As a back-up, a pair of 1 MHz transducers was purchased from Scarpa Laboratories, Inc. Scarpa has been marketing commercial ultrasonic flowmeters for a number of years. It seemed reasonably probable that use of his transducers might circumvent a development effort on this contract. The Scarpa transducers are rugged and utilize a degree of focusing to obtain some colimation of the sonic beam. They are not designed for frequency chirp operation, but in the opinion of Mr. John Scarpa, they should operate in this mode. In the Scarpa design, the transducer assembly floats on two O-ring seals, and does not contact the stainless-steel flow cell directly. This design feature would not be directly applicable to an RCS gaging system, but it seemed possible that the Scarpa internal design would permit hard mounting when used with a frequency chirp system.

6C   INITIAL ZERO-FLOW TEST RESULTS AND CONCLUSIONS

The results obtained in the initial testing at component level are summarized here. While the major conclusions drawn at the time were valid, subsequent work revealed that faulty crystal bonding, for example, compromised the quality of the data obtained. The major no-flow test results and conclusions, essentially in chronological order, were as follows:

- No appreciable signal was received for off-resonance operation. This was the most significant finding, since it precluded the possibility of breadboard operation of the transducers without using more elaborate designs

- The received RF signal was amplitude modulated by a sinusoidal function having the frequency of the IF signal. This caused by multiple reflections between the transducers, with transit times of 3τ, 5τ, etc.

- The use of a square transmitted wave greatly confuses any attempt to correlate the received RF with the IF signal, and makes detailed analysis much more difficult. This is a consequence of the high harmonic content of square waves, the fact that f_m for the nth harmonic is equal to nf_m, and (probably) the fact that the phase shift for each harmonic is different. It was concluded that transmitting a sine wave was essential for the acquisition of a better understanding of the system, even if it is ultimately found to be unnecessary for a flight system.

- The received RF signal and the IF signal obtained for 2.5 MHz and 1.0 MHz crystals, and for both crystal diameters, were found to be of essentially equal quality. Accordingly, it was decided to use 0.25-inch diameter, 2.5 MHz, crystals for further evaluation of transducer designs.

- Transducers having 0.125-inch-thick stainless-steel crystal mounts gave received RF and IF signals that were fairly comparable to those obtained with crystals mounted on 0.005-inch-thick stainless steel. This lead to fabrication of a second set using 0.5-inch-thick stainless steel, in an attempt to establish the practical limit.

- The Scarpa transducers (1 MHz) were found to be comparable to the 0.125-inch-thick stainless-steel mounted, 2.5-MHz crystals, transducers, at least with regard to received RF and IF signal quality.

- The 0.5-inch-thick stainless-steel crystal mounts provided useful received RF and IF signals over a very narrow frequency range compared to those with 0.125-inch-thick mounts. It was concluded that this was due to the fact that they corresponded to 10 quarter-wave thicknesses, which by analogy to optical interference filters would make them have a narrow bandpass. (While this is valid, it was discovered at a much later date that one crystal of the pair was very poorly bonded, which compromised the value of the data.)

- Retest of the 0.125-inch-thick stainless-steel mounts (2.5 quarter-wave thick at 2.5 MHz) revealed that the peak signal occurred at about 2.8 MHz, at which the thickness corresponded to about 2.2 quarter waves. It was concluded that thicknesses of one-half wave or less were preferred, but that no further changes would be made until flow tests were performed.

- A digitally controlled frequency ramp generator was fabricated. While this approach yields a series of small step increases in frequency, rather than a smooth sweep, it is capable of generating a constant average f_m to provide a high degree of frequency ramp linearity. No apparent problems with this ramp generator were seen in the initial zero-flow tests. It was believed that the trade-off between superior sweep linearity and jitter due to the small steps in frequency would be favorable. This generator was subsequently replaced with a Teledyne Model 4707 VFC, primarily to remove the analytical uncertainties of the digital system, in the interests of achieving a better understanding of the problems encountered in flow testing.

6D INITIAL FLOW TEST RESULTS AND CONCLUSIONS

Initial flow test results were not encouraging. The circuit design permitted measurement of the difference of IF periods for the two directions of sound transmission for 2, 3, or 5 IF cycles. By varying the time after start of the T/R half cycle at which the Flow Counter Reset Pulse occurred, it was possible to determine the flow sensitivity for groups of IF cycles, beginning at the first cycle with significant amplitude and progressing in time, one cycle at a time, to the end of the T/R half cycle. It was found that the sensitivity to flow varied from about ten times the theoretical value to virtually zero. Reversed sensitivity was also observed for some cycles of the IF signal. This poor performance is characteristic of poor IF period uniformity, and the major problem was to identify the source of the poor uniformity. The two most probable sources were: the phase shifts of the transmitted and received signals due to operation across the resonant frequency band and/or the complicating factor associated with the multiple reflections of the signal; and the problems due to imperfections of the digital frequency sweep generator. The following considerations resulted in replacement of the digital sweep generator with a Teledyne Model 4707 voltage-to-frequency converter (VFC):

- The visual quality of the IF signal was very dependent on the starting frequency, f_O. In particular, adding or removing the least significant bit which determined f_O appeared to always upset the IF signal more than did operation of more significant bit switches. This illogical result cast doubt on the performance of the digital generator, although no fault could be identified.

- The difficulty of analytically isolating the effects of the digital generator parameters on the quality of the IF signal made it very difficult to establish whether the problem was actually due to the transducers and/or multiple reflections, or not.

6E MISCELLANEOUS TEST RESULTS (ZERO FLOW) OBTAINED DURING CIRCUIT REVISION ACTIVITY

While awaiting delivery of the Teledyne VFC, an attempt was made to substitute a delay line to simulate flow, to facilitate isolation of the source of the problem. The results were neither predictable nor reproducible, probably due to increased stray coupling of the transmitted into the received signal. This series of tests did reveal that even under zero flow conditions (no delay line) there were large shifts of output zero as different sets of IF cycles were monitored. This may have been due to a systematic error in the digital generator for successive T/R half cycles, due to a design or fabrication error. The point was not pursued since this generator was to be replaced as soon as possible.

Some basic transducer tests were also performed using a Wavetek Model 146 Dual Signal Generator, with frequency modulation capability. Oscilloscope photographs such as those shown in FIGURE 6-1 indicate the differences in transducer performance when operating from the same frequency ramp generator. As noted
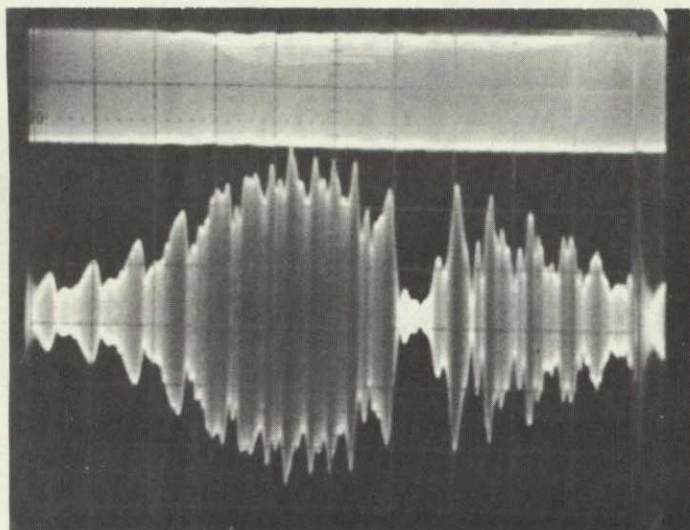
TEST CONDITIONS

A VERT: TRANSMITTED   2 V/DIV

B VERT: RECEIVED   0.1 V/DIV

HORIZ: 2 MS/DIV

fm ≈ 8.3 MHZ/S

HORIZONTAL ≈ 16.7 kHz/DIV

0.125 INCH STAINLESS STEEL MOUNTS.
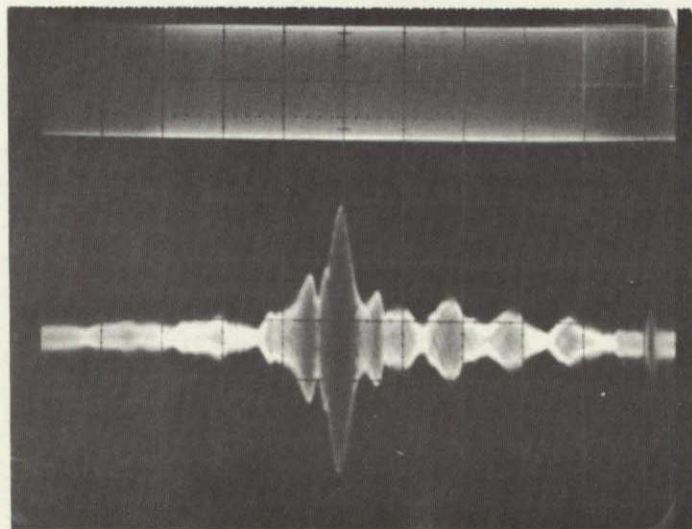
TEST CONDITIONS

A VERT: TRANSMITTED   2 V/DIV

B VERT: RECEIVED   0.02 V/DIV

HORIZ: 2 MS/DIV

fm ≈ 8.3 MHz/SEC

HORIZONTAL ≈ 16.7 kHz/DIV

0.5 INCH STAINLESS STEEL MOUNTS.

Figure 6-1.   Comparative Data for 0.125- and 0.500-Inch Thick Stainless Steel
Crystal Mounts, Using Wavetek FM Signal Generator.

above, it was found much later that one of the pair of 0.5-inch-thick stainless-steel transducers had a defective crystal bond, making the significance of the two photographs somewhat unclear. The most important feature shown in FIGURE 6-1 is the striking loss of received RF amplitude for the 0.125-inch-thick crystal mounts near the center of the frequency sweep. The sweep across resonance occurred in 20 ms for the photographs of FIGURE 6-1.

After incorporation of the Teledyne VFC, data similar to that shown in FIGURE 6-1 for the 0.125-inch mounts were obtained. The series of oscilloscope pictures of FIGURES 6-2, 6-3, and 6-4 show the received RF, the mixer output, and the four successive IF filter stage outputs. All but the bottom photograph of FIGURE 6-4 were obtained with an expanded oscilloscope sweep rate, and show only about the first 1.8 ms data of the 4 ms ramp time. The bottom photograph of FIGURE 6-4 shows the full ramp (0.5 to 8.5 horizontal divisions). This series of photographs illustrates the following:

● The received RF is modulated by several periodic functions, one of which appears to have the IF frequency.

● The RF frequencies at which the received RF signal shows marked changes in modulation pattern create near phase reversals in the mixer output. The IF filters smooth out these phase reversals, making them undiscernible to the eye (on this scale) after the second stage.

● Each IF stage contributes a group delay and a rise-time delay which result in a delay time of about one millisecond before the IF signal from the fourth stage has significant amplitude.

● Comparison of the top photographs of FIGURES 6-1 and 6-2 reveal distinct differences in the received RF waveform. The fuzzy appearance of the photograph of FIGURE 6-2 compared to that of FIGURE 6-4 probably arises from the higher harmonic content of the driver stage used with the VFC compared to that of the Wavetek generator. There is also an effect on the received RF of the varying transmitted amplitude with the VFC driver, which went from essentially zero, to peak, to zero, across the frequency sweep pictured. The marked differences in the amplitude modulation near center frequency is believed to be primarily due to the difference in ramp time. The Wavetek was using a ramp time of 20 ms compared to 4 ms for the VFC. For slow sweep rates the cavity resonance effect (due to standing waves) results in modulation of the received RF at intervals of 9.4 kHz, for which the path length (8 cm) corresponds to one-half of a wavelength of sound in water. It can be shown that multiple reflections, in a frequency chirp system, contribute received RF signals related to the transmitted signals, but time delayed by 3τ, 5τ, etc. These signals have frequency differences which are integral multiples of f_{IF}, and using trigonometric identities it can be shown that the net effect is to modulate the received RF at the IF frequency. For fast sweep rates the modulation at the IF frequency appears to dominate the modulation at the cavity resonance frequency. This is simply due to the fact that the multi-reflected signals cannot "reinforce" the transmitted signal in the same manner
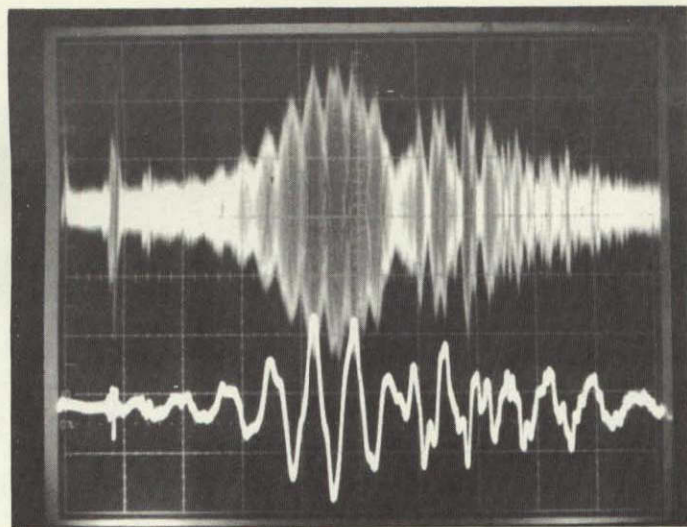
TEST CONDITIONS

A VERT: RECEIVED   50 MV/DIV

B VERT: MIXER OUTPUT 0.5 V/DIV

HORIZ: 0.2 MS/DIV

$fm \approx 1.06 \times 10^{8}$ HZ/S

(RF HORIZONTAL $\approx$ 21.2 KHZ/DIV)

2.5 MHZ CRYSTALS ON 0.125 INCH
STAINLESS STEEL MOUNTS.

6.4 KHZ IF

TEST CONDITIONS

A VERT: 1ST IF STAGE   1 V/DIV
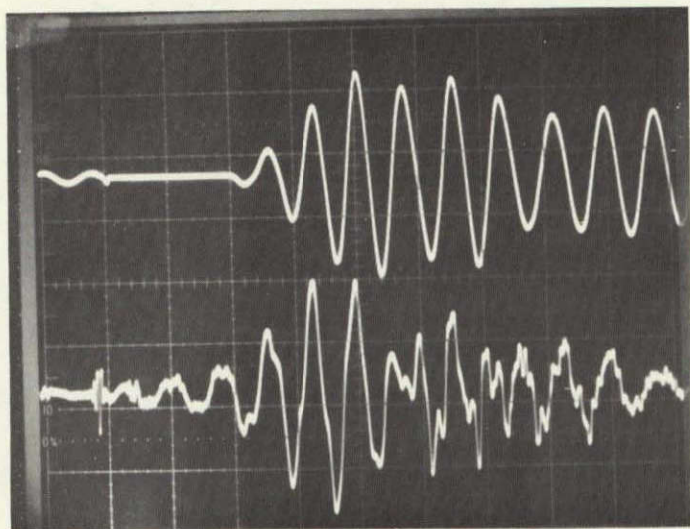
B VERT: MIXER   0.5 V/DIV

HORIZ: 0.2 MS/DIV

$fm \approx 1.06 \times 10^{8}$ HZ/S

(RF HORIZONTAL $\approx$ 21.2 KHZ/DIV)

2.5 MHZ CRYSTALS ON 0.125 INCH
STAINLESS STEEL MOUNTS.

6.4 KHZ IF

Figure 6-2.   Comparative Data for Received RF, Mixer Output, and First Stage IF
Filter Output, for System Using Teledyne VFC.
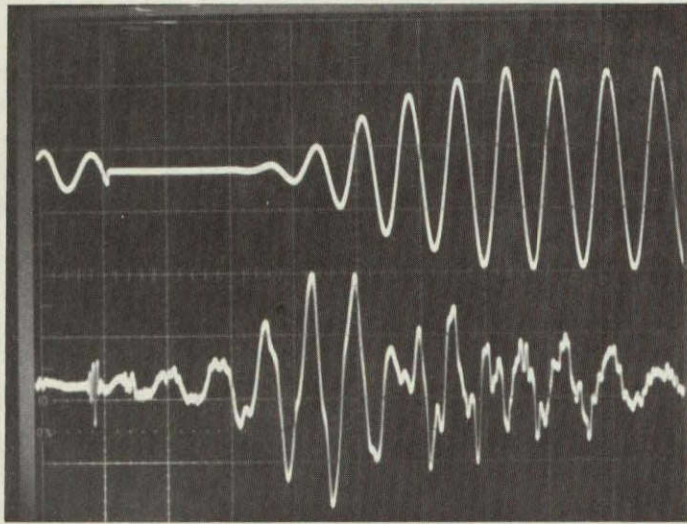
TEST CONDITIONS

A VERT: 2ND STAGE IF   1 V/DIV

B VERT: MIXER OUTPUT 0.5 V/DIV

HORIZ: 0.2 MS/DIV

$fm \approx 1.06 \times 10^8$ Hz/S

2.5 MHz CRYSTALS ON 0.125 INCH STAINLESS STEEL MOUNTS.

6.4 KHz IF

TEST CONDITIONS

A VERT: 3RD STAGE IF   1 V/DIV

B VERT: MIXER OUTPUT 0.5 V/DIV

HORIZ: 0.2 MS/DIV

$fm \approx 1.06 \times 10^8$ Hz/S

2.5 MHz CRYSTALS ON 0.125 INCH STAINLESS STEEL MOUNTS.

6.4 KHz IF

Figure 6-3.   Comparative Data for Mixer Output and Second and Third IF Filter
              Stage Outputs, for System Using Teledyne VFC.

TEST CONDITIONS

A VERT: 4TH STAGE IF   1 V/DIV

B VERT: MIXER OUTPUT, 0.5 V/DIV

HORIZ: 0.2 MS/DIV

$fm \approx 1.06 \times 10^{8}$ MHz/SEC

2.5 MHz CRYSTALS ON 0.125 INCH
STAINLESS STEEL MOUNTS.

6.4 KHz IF

NOTE: COMPARE TO FIGURES 6-2
        AND 6-3.

TEST CONDITIONS

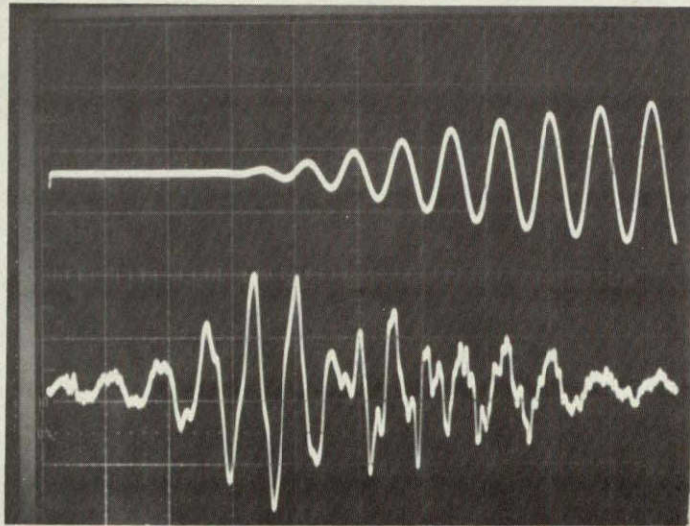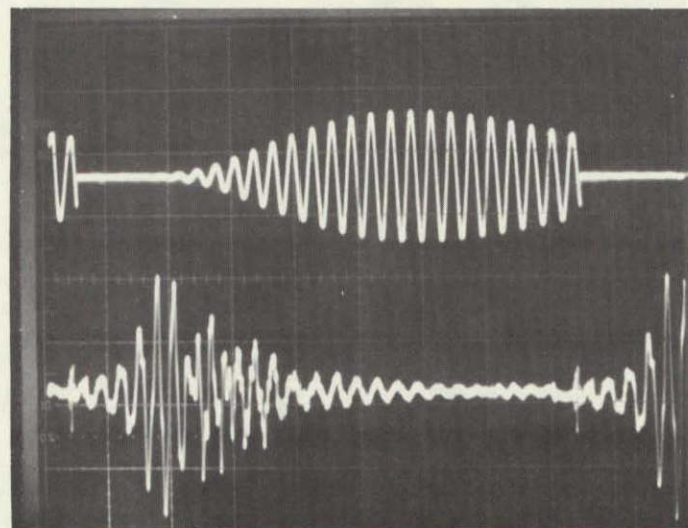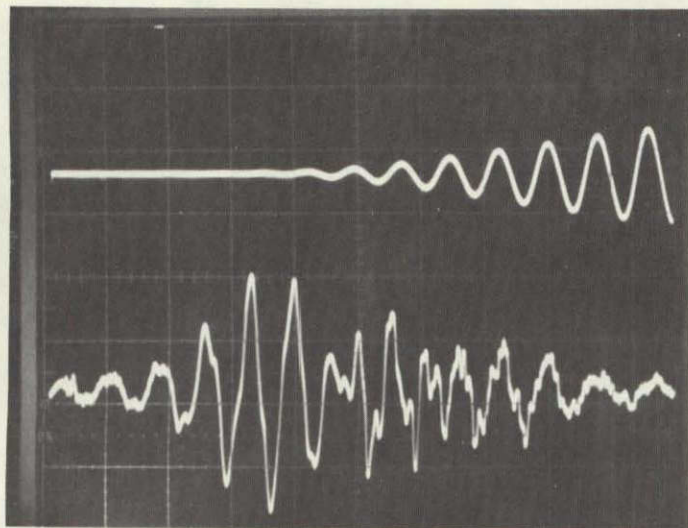A VERT: 4TH STAGE IF   1 V/DIV

B VERT: MIXER OUTPUT, 0.5 V/DIV

HORIZ: 0.5 MS/DIV

$fm \approx 1.06 \times 10^{8}$ MHz/SEC

2.5 MHz CRYSTALS ON 0.125 INCH
STAINLESS STEEL MOUNTS.

6.4 KHz IF
(FULL T/R HALF-CYCLE PLUS END OF
PRECEEDING AND BEGINNING OF
SUCCEEDING HALF-CYCLES)

Figure 6-4.   Comparative Data for Mixer Output and Fourth IF Filter Stage Output for System
              Using Teledyne VFC.

they do for a steady (or slowly swept) transmitted signal. Each rein-
forcement of the direct signal (one pass) by a double, reflected signal
(three passes) occurs at a frequency which is $2f_{IF}$ lower.

The Scarpa transducers were examined in a similar fashion. It was found that
they also provided a received RF which was amplitude modulated. The basic per-
formance was not significantly different from that of the Beckman design using
0.125-inch-thick stainless-steel mounts.

It was concluded that it would be necessary to generate a broadband transducer
design. A broader resonance reduces the rate of phase shift with frequency,
which reduces the IF phase shift. The usual approach to making a broadband
transducer is to load the backside of the crystal to prevent multiple reflec-
tions within the crystal, which are the cause of resonance. It also appeared
desirable to investigate the effects of impedance matching the transducers to
the water to improve the ratio of transmitted to reflected power. The modu-
lation of the received RF at the IF frequency due to multiple reflections
should be reduced by both impedance matching the transducers to the load, and
by back-loading the crystals. The analytical and design work discussed in the
following section was initiated for these reasons.

7A   ACOUSTIC IMPEDANCE MATCHING CONSIDERATIONS

The generally accepted equations describing the transmission and reflection of acoustic waves (longitudinal) at an interface of two materials are those employed in transmission line theory. They also describe optical reflection and transmission, with proper use of the analogs. In the case of acoustic waves, the acoustic impedance is defined as the product of the density and the acoustic velocity (longitudinal, in the case of interest) in the medium. The commonly used symbol for the acoustic impedance is ρ_C, in agreement with the notation employed thus far in this report. The acoustic impedance is generally expressed in complex notation, as is electrical impedance.

The plot of FIGURE 7-1 is a convenient means of estimating the fractions of an acoustic signal (power) that are reflected and transmitted as a function of the ratio of the acoustic impedances of the materials forming the interface. The following are relevant equations for the fractions of the power reflected and transmitted:

$$\frac{P_R}{P_{in}} = \left(\frac{Z_L/Z_t - 1}{Z_L/Z_t + 1}\right)^2 \quad \text{for the fraction of power reflected} \tag{12A}$$

$$\frac{P_t}{P_{in}} = \frac{4Z_L/Z_t}{\left(Z_L/Z_t + 1\right)^2} \quad \text{for the fraction of sound transmitted.} \tag{12B}$$

The impedance of the medium in which the sound is initially propagating is Z_t and that into which it is traveling has impedance Z_L. The acoustic power is proportional to the amplitude (pressure) squared. The reflected amplitude fraction is as follows:

$$\frac{A_r}{A_{in}} = \frac{Z_L/Z_t - 1}{Z_L/Z_t + 1} \tag{12C}$$

The reflected signal exhibits a phase reversal, therefore, when the sonic wave is traveling from a material of higher to one of lower acoustic impedance.

The concept of impedance matching may be explained by consideration of the following equation in complex variable notation:

$$Z_{in} = Z_m \frac{Z_L \cos G + jZ_m \sin G}{Z_m \cos G + jZ_L \sin G} \tag{12D}$$
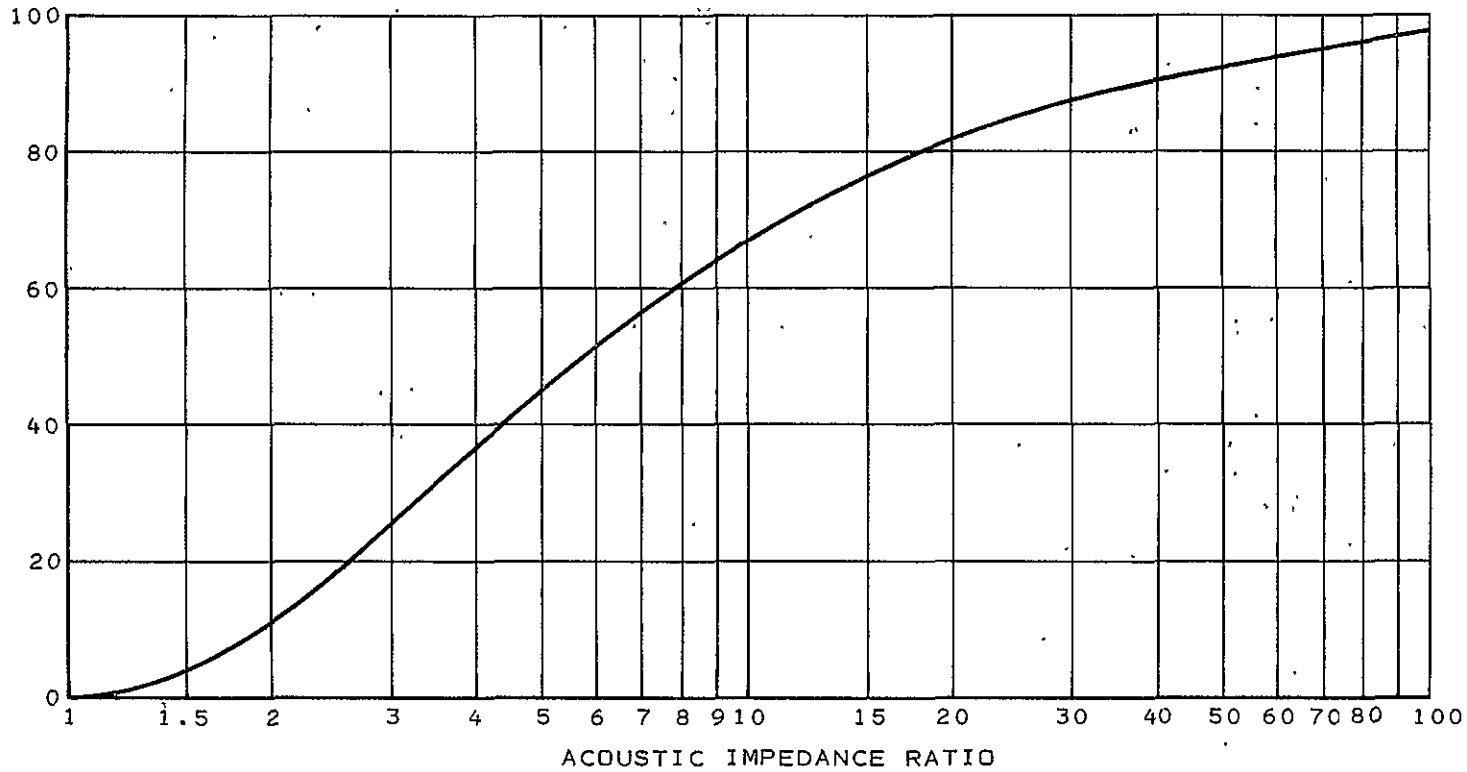
RELATIVE
REFLECTION, %

ACOUSTIC IMPEDANCE RATIO

Figure 7-1. Plot of Fraction of Power Reflected at an Inteface of Materials of Different
Acoustic Impedance as a Function of the Impedance Ratio.

In this equation,

Z_{in} = the input impedance as viewed from outside a layer of material having an impedance of Z_m and thickness d;

Z_L = the impedance of a load on the opposite side of the plate having impedance Z_m;

$G = 2\pi d/\lambda$, in which d is the thickness of the matching plate having impedance Z_m;

λ = the wavelength of the sound in the plate of impedance Z_m;

j = the square root of minus one.

The phase shifts that occur at interfaces are accounted for by this complex impedance. Several marked simplifications arise when certain conditions are met. These special cases are as follows:

$$\text{IF}\, Z_L = Z_m; \quad Z_{in} = Z_m \text{ for any value of } d/\lambda \tag{12E}$$

This is a rare case in acoustics, in which the coupling material impedance matches the load impedance.

$$\text{IF}\, d = \lambda/2,\ 3\lambda/2,\ \text{etc};\quad \sin G = 0,\ \cos G = 1,\ \text{and}\ Z_{in} = Z_L \tag{12F}$$

This is the case for "half-wave plates" which are essentially transparent at the frequency for which they are exactly odd multiples of one-half-wave thick.

$$\text{IF}\, d \ll \lambda;\quad \sin \frac{2\pi d}{\lambda} \approx G \approx 0,\ \cos G \approx 1,\ \text{and}\ Z_{in} \approx Z_L \tag{12G}$$

This is the case for thin layers of any material. They are essentially transparent over a fairly broad band. Crystal bonding layers are in this category, ideally, and do not significantly affect the performance of a transducer. Best results are obtained with a Z_m which is the geometric mean of Z_{in} and Z_L. A thin film of air, for example, transmits with little phase shift, but it transmits only a very small fraction of the energy.

$$\text{IF}\, d = \lambda/4,\ 3\lambda/4,\ \text{etc};\quad \sin G = \pm 1,\ \cos G = 0,\ \text{and}\ Z_i = Z_m^2/Z_L \tag{12H}$$

This is the case for "quarter-wave plates," which are also called "impedance transformers," because they alter the apparent input impedance of the load. In particular, if the load is to be matched to a transducer of impedance Z_t, the apparent input impedance is made equal to that of the transducer by making Z_m the geometric mass of Z_t and Z_L, which is:

$$Z_m = \sqrt{Z_t Z_L},\ \text{for matching } Z_t \text{ to } Z_L \tag{12I}$$

Unfortunately, the available materials provide a very limited choice of impedances for matching layers. For the NIGS application, $Z_t = 20.4$ (lead metaniobate) and $Z_L = 1.5$ (water) kilogram $m^{-2}s^{-1}$. The ideal value for Z_m would be 5.5. No material (much less a compatible material) has this desired impedance. In such cases, it is sometimes possible to use two (or more) quarter-wave layers to achieve an acceptable match with available materials. In the RCS application, 305L stainless steel is the preferred material, but it has an impedance (about 47) that is higher than that of either the crystal or water, further complicating the situation. Aluminum alloys apparently can also be compatible with MMH and N_2O_4 when properly treated, although aluminum is less desirable than 305 stainless steel. Aluminum and its alloys happen to have an impedance (17) close to that of lead metaniobate (20.4) which means that aluminum alloy mounts should provide significantly better signals than stainless-steel mounts. From FIGURE 7-1, only about 0.8% of the power (9% of the amplitude) will be reflected at an aluminum interface. For a stainless-steel interface, about 16% of the power (39% of the amplitude) will be reflected. From the liquid side, for water, the aluminum interface would result in 70% power reflection against 88% for the stainless steel. The corresponding amplitude reflections are 83% and 94%, respectively, for aluminum and stainless steel.

At the liquid interface, Teflon is the only compatible material having a useful acoustic impedance (3). A Teflon outer jacket could also make incompatible intermediate layers acceptable. For water testing, Lucite and polystyrene have useful properties, and they are easier to bond than is Teflon. Recognizing that Teflon could be used for a flight model if impedance matching should prove to be justified, the least expensive approach was selected. It was decided that Lucite and/or polystyrene would be utilized for water testing to determine the benefits of impedance matching.

The apparent input impedance for two quarter-wave layers may be computed using Equation (12H) twice. The general case relationship derived in this manner, for two layers having impedances of Z_1 and Z_2 which are to match a "first" impedance, Z_f to a "last" impedance, Z_L is:

$$\frac{Z_1}{Z_2} = \left(\frac{Z_f}{Z_L}\right)^{1/2} \text{ for two quarter-wave layers.} \tag{12J}$$

This relationship does not specify which layer has impedance Z_1 and which has Z_2. Best results are obtained when the impedance of each successive layer is the geometric mean of the two on either side of it. An increase in impedance followed by a decrease for succeeding impedances is not desirable. Since the impedance of stainless steel is higher than that of the desirable crystals, it is not the best interface.

One approach to reducing the undesirable features of stainless steel is to make it one-half-wave thick. At the nominal sonic frequency it is, then, transparent. The frequency band over which it is satisfactorily transparent is only half as wide as the band for which quarter-wave plates provide satisfactory

matching, but it could be a worthwhile compromise. Examples are shown in FIGURE 7-2 for Keramos, Inc., K-81 crystals (lead metaniobate) coupling into water. The apparent input impedance from each substance into the next differs in the two directions. The half-wave-thick materials are shown as two successive quarter-wave thicknesses to stress the basic undesirable effects of having a poor impedance match in the system. The apparent input impedances are calculated using Equation (12H), starting with the load and adjacent layer as Z_L and Z_m, respectively. The calculated value of Z_{in} is then used as Z_L, and the next plate as Z_m to compute the next input impedance. The disagreement in apparent impedance looking in opposite directions from each material provides a figure of merit for the matching. From the first two examples, it may be seen that magnesium is a better "impedance transformer" than aluminum for matching K-81 to polystyrene. The last two examples indicate that polystyrene is a slightly better material for matching magnesium to water than are Lucite and Teflon. The large apparent impedance between the two quarter-wave thicknesses of stainless steel (second example) is the main factor in FIGURE 7-2, indicating that one-half-wave-thick stainless steel will not be as good as aluminum of the corresponding thickness.

Another approach not shown in FIGURE 7-2, but comparable to the second example, is to use a thin section of 305L stainless steel. A thin section also approximates transparency. The second example, with the two left-hand apparent impedances (and half-wave plates) deleted, describes this transducer. Specifically, the transducers used for the Final Feasibility Demonstration Test utilized 300 series stainless-steel mounts which were 0.017-inch thick. This thickness corresponds to $\lambda/40$ at 0.75 MHz, and to $\lambda/80$ at 0.375 MHz, the two test conditions. At these frequencies, the sine terms of Equation (12D) are 0.156 and 0.078, respectively. This means that the stainless steel was not really transparent in either case, but the approximation is fair. These transducers were tested both with and without magnesium and Lucite impedance matching facings which were each $\lambda/4$ thick at 0.75 MHz. At 0.375 MHz the facings were each $\lambda/2$ thick and should have been transparent. The test results, discussed in paragraph 7E, indicated that the impedance matching was beneficial but not essential.

7B   BACK-LOADING OF CRYSTALS TO MAKE BROADBAND TRANSDUCERS

As discussed above, it was found that no usable RF signal was received when the operating frequency was off resonance. This result meant that a wide frequency sweep without phase shifts was not feasible, and that a limited frequency sweep in the region of a resonance response was required. The literature contains a great deal of information regarding both impedance matching and back-loading, but in all instances peak power output has been the major concern. Flow sensing requires only moderate power transmission, but with high fidelity. A literature search revealed much relevant, but no directly applicable, art.

Crystal resonance is caused by reinforcement of internally reflected sound waves. An undamped crystal loaded only by air (near total reflection) has a high Q, and is "narrow band." If the sonic energy reaching the rear face of the crystal can be transmitted into a perfect absorber so that it does not

K81 Z=20.46	305L 47	305L 47	Al 17.3	POLYSTYRENE 2.8	WATER 1.5

→ 57.6	→ 39	→ 57.6	→ 5.2	→ 1.5	LOOKING TO RIGHT
← 20.46	← 108	← 20.46	← 14.6	← 0.54	LOOKING TO LEFT

} APPARENT INPUT IMPEDANCES

K81 Z=20.46	305L 47	305L 47	MG 9.9	POLYSTYRENE 2.8	WATER 1.5

→ 18.8	→ 118	→ 18.8	→ 5.2	→ 1.5
← 20.46	← 108	← 20.46	← 4.8	← 1.6

SCHEMATIC

$Z_i \rightarrow$ | Z_m | Z_L |

EQUATION: $Z_i = \dfrac{1}{Z_L} Z_m^2$

K81 Z=20.46	Al 17.3	Al 17.3	Mg 9.9	LUCITE (OR TEFLON) 3.0	WATER 1.5

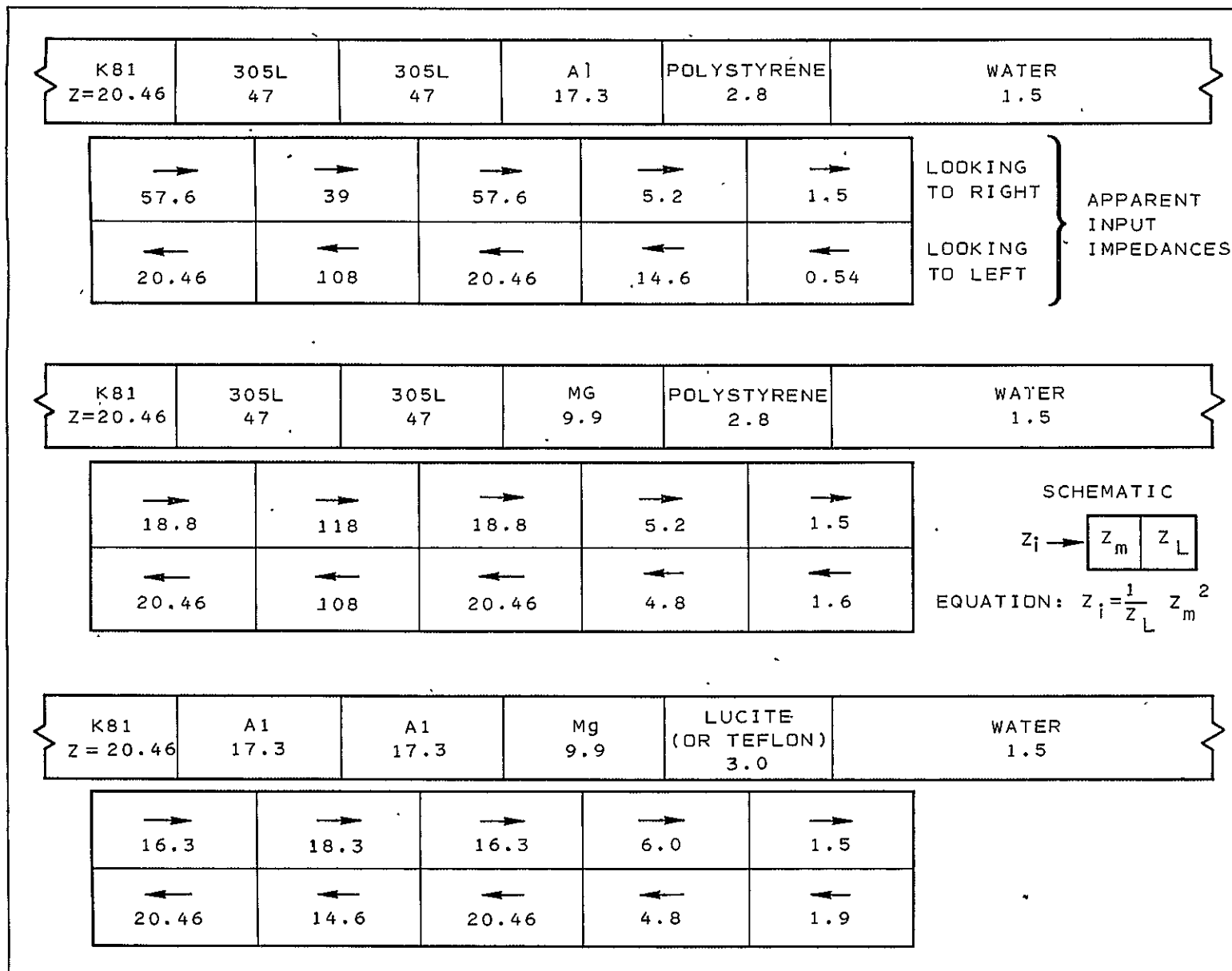|				
→ 16.3	→ 18.3	→ 16.3	→ 6.0	→ 1.5
← 20.46	← 14.6	← 20.46	← 4.8	← 1.9

Figure 7-2. Example Calculations of Impedances for Various Matching Layers.

reflect back, the Q will be lowered and the transducer will be "broadband."
The resonance is essentially destroyed if no internal reflection, or "compound"
reflection from the mounting structure surfaces, is allowed. The back-loading
material must match the impedance of the crystal, and must absorb and/or other-
wise prevent reflection of the energy leaving the crystal back to the crystal.

Plastics and elastomers filled with tungsten powder have been widely used for
back-loading. The impedance of the mixture can be controlled by control of the
tungsten powder loading. The tungsten powder disperses and absorbs the energy.
This mixed material, therefore, provides a means of both impedance matching and
of absorbing the transmitted energy. Stacks of alternate half-wave layers of
tungsten-filled plastics (and elastomers) and metal plates, having an effective
acoustic impedance matching the crystal employed, have been reported in the
literature. These structures cannot, however, be truly broadband since their
thicknesses are one-half-wave only at a specified frequency. Furthermore,
relatively close control of the impedance of the tungsten mixture is required
to achieve overall impedance matching. The conical structure described below
avoids this problem, and is truly broadband.

An aluminum cone, shown in FIGURE 7-3, was designed for back-loading. As pre-
viously noted, 99.2% of the power can be transmitted into aluminum from K-81
ceramic crystals. The cone was bonded directly to the back side of the crystal
with silver-filled conductive epoxy. The inner and outer walls were cones of
different angles. The apex of the inner wall cone was formed about 0.127 cm
(0.05 inch) from the flat surface which was bonded to the crystal. Most of the
energy entered the aluminum, and was then repeatedly reflected between the non-
parallel conical walls. The cone was filled with 100 mesh tungsten powder/
epoxy mixture in the ratio of about 1:1 by volume. No attempt was made to mea-
sure the impedance of this mixture. It could vary between about 8.5 and 34,
and still provide an impedance ratio of 1/2 to 2 with aluminum. From FIGURE
7-1, this factor of 1/2 to 2 would cause less than 12% reflection (power) at
each collision with the aluminum-tungsten/epoxy interface. Three collisions
should transmit all but 0.17% of the power into the absorbent material.
Strictly speaking, these figures are for normal incidence, but for angles sig-
nificantly less than the critical angle, the approximation is good. Furthermore,
the converging conical-wall configuration results in an increasing angle of inci-
dence for successive reflections, and the angles were chosen to provide more than
three collisions before the power could reflect back to the crystal.

The design of FIGURE 7-3 was generated by elementary geometrical optics ray-
tracing techniques for a first test of performance. It would be possible to
use computer ray tracing techniques to generate an optimum design. It would
also be possible to use an ideal tungsten/epoxy mixture to match the aluminum
alloy. For purposes of this contract, adequate performance was achieved with
the first attempt (FIGURE 7-3). Minor changes in cone angle were made before
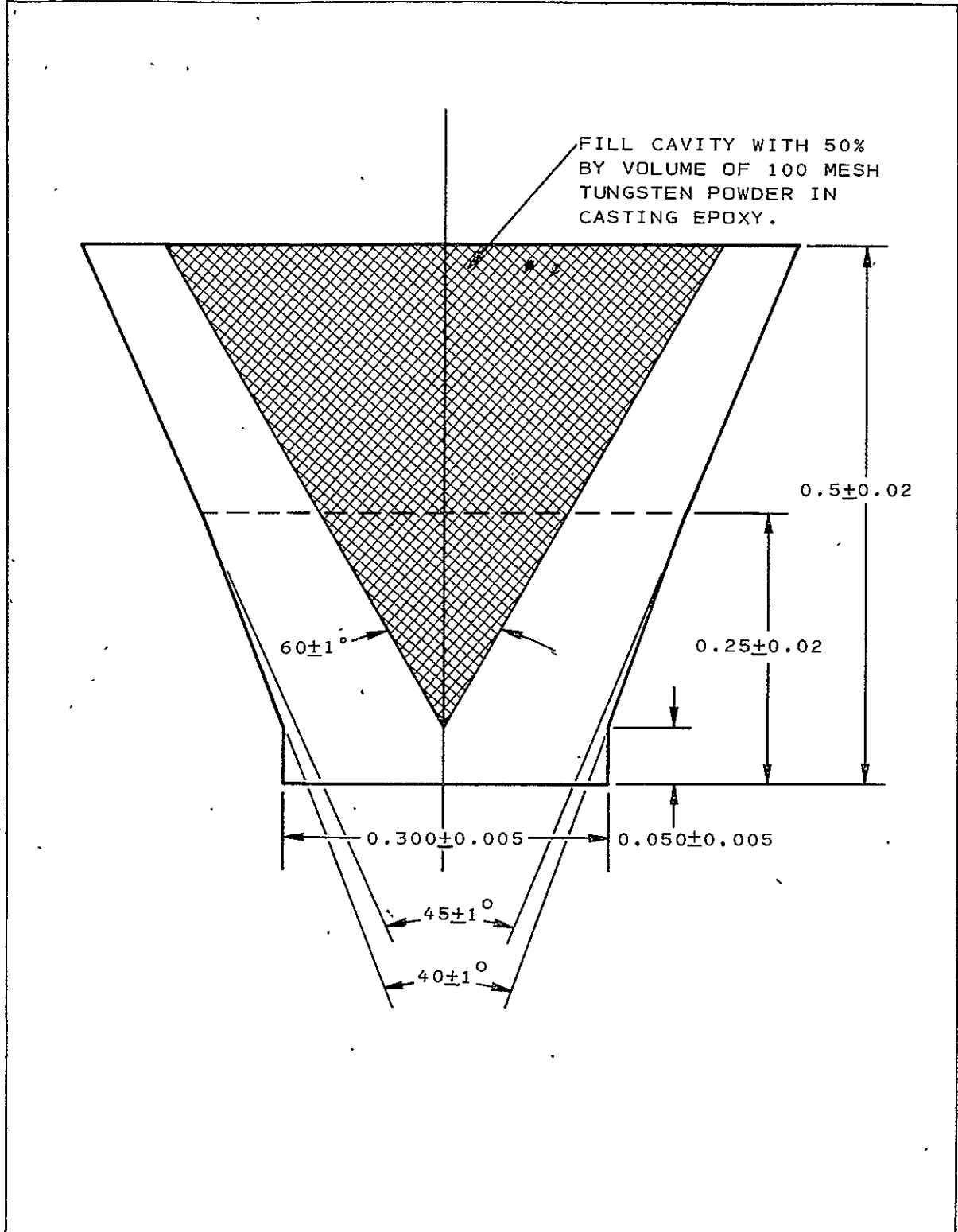fabrication of subsequent parts, but no significant change in performance was
seen.

Figure 7-3.   Design of Back-Loading Cone for K-81 Piezo Ceramic Crystals.

The oscilloscope photographs of FIGURES 7-4 through 7-6 illustrate the effects
of back-loading and, to some extent, of impedance matching the front face of
the transducers. A change from 2.5 MHz to 0.75 MHz crystals was made to re-
duce the phase shift sensitivity of the system. The photos of FIGURE 7-4
through 7-6 were obtained during fabrication of one of the pair of transducers
used in Final Design Feasibility Testing. The top photo of FIGURE 7-4 shows
the voltage across 47 ohms connected in series with the transducer and a Wave-
tek signal generator (50-ohm output impedance). The frequency sweep (hori-
zontal) is 0.5 to 1.0 MHz. The nominal crystal resonance is 0.75 MHz. The
vertical input (the voltage across the 47-ohm load) has a sensitivity of 20 mV/
division. This sensitivity corresponds to 0.42 mA/division for current through
the transducer. The peak-to-peak current varied from about 17 to 30 mA. The
applied voltage was 12 V peak-to-peak, which means that the minimum transducer
impedance was about 400 ohms and the maximum value was about 700 ohms. The
parallel impedance due to stray wiring capacitance was probably greater than
4000 ohms.

The vertical and horizontal scales, and the transmitted voltage, were constant
for all of the photographs of FIGURES 7-4 through 7-6. The lower picture of
FIGURE 7-4 shows the effect of loading the transducer to a Formica bench top,
using water (plus a detergent) to eliminate the possibility of an air film at
the interface. The effect on the fine-structure of the current versus the fre-
quency is apparent. There was also a slight shift toward a higher frequency of
several resonance features. The photographs of FIGURE 7-5 were obtained after
bonding an unfilled aluminum alloy cone to the rear face of the 0.75 MHz crys-
tal. The top and bottom photographs, respectively, were obtained with and with-
out loading to the work bench. The empty cone alters the resonance pattern
(variation of current with frequency) noticeably, and loading to the bench elim-
inates fine-structure as it did before the cone was added. Finally, FIGURE 7-6
illustrates the marked reduction in current variations with frequency when the
aluminum cone was filled with the absorbent mixture. The top and bottom photo-
graphs were, respectively, with and without loading to the bench top. Loading
to the bench top reduced the residual fine-structure, as it did under the
previous test conditions. The linear increase of transducer current with fre-
quency is about that to be expected for a capacitive load plus a series resistor
(47 ohms plus the 50-ohm output impedance of the generator). The residual devi-
ations from a linear current increase with frequency are indicative of the
residual resonances of the compound transducer, which appear to be much broader
than the resonances of the unloaded crystal.

As noted above, the photographs of FIGURES 7-4 through 7-6 were obtained when
assembling one of the pair of transducers used in Final Design Feasibility
Testing. Corresponding photographs taken at corresponding steps in the fabri-
cation of the matching transducer were virtually identical.
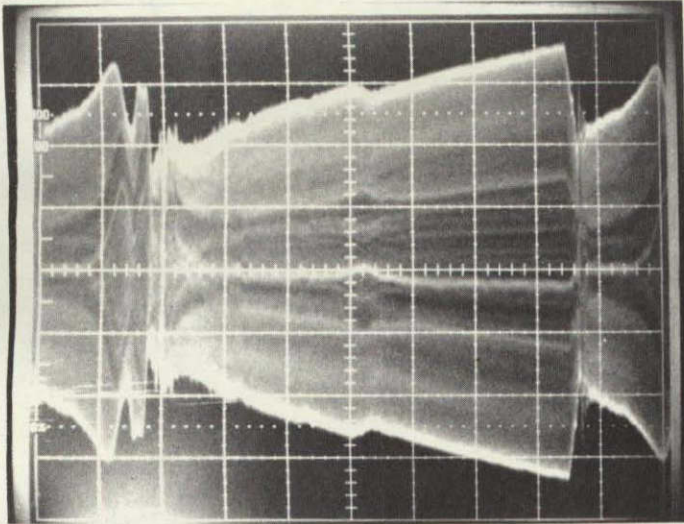
TEST CONDITIONS

A VERT: ACROSS LOAD,   20 MV/DIV

HORIZ: 0.5 MS/DIV

LOAD: 47 OHMS

0.5 TO 1.0 MHz SWEEP, USING
WAVETEK FM SIGNAL GENERATOR,
12 V P-P AMPLITUDE.

TEST CONDITIONS

A VERT: ACROSS LOAD,   20 MV/DIV

HORIZ: 0.5 MS/DIV

LOAD: 47 OHMS

0.5 TO 1.0 MHz SWEEP, USING
WAVETEK FM SIGNAL GENERATOR
WITH 12 V P-P AMPLITUDE.
TRANSDUCER LOADED TO BENCH TOP
WITH WATER FILM.

Figure 7-4.   Comparative Data for One of Pair of Final Transducers, Using
0.75 MHz Crystal Mounted to 0.017 Inch Stainless Steel.

TEST CONDITIONS

A VERT: ACROSS LOAD,   20 MV/DIV

HORIZ: 0.5 MS/DIV

LOAD: 47 OHMS

0.5 TO 1.0 MHz SWEEP, USING
WAVETEK FM SIGNAL GENERATOR,
WITH 12 V P-P AMPLITUDE.

TEST CONDITIONS

A VERT: ACROSS LOAD   20 MV/DIV

HORIZ: 0.5 MS/DIV

LOAD: 47 OHMS

0.5 TO 1.0 MHz SWEEP, USING
WAVETEK FM SIGNAL GENERATOR,
WITH 12 V P-P AMPLITUDE.
TRANSDUCER LOADED TO BENCH TOP
WITH WATER FILM.

Figure 7-5.   Comparative Data for One of Pair of Final Transducers, Obtained After Back Loading With
Unfilled Aluminum Cone.

TEST CONDITIONS

A VERT: ACROSS LOAD,   20 MV/DIV

HORIZ: 0.5 MS/DIV

LOAD: 47 OHMS

0.5 TO 1.0 MHz SWEEP, USING
WAVETEK FM SIGNAL GENERATOR,
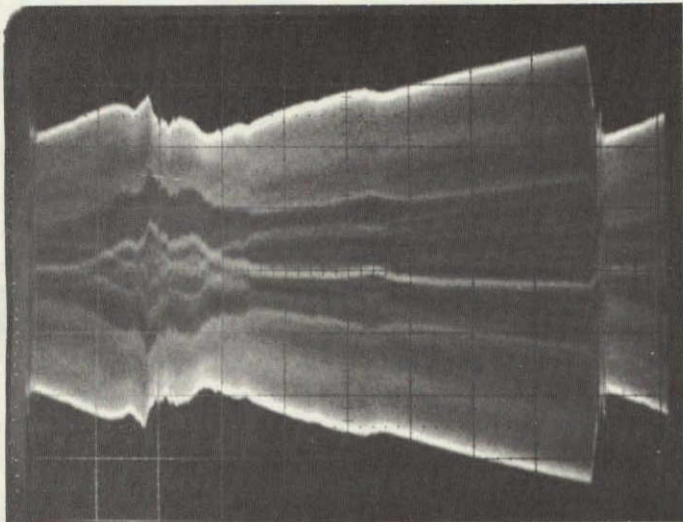WITH 12 V P-P AMPLITUDE.
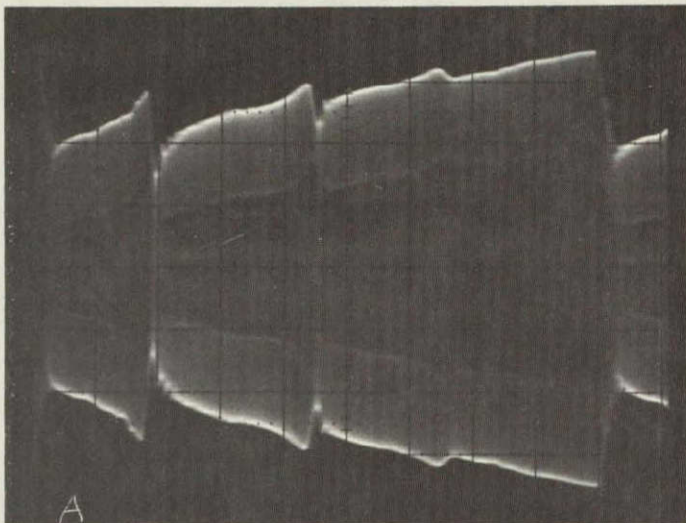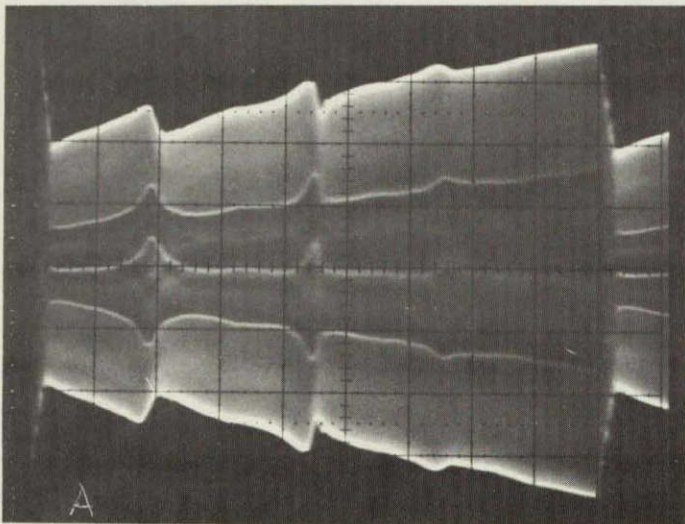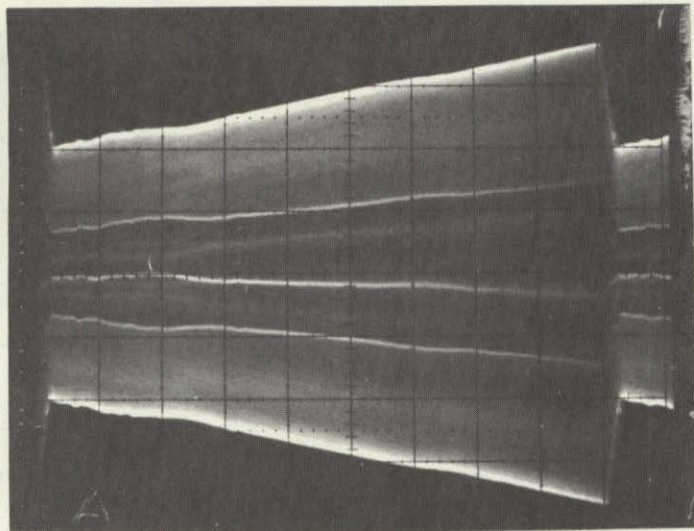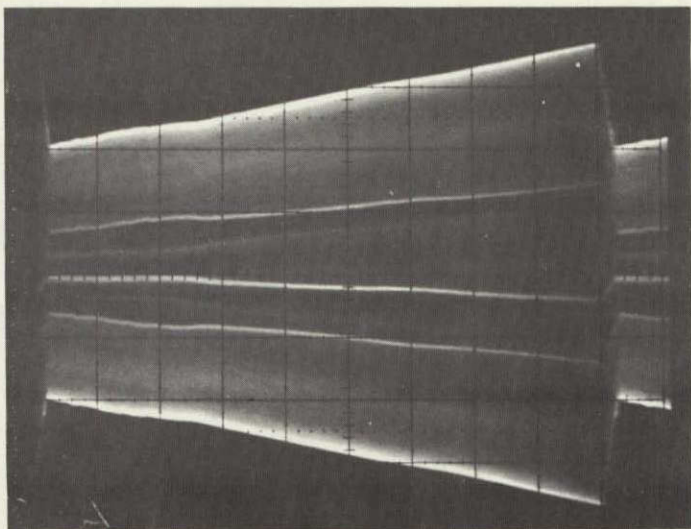
TEST CONDITIONS

A VERT: ACROSS LOAD,   20 MV/DIV

HORIZ: 0.5 MS/DIV

LOAD: 47 OHMS

0.5 TO 1.0 MHz SWEEP, USING
WAVETEK FM SIGNAL GENERATOR,
WITH 12 V P-P AMPLITUDE.
TRANSDUCER LOADED TO BENCH TOP
WITH WATER FILM.

Figure 7-6.   Comparative Data for One of Pair of Final Transducers, Obtained After Filling Aluminum
Cone With Tungsten Powder/Epoxy Mixture.

The uniformity of successive IF periods was found to be improved for both stainless-steel and aluminum transducers by impedance matching to the load. For stainless-steel transducers, the received RF signal _appeared_ to be reduced by about ten-fold, while the uniformity of the IF periods improved about two-fold. It was concluded that the higher "signal" originally received was basically noise due to multiple reflections between the transducer faces. Impedance matching water to the transducers may have improved the true signal-to-noise ratio by up to a factor of twenty. It was impractical to increase the drive voltage a factor of ten (due to T/R switch voltage ratings) in the time available to prove this point. However, a factor of two increase in drive voltage (made with aluminum mounted 2.5 MHz crystals and 6.4 kHz IF) made the full sensitivity to flow available after 3 IF cycles instead of 6 cycles, and also reduced the noise in the output noticeably.

In a later set of tests with different pairs of aluminum transducers, it was found that the IF periods varied $\pm$ 1.6 percent with no impedance matching (2.5 MHz crystals, 6.4 kHz IF, λ/2 Al thickness). With impedance matching, a second set provided less than $\pm$ 0.2% variation of IF period (0.75 MHz crystals, 2 kHz IF, λ/2 Al thickness). The apparent improvement of eight-fold due to impedance matching in this test is believed to be valid, even though two different sets of transducers were involved. The improvement for aluminum was generally better than for stainless-steel transducers, probably because the aluminum inherently provides a wider bandpass capability with K-81 crystals.

Unfortunately, the improvement in IF cycle uniformity due to back-loading alone was not reliably determined, due to an inability to repeat experiments with a given pair of transducers. Once aluminum cones were bonded to crystals they could not be removed non-destructively. The best, although somewhat indirect, evidence is that the typical unloaded 2.5 MHz crystal provided an output IF period which varied $\pm$ 2.2% of the average value from one end of the ramp to the other. (This corresponds to $\pm$ 300% of the period difference for full-scale flow, but because of symmetry of the two IF signals for transmission in opposite directions, the net shift in zero-flow output for successive groups of two or three IF cycles scanned across the ramp was only a few percent of full scale.)

The effect with flow (up to 20% of full scale) was more pronounced. With back-loading, the flow sensitivity for successive pairs of IF cycles was a smooth function, even when it was not constant. Prior to back-loading the crystals, up to two polarity reversals of the output were found in the plot of flow sensitivity _versus_ the position in time of the IF cycles being measured. The cycle sensitivity scan was done using two cycles for the period measurement, scanned by varying the time delay of the IF Counter Enable Pulse across the ramp.

Another factor which made it difficult to establish the benefits of back-loading _per se_ is that the electronics were "debugged" in a parallel effort while the back-loading and impedance matching schemes were being developed.

Consequently, an unknown portion of the improvement in performance was due to improvements in the electronics. Time and cost constraints did not permit a truly systematic study to isolate the magnitudes of the various effects. Impedance matching to water, on the other hand, was a reversible operation, and repeated tests with given transducer pairs clearly established that the uniformity of the IF cycles was improved at least two-fold at zero flow, and more than two-fold at 20% of full-scale flow.

After stating the above qualifications, back-loading of the crystals is believed to have improved the uniformity of response to flow for successive IF cycles by up to a factor of ten. It was still necessary to use a frequency sweep in the vicinity of a transducer resonance for drive voltages of 17 V peak-to-peak or less. It is not known whether off-resonance operation would be possible with higher drive voltages, but it is considered probable that operation at 100 V rms would greatly improve the signal-to-noise ratio. However, the lead metaniobate crystals exhibit many small "narrow-band" resonances, located at random frequencies, which might introduce spurious phase shifts which could compromise the performance even at higher drive voltages by limiting the width of the usable frequency sweep.

The predicted benefits of aluminum mounts compared to stainless-steel mounts are shown in FIGURES 7-7 and 7-8. Both figures were obtained at zero flow, with 2.5 MHz crystals and 6.4 kHz IF filters. The transducers of FIGURE 7-7 were $\lambda/2$ thick (0.05 inch) stainless steel, while those of FIGURE 7-8 were $\lambda/2$ thick 0.127 cm (0.050 inch) aluminum alloy with a 0.005 cm (0.002-inch) thick nickel plating. Both were impedance matched to water with $\lambda/4$ thick layers of magnesium and polystyrene, epoxy bonded. The top photographs of each figure indicate the transmitted voltage (upper trace) and the received voltage (lower trace). The circuit made provisions for removing the transmitter power during T/R switching, which accounts for the time of zero amplitude at the beginning of each ramp. The transmitted signal amplitude decreased with frequency becaue it was low-pass filtered to reduce the harmonic content. The important difference in the upper photographs of FIGURES 7-7 and 7-8 is that the aluminum mount provides a relatively broadband received RF. The stainless-steel mounts provide a received RF which exhibits a narrow-band resonance at the low frequency end (steel thickness less than $\lambda/2$), a narrow band of "broadband quality" near the center of the frequency sweep (steel thickness near $\lambda/2$), and another minor narrow-band resonance at higher frequencies (for which the steel thickness was greater than $\lambda/2$). The impedance matching layers also limit the bandpass, but they were identical for the two sets of transducers. The superior coupling and broadband behavior with aluminum mounts is apparent.

The lower photographs of FIGURES 7-7 and 7-8 show the fourth stage IF filter output (upper trace) and the mixer output (lower trace). The four IF filter inputs were clamped (electrically shorted) for a time greater than that required for T/R switching, resulting in zero IF amplitude for the first millisecond of the traces (two horizontal divisions). The mixer output exhibits a high frequency component at the beginning of the ramp cycle, which is generated by transients in the transmitted and received mixer inputs as the
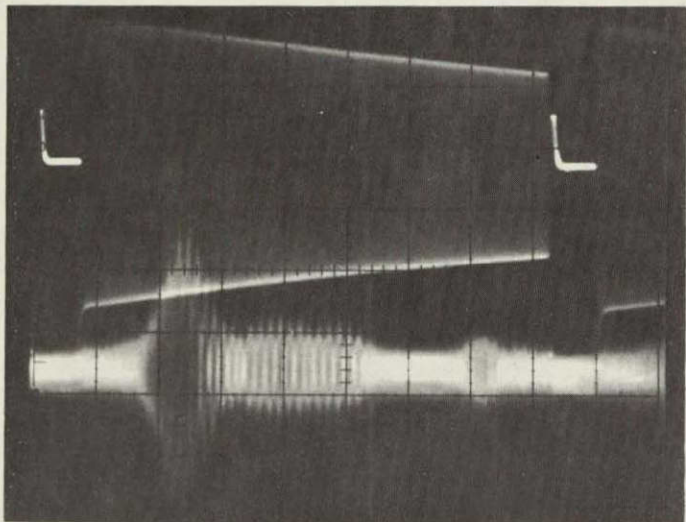
TEST CONDITIONS

A VERT: TRANSMITTED,   2 V/DIV

B VERT: RECEIVED,   20 MV/DIV

HORIZ: 0.5 MS/DIV

TEST CONDITIONS

A VERT: 4TH STAGE IF, 0.5 V/DIV

B VERT: MIXER OUTPUT, 50 MV/DIV

HORIZ: 0.5 MS/DIV

NOTE: MIXER POST AMPLIFIER
        GAIN IS UNKNOWN.

Figure 7-7.   *Oscilloscope Photographs of Basic Signals With 6.4 kHz IF, 2.5 MHz Crystals, 0.050 Inch Thick Stainless Steel Mounts, and With Impedance Matching Facings.*

TEST CONDITIONS

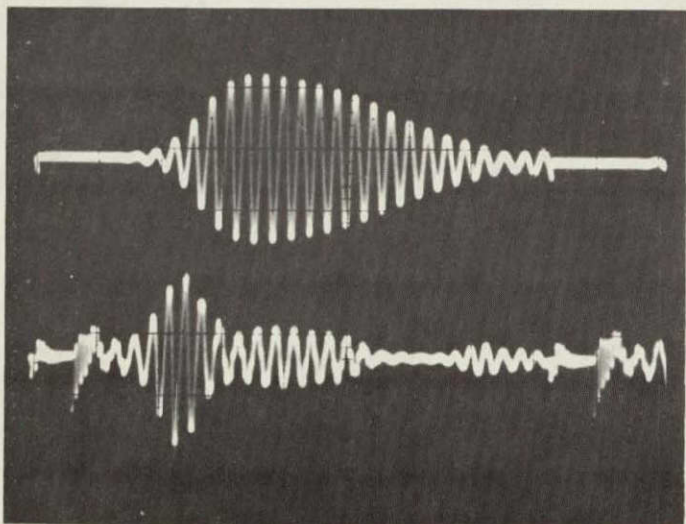A VERT: TRANSMITTED, 5V/DIV

B VERT: RECEIVED, 20 MV/DIV

HORIZ: 0.5 MS/DIV

TEST CONDITIONS

A VERT: 4TH STAGE IF   2V/DIV

B VERT: MIXER OUTPUT 0.5V/DIV

HORIZ: 0.5 MS/DIV

NOTE: MIXER POST AMPLIFIER
        GAIN IS UNKNOWN

Figure 7-8.   Oscilloscope Photographs of Basic Signals With 6.4 kHz IF, 2.5 MHz Crystals, 0.050
Inch Thick Aluminum Alloy Mounts, and With Impedance Matching Facings.

power is removed from the T/R switches. This noise is eliminated by clamping the IF filter input until the transients are over and the desired mixer output of the new ramp cycle is available. The mixer output for the aluminum transducer is obviously superior to that for the stainless steel, and closely approximates the "idealized system" which was analyzed in the study phase. In particular, if the transmitted signal amplitude had been constant the mixer output would have been very nearly constant. There is a discernible "step" in the received RF amplitude (upper photograph of FIGURE 7-8) which is more apparent in the amplitude of the mixer output (lower photograph). This amplitude change is not apparent in the fourth stage IF output (upper trace of lower photograph) because its response rate is limited. There was, however, a discernible change in IF period corresponding to the amplitude step. The amplitude step was probably due to a residual narrow-band transducer resonance, which caused a phase shift of the transmitted and received RF signals with frequency. Sweeping the frequency above this point only, and below the next residual resonance (not shown), should provide excellent IF quality.

Comparison of FIGURE 7-9 to FIGURE 7-7 reveals that impedance matching of the stainless-steel transducers to the load (water) does improve the quality of the received RF (and IF) in the region for which the stainless steel is $\lambda/2$ and the magnesium and polystyrene plates are $\lambda/4$ thick. The improvement is apparent, but the frequency band over which it is effective is still very small compared to that for aluminum shown in FIGURE 7-8.

The fundamental superiority of aluminum over stainless steel for use with K-81 crystals arises from the near equality of the acoustic impedances, which greatly reduces both the percentage of energy reflected, and the phase shift of the energy reflected, at the aluminum/K-81 interface. The thickness of the aluminum is less critical with frequency variations for this reason. FIGURE 7-10 shows the behavior of the aluminum transducers at a frequency below the first resonance for which the aluminum, magnesium, and polystyrene thicknesses were not optimum. The received RF and IF are of reduced quality (compared to FIGURE 7-8), but they compare favorably to those of the stainless-steel transducers when operating in their optimum frequency band.

7E   RESULTS OF PRELIMINARY FLOW TESTS OF IMPROVED TRANSDUCERS
      AT BECKMAN

In the interests of economy the Beckman flow test capability was restricted to the flow available from the two-inch pipe water main at the point where it entered the building. The water pressure was observed to randomly fluctuate between 40 and 80 psig during all tests. The maximum flow rate attainable was about 3.6 kg/s (8 lb/s or 66 gpm), corresponding to about 25% of the required full-scale flow rate of 16 kg/s (35 lb/s). Independent flow rate monitoring was limited to the range of zero to 1 kg/s (2.2 lb/s or 16 gpm) with an available Fisher-Porter (float in tapered tube) flowmeter. The specified minimum flow rate for the RCS application is 1 kg/s (2.2 lb/s) which is nearly full scale for the Fisher-Porter meter. The response in the zero to 1 kg/s (2.2 lb/s) range was of considerable theoretical

TEST CONDITIONS

A VERT: TRANSMITTED   20 MV/DIV

B VERT: RECEIVED   2 V/DIV

HORIZ: 0.5 MS/DIV

NOTE: COMPARE THESE PHOTOGRAPHS TO
      THOSE SHOWN IN FIGURE 7-7.
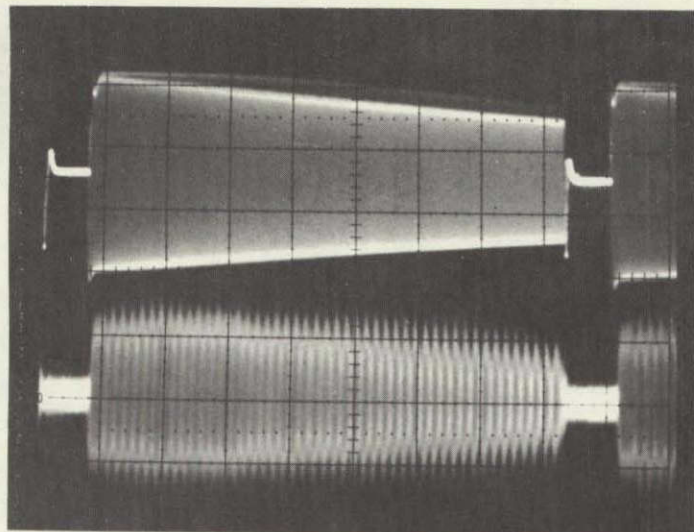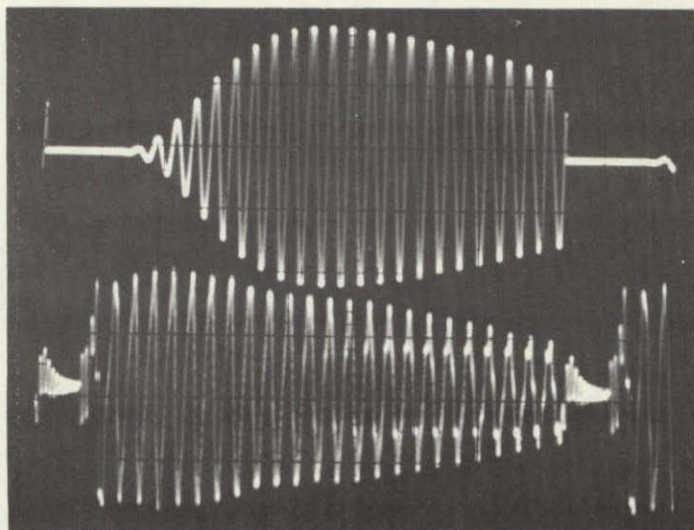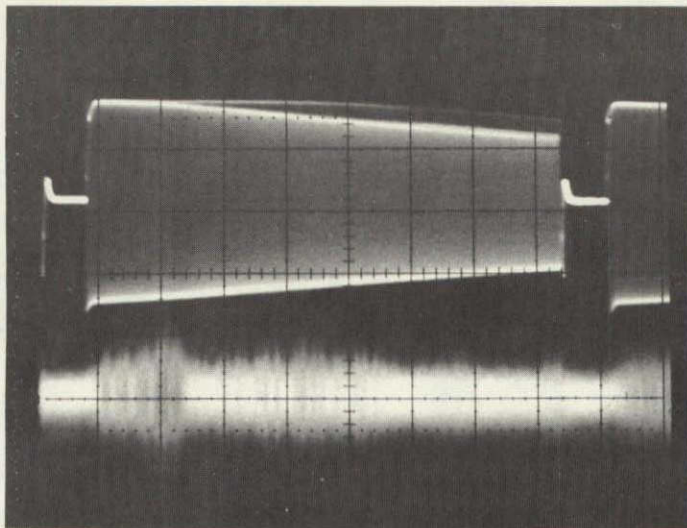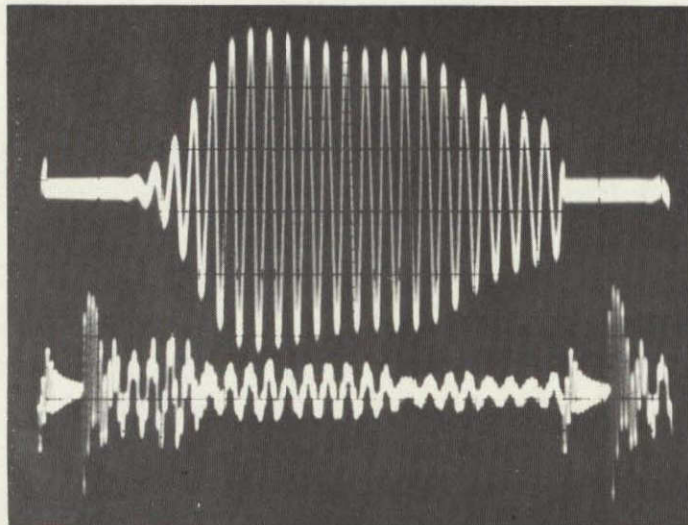
TEST CONDITIONS

A VERT: 4TH STAGE IF   0.5 V/DIV

B VERT: MIXER OUTPUT   0.2 V/DIV

HORIZ: 0.5 MS/DIV

NOTE: MIXER POST AMPLIFIER
       GAIN SETTING IS UNKNOWN.

Figure 7-9.   Oscilloscope Photographs of Basic Signals With 6.4 kHz IF, 2.5 MHz Crystals, 0.050
Inch Thick Stainless Steel Mounts, and Without Impedance Matching Facings.
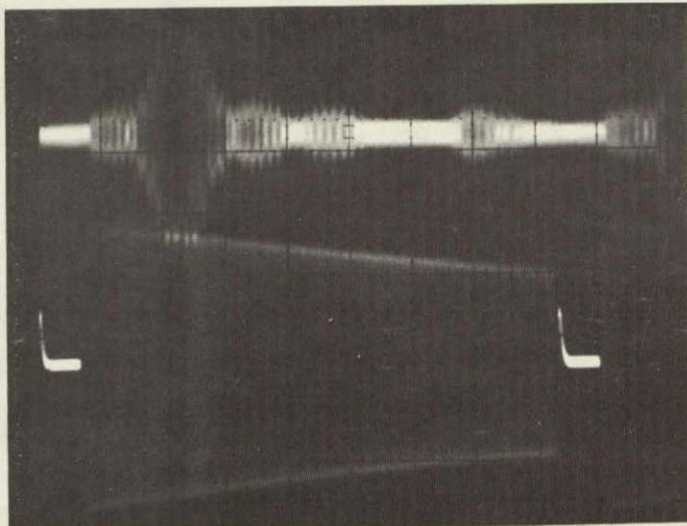
TEST CONDITIONS

A VERT: TRANSMITTED,   5 V/DIV

B VERT: RECEIVED,   5 MV/DIV

HORIZ: 0.5 MS/DIV

NOTE: COMPARE THESE PHOTOGRAPHS TO
      THOSE SHOWN IN FIGURE 7-8.
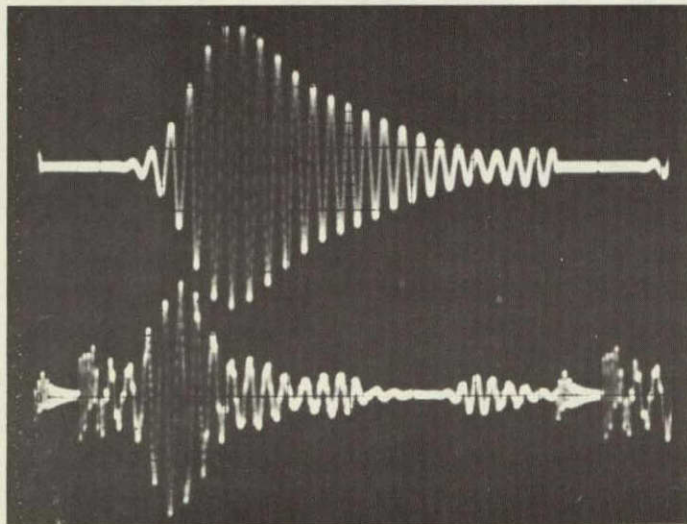
TEST CONDITIONS

A VERT: 4TH STAGE IF 0.2 V/DIV

B VERT: MIXER OUTPUT 0.1 V/DIV

HORIZ: 0.5 MS/DIV

NOTE; MIXER POST AMPLIFIER
       GAIN SETTING IS UNKNOWN.

Figure 7-10.   Oscilloscope Photographs of Basic Signals With 6.4 kHz IF, 2.5 MHz Crystals, 0.050
          Inch Thick Aluminum Alloy Mounts, With Impedance Matching Facings, and With Frequency
          Sweep at Resolance Lower Than Design Nominal.

interest, because the analysis performed in the study phase of the contract had assumed that the sonic technique would average the flow profile with adequate accuracy to permit accurate measurement in the laminar, transition, and turbulent flow ranges. The calculated Reynolds number indicated turbulent flow should occur well below a flow rate of 0.5 kg/s (1.1 lb/s). The curve of FIGURE 7-11 was obtained with the stainless-steel transducers 0.127 cm (0.05-inch) thick (2.5 MHz crystals, and 6.4 kHz IF) used in obtaining the zero flow rate data of FIGURES 7-7 and 7-9. They were operated in the period-mode, using the ten best IF cycles (1.56 ms measurement time) and T_r = 4.2 milliseconds. FIGURE 7-11 indicates the excellent linearity of the system through the flow transition region. The Fisher-Porter average reading (abscissa) is plotted against the reciprocal of the time of integration required to produce an 8.16 volt change in the integrator output (ordinate), which is proportional to the average flow rate. The time was read from an analog recorder chart, between automatic resettings of the integrator (which occurred after an 8.16 V swing). Within the limits of readability of the Fisher-Porter flowmeter and the time of integration (probably about $\pm$ 2% total), the output was linear. This result is in agreement with the performance of the Beckman respiratory flowmeter, and was later confirmed in the Final Design Feasibility Tests performed at NASA-JSC. A small negative zero offset, causing the integrator to drift at no-flow, is apparent. It will be necessary in a flight model to impose a minimum-value test upon the digital flow rate data to prevent large total mass errors (over very long time periods) due to such slight zero offsets. If, for example, the digital counts at the end of a T/R ramp cycle represent less than $\pm$ 0.5% of full scale, they will not be transferred to the summing register.

It should be noted that some of the tests discussed above were performed with transducers using 2.5 MHz and others with 0.75 MHz crystals. Flow testing of both stainless-steel and aluminum transducers using 2.5 MHz crystals with back-loading, and with and without impedance matching, demonstrated that the uniformity of the IF cycle periods was too poor to permit operation in the period-mode without regard to which cycles were being monitored. Therefore, the major theoretical benefit of the period mode of operation was not achievable. It was necessary to limit the phase shift sensitivity to prevent shifts of more than $\pm \pi$ radians due to full-scale flow. Under these circumstances the phase mode was expected to provide better performance than the period mode. This was confirmed in later tests. New transducers were fabricated with 0.75 MHz crystals, instead of 2.5 MHz, to lower the phase shift sensitivity by a factor of three. The reduction to f_o = 0.75 MHz was expected to permit full-scale operation without experiencing a phase shift greater than $\pm \pi$ radians. However, subsequent tests at the NASA-JSC Thermochemical Test Area indicated that a reduction to 0.3 to 0.4 MHz (crystals) would have avoided most of the operational problems encountered in the Final Design Feasibility Tests, and would have provided superior performance. This factor is discussed further in Sections 8 and 9.
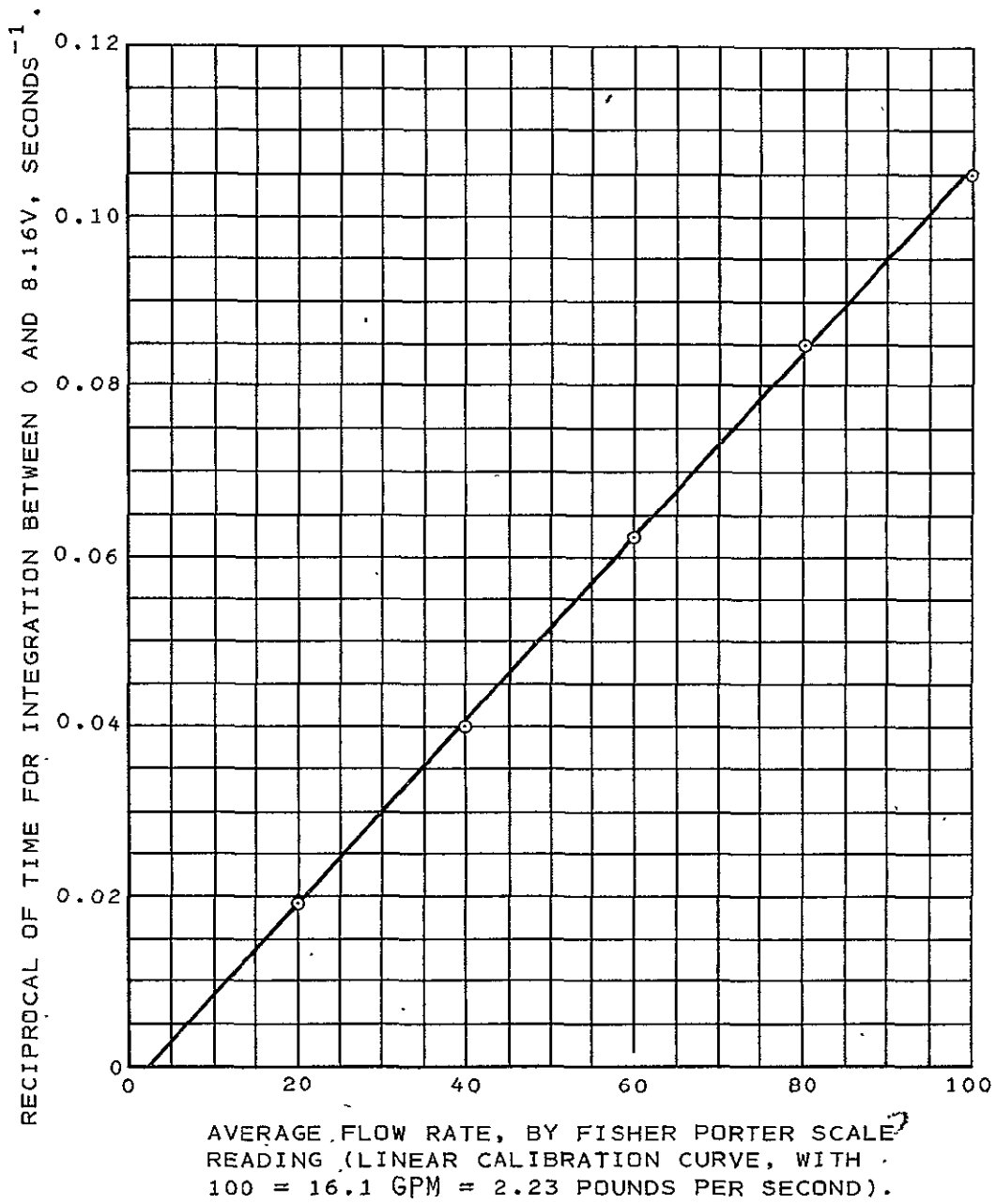
Figure 7-11. *Linearity of Prototype Gaging System Integrator*
Output Versus Flowrate in the Zero to 2.2 lb/S Range.

DESIGN FEASIBILITY TESTING

8A   GENERAL COMMENTS

The Tentative Test Plan For The Nonintrusive Flowmeter, Document No. TTA-TP-2P230, dated 1-26-76, was prepared by NASA-JSC-TTA personnel. A summary of the tests which were planned, with comments regarding the degree to which the tests were actually performed, is given in Section 2 of this report, "Design Feasibility Test Outline and Results." The tentative plan was modified slightly during the course of the tests. In particular, the sequence of the tests was varied at the discretion of the Test Engineer to ensure that the tests less likely to destroy the previously untested Prototype NIGS were performed first. For example, the system linearity was checked against a catch-weigh system to the maximum flow rate attainable with 80 psig pressure before increasing the pressure, in steps, to 250 psig. As another example, it was hoped that test time would permit determination of the effect of a turbulence generator inserted into the plumbing ahead of the NIGS flow cell, but this test was waived in the interests of obtaining more basic data.

These tests were performed in two one-week periods at the NASA-JSC Thermochemical Test Area previously indicated with contractor participation. The first week of testing, in April 1976, was the first time the prototype gaging system had been exposed to greater than 25% of full scale flow, to pressures greater than 80 psig, and to rapidly pulsed flows. Although five pairs of transducers of different configurations were available for testing, it was decided that obtaining the most complete set of data for one pair of transducers within the available test time would provide maximum essential information. Although preliminary tests had verified that aluminum transducers provided superior performance, it was decided that the best stainless-steel transducers should be tested. The reasoning was simply that the performance of the least complicated (lowest development cost for flight hardware) transducer was of greatest interest.

8B   FIRST TEST AT JSC (APRIL, 1976)

The transducers tested in April may be characterized as follows:

- Transducer Mounts — 300 series stainless steel, 0.4-inch-diameter counter bore from the inside to 0.017-inch thickness for mounting 0.25-inch-diameter crystal (thickness of stainless steel = $\lambda/40$ at 0.75 MHz).

- Crystals — 0.75 MHz fundamental resonance, K-81 material (Keramos, Inc.). Pair were frequency matched to within 1% by vendor.

- Back-loading - Aluminum alloy cone, filled with tungsten powder/epoxy mixture. (Rear cavity was not potted to facilitate repair in case of accidental damage.)

- Impedance Matching — Magnesium 0.070-inch-thick and Lucite 0.030-inch-thick (each $\lambda/4$-thick at 0.75 MHz, and $\lambda/2$-thick at 0.375 MHz). Layers were bonded together and to stainless steel with epoxy cement.

These transducers were also tested in the final tests in May 1976, the only change being removal of the impedance matching facings. This change was in keeping with the philosophy of determining the performance of the least complicated transducer, since this would provide the best indication of development costs for a flight system. Welding the transducers tested in May into the flow cell will make the nonintrusive gaging system equivalent to the basic plumbing of the OMS and RCS fuel and oxidant supply systems.

The balance of the system tested in April may be characterized as follows:

- Period mode of operation only, monitoring either 2, 3, or 5 cycles by selector switches.

- Ramp time, T_r, of either 4.2 or 8.4 ms, but only 8.4 ms was tested to ensure that the DCA minicomputer could update the digital display.

- 2 kHz IF filter, ±300 Hz at -3dB point.

- No control of phase shift for C_o (thermal) changes.

- f_o adjustable. About 0.75 MHz and 0.38 MHz were tested.

- f_m adjustable. The nominal value of 33.3 MHz was trimmed to obtain maximum IF signal for the nominal value of f_o chosen.

- Analog and digital display outputs for flow rate and total mass were provided. (They required calibration for various selectable operating conditions.)

The major positive results of the April tests were:

- Successful proof pressure test of the flow cell structure to 375 psig (150% of nominal operating pressure of 250 psig).

- Operation of the prototype gaging system at 250 psig nominal, with severe water hammer conditions.

- Measurement of pulsed flows at (or below) the minimum specified flow rate at 5, 1, and 0.5 Hz. The sensitivity to pulsed flows was within 7% of that for steady flow at the same rate, which is within 0.5% of the full-scale flow rate. This result is discussed further in paragraph 9C, in relation to the tests performed in May.

- The system was proven to be linear in the 0 to 75 gpm (0 to 30% of full scale) range in all tests performed with f_o approximately 0.75 MHz, for which it was nonlinear above about 66% of full scale.

- The system was proven to be linear in the 15 to 250 gpm (2 to 35 lb/s, the specified range) using f_o = 0.38 MHz.

- The ability of the system to monitor bidirectional flow was demonstrated. When a large air bubble was trapped downstream of the flow cell, valve closure resulted in a damped oscillatory flow through the flow cell. Both outputs responded, and no net flow error as a result of such "ringing" was detected. The transducers were also interchanged electrically for one test, verifying equal but opposite response to flow.

- When linear to full scale (f_o = 0.38 MHz) the deviations from the mean sensitivity value (across the flow rate range) measured against a catch-weigh system of high precision, were within the requirement, but larger than desired, for the RCS system. However, the deviations for repeat measurements at any given flow rate were often comparable to the deviations for widely different flow rates. Unnecessary circuit temperature dependence and the difficulty of accurately timing the flow runs are believed to account for most of the error.

The major negative factors revealed by the April test may be summarized as follows:

- One or more of the circuits had an unnecessarily large thermal coefficient, causing large changes in performance (sensitivity, range of linear response, etc.) with ambient temperature.

- The circuit adjustments for establishing f_o and f_m were rather critical, and thermal effects occasionally drastically affected the adjustments. The marginal IF quality made the alignment critical.

- The phase shift due to water temperature variations (C_o) was larger than anticipated. A change of several degrees Celsius resulted in a noticeable loss of full-scale range (i.e., the flow at which one IF cycle shift occurred for the period measurement in one direction). With uniform IF cycles, this would not have been a problem.

- The output noise with flow was larger than anticipated. It was erroneously concluded that this was probably a result of flow-generated sound. This noise was generally random, and did not affect the integrator output detectably. (The May tests results proved that the noise was not flow generated, and was probably due to faulty electronics. See paragraph 9D.)

- In one test at very low flow rate, a very loud "squeal" was heard. This sound apparently <u>directly</u> <u>interfered</u> with the measurement. The flow rate output had a series of low amplitude, damped, oscillations superimposed upon the normal random noise pattern. It is doubtful that this effect would introduce a systematic error into the integrator output, but its presence suggests the desirability of further testing of any future model. (This effect was observed in only one of about 175 tests.)

● Large air bubbles passing through the flow cell caused large tran-
sients in the flow rate and integrator outputs. The integrator in a
flight model will be designed to ignore signals if greater than full-
scale flow. The large noise in indicated flow rate will be a useful
indicator of the presence of large bubbles. The effect of small
bubbles is not known. Further testing with deliberate injection of
bubbles would be worthwhile. A reduction in the IF amplitude will
almost certainly indicate their passage, because of scattering
effects.

By 29 April, it was apparent that the test transducers were incapable of meet-
ing the requirements above 40 to 50% of full-scale flow when operating with f_0
at 0.75 MHz, which was the design condition. Careful review of preliminary
test data obtained at the Beckman facility indicated that while the IF period
uniformity with zero flow was probably better at $f_0 = 0.75$ MHz, the uniformity
of response to flow was definitely better with f_0 at 0.38 MHz. Accordingly,
after semi-formal testing was completed, flow response uniformity (versus
initial cycle number) data were obtained. Analysis of the data obtained on
29 April revealed that the three very nonlinear curves obtained for two,
three, and five IF cycle measurements all normalized to the same nonlinear
curve. When the same test was repeated on the morning of 30 April, three
totally different curves were obtained. They were only slightly nonlinear
above about 150 gpm (66% of full scale), whereas all three curves obtained on
the afternoon of 29 April were badly nonlinear above 100 (or less) gpm. It
appeared, therefore, that an IF signal which did not provide uniformity of
flow response would also change its characteristic nonlinear behavior drasti-
cally with temperature. This was typical of the poor results obtained at flow
rates above 100 to 150 gpm prior to 30 April. In one case, for example, it
was found that the flow output was negative for a flow rate of 100 gpm, while
on the previous day it had appeared to be only slightly nonlinear from data
obtained at 75 and 150 gpm. All prior data obtained at flow rates of less
than about 80 gpm had been reasonably repeatable. A possible error in inter-
pretation of these observations is discussed at the conclusion of Section 5,
in connection with excessive phase shift.

The system was realigned for operation at $f_0 = 0.38$ MHz on the morning of 30
April and it was verified that flow response in the ratios 2:3:5 for two,
three, and five IF cycles, was obtained with f_0 at 0.38 MHz. This had defi-
nitely not been the case with f_0 at 0.75 MHz.

After realigning the gaging system for operation with f_0 at about 0.38 MHz to
achieve full scale linearity, excellent data were obtained on April 30. In
a fast check of several flow rates against a facility flowmeter (FM-804) the
flow sensitivity was verified to be linear and uniform for two, three, and
five IF cycles. Ten tests using five IF cycles were then made against the
facility catch-weigh system. The results are presented in TABLE 8-1 and in
FIGURES 8-1 and 8-2. FIGURE 8-1 is a plot of the cumulative mass transferred
calculated from the NIGS integrator output versus that measured by the catch-
weigh technique. The linearity and accuracy of the NIGS indicated by FIGURE

TABLE 8-1. SUMMARY OF ALL STEADY-STATE FLOW DATA OBTAINED ON 30 APRIL, USING PERIOD MODE AND WITH IMPEDANCE MATCHING FACINGS. AMBIENT TEMPERATURE WAS REASONABLY STABLE DURING THESE RUNS.

Run No.	Calculated Average Flow Rate Catch-Weigh		Transferred Mass By Catch-Weigh System	Transferred Mass By NIGS Integrator Output, Calculated	NIGS Integrator Voltage Change	Cumulative Mass Transferred (NIGS Mean SENS. = 19.311 lb/volt) Catch-Weigh System	NIGS Integrator Times Sensitivity	NIGS Integrator Error	NIGS Error, % of Total Mass
	(gpm)	(lb/s)	(lb)	(lb)	(volts dc)	(lb)	(lb)	(lb)	
41	212	29.4	440.7	440.7	22.82	440.7	440.7	0	0
42	216	30.0	449.4	462.9	23.97	890.2	903.6	+13.5	+1.5
43	160	22.2	440.0	454.2	23.52	1334.2	1357.8	+23.6	+1.8
44	162	22.5	450.7	438.8	22.72	1784.9	1796.6	+11.7	+0.7
45	106	14.7	442.2	448.2	23.21	2227.1	2244.8	+17.7	+0.8
46	109	15.1	453.6	452.3	23.42	2680.7	2697.1	+16.4	+0.6
47	54	7.5	224.9	225.2	11.66	2905.6	2922.3	+16.7	+0.6
48	16	2.2	134.9	135.6	7.02	3040.5	3057.9	+17.4	+0.6
49	16	2.2	138.3	139.2	7.21	3178.8	3197.1	+16.3	+0.6
50	13	1.8	104.6	99.8	5.17	3283.4	3296.9	+13.5	+0.4

Figure 8-1. Linearity of NIGS Integrator Versus Catch-Weigh System.
Data of 30 April, period mode, using impedance matching facings.
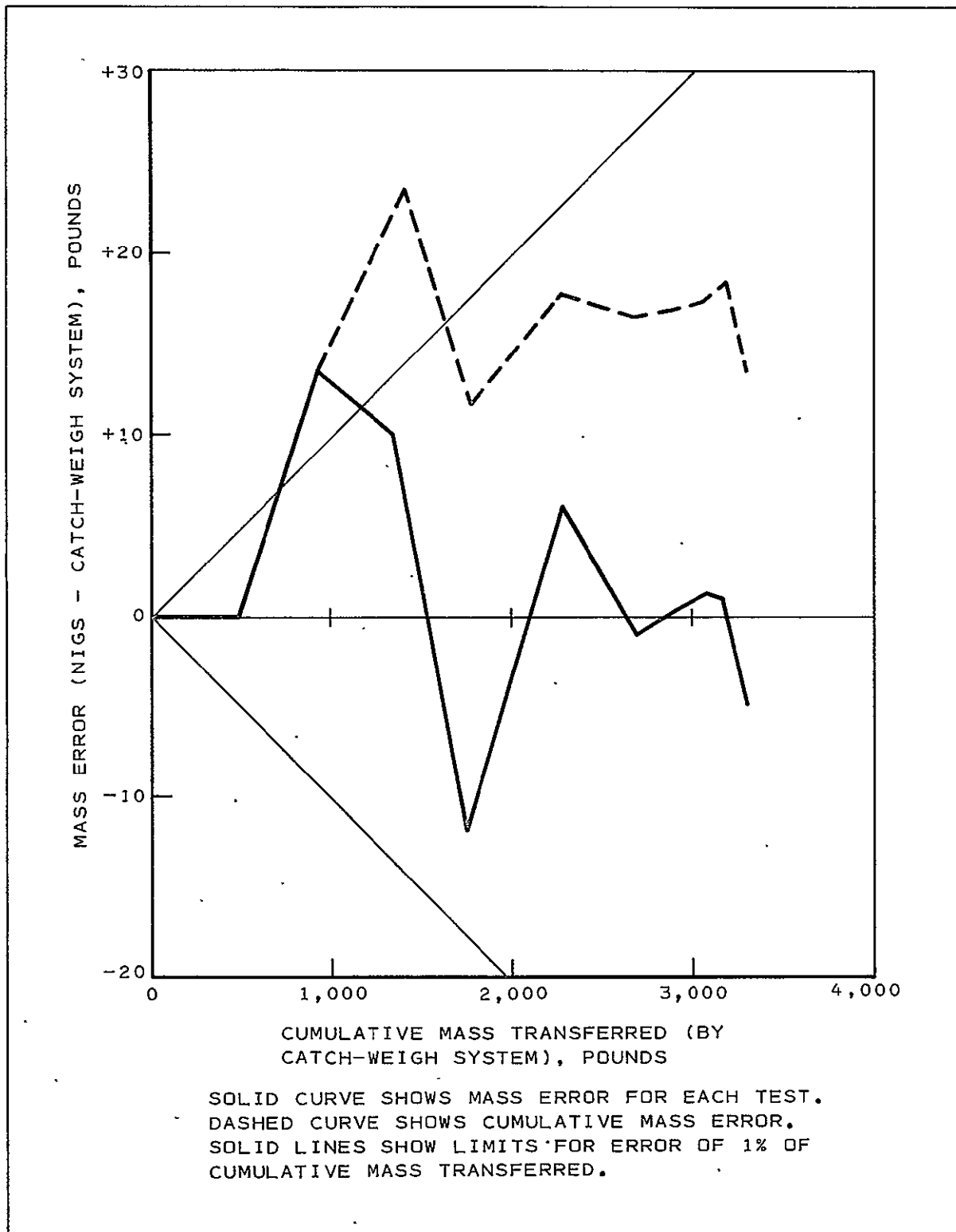
Figure 8-2. Mass Error in Pounds Versus Cumulative Mass Transferred for Period Mode Test of 30 April.

8-1 are excellent. TABLE 8-1 contains all of the original data for runs 41 through 50, made on the afternoon of April 30, 1976. The average sensitivity of the NIGS in pounds per volt (integrator output), using all ten sets of data obtained, was 19.311 pounds per volt. The table includes the mass transferred as calculated from the measured integrator voltage change in each test multiplied by the mean sensitivity (determined after the test). The cumulative mass outputs are given in the table along with the cumulative mass output error for the NIGS. The maximum error at the end of any test was 1.8% of 1334.2 pounds (run 43). The percentage of total mass error decreased from that point to 0.4% (14 pounds out of 3283 pounds) at the end of the test. There was a maximum mass error for one run (run 42) of about 13.5 pounds/450 pounds or 3%. The maximum percentage error was -4.8 pounds/105 pounds or -4.6% (run 50), which corresponds to only about -0.23% of full-scale flow-rate error. Two other flow tests at about the same flow rate had errors about one-eighth as large (runs 48 and 49), suggesting a possible error in the data taken in run 50.

The dashed curve of FIGURE 8-2 shows the cumulative mass error _versus_ the total mass transferred. This view of the data (dashed curve) makes it apparent that the 13.5 and 10.2 pound errors for runs 42 and 43 resulted in the major portion of the cumulative mass error for the balance of the runs. At the same time, the solid curve of FIGURE 8-2 suggests that the errors were probably random, and that if more tests had been performed the mean values would have been more accurate. The solid curve shows the individual mass errors for each run versus the cumulate mass.

If a tank containing 3300 pounds of water had been the supply for the ten runs on 30 April, the mass left within the tank would have been known to within better than 0.7% (which meets the basic RCS requirement) at the end of each and every run. This assertion follows from the fact that the maximum cumulative mass error was 23.5 pounds, which is about 0.7% of 3300 pounds. Furthermore, a total of 378 pounds (11.5%) was transferred at the minimum specified flow rate (about 16 gpm) which is comparable to the best estimate of the RCS requirement. However, the water and ambient temperatures were both relatively constant during this test, which prevented the marginal electronics from introducing large errors.

There may have been a major oversight in the April tests which caused similar problems in May. It is possible that the IF phase shift (not measured directly in the April tests) was twice as sensitive as it was expected to be, and if so it escaped notice. This factor may have accounted for both the gross discontinuities in the period mode output at about 50 to 66% of full scale when operating with f_0 = 0.75 MHz, and the large effect of temperature upon the maximum linear flow rate, which were attributed to other causes at the time. One test was made deliberately to determine the phase shift at full-scale flow (by viewing an oscilloscope pattern) which seemingly confirmed the calculated sensitivity. In retrospect, it appears possible that the measurement was made when there was an undesirable alignment of f_0 and/or f_m, resulting in reduced phase sensitivity by virtue of distortion in the IF cycles.

At any rate, the problem escaped attention until the May tests were conducted, at which time it appeared that the phase shift sensitivity was about twice that calculated. The derivation (see Appendix) has been checked without revealing a factor-of-two error. This means, of course, that the phase shift sensitivity may have been twice as sensitive as it should have been in the May tests, due to distortion of the IF cycles. At any rate, as shown in the May test results, (Section 9), replacement of the 0.75 MHz K-81 crystals by 0.3 to 0.4 MHz crystals would have been advantageous.

8C   REVISIONS BEFORE DELIVERY FOR FINAL TESTING

Based on the April test results, the following design revisions were made to the Prototype Nonintrusive Gaging System prior to delivery for Final Design Feasibility Testing:

- The impedance matching layers were removed from the stainless-steel transducers.

- Circuitry to provide an analog output proportional to the average IF period was added to the Flow Cell Electronics.

- The average period dc output (C-DAC output) was fed back to the f_o (starting frequency) dc set voltage to vary f_o in proportion to C_o (as measured by the average IF period). This was an open-loop feedback system, providing about a ten-fold reduction in phase shift due to the sample temperature. A closed-loop system will be required for a flight model. This mode of feedback, incidentally, cancels the speed-of-sound sensitivity from the phase mode output without additional circuitry.

- A design error in the dc voltage ramp generator used to drive the voltage-to-frequency converter (VFC) was corrected. This was the major thermal coefficient which caused problems in the April test. In effect, f_o had shifted about 0.33% per degree Celsius due to improper use of a diode in the dc ramp generator. This caused excessive IF phase shift, which mattered only because of the poor IF cycle uniformity.

- Several temperature-sensitive capacitors were replaced with capacitors having lower coefficients. Optimum components were not available within the time constraints.

- Switches, a fixed-time pulse to initiate the Phase Mode Counter Enable signal (plus associated circuitry), and a 20 MHz clock divide-by-five were added to the Flow Cell Electronics to permit operation in the phase shift mode as well as in the period mode.

- The T/R half-cycle time was changed to either 5 or 10 ms (from either 4.2 or 8.4 ms) to reduce interference from 60 and 120 cycle EMI.

● An apparent error in logic in the IF cycle counter was found. It had
  never been noticed before. It resulted from a "race" condition, under
  which the system normally functioned properly. The effect observed
  was that the Period Mode IF Cycle Counter Enable signal would sometimes
  lock-in on the negative- and sometimes on the positive-going square-
  wave IF output. This may have caused some of the gross errors in the
  April test, since it caused optimum alignment to suddenly become the
  worst possible alignment for the period mode of operation.

8D   RESULTS OF TESTING AT BECKMAN AFTER REVISION

After the circuit revisions and modifications described above were made, pre-
liminary flow test data were obtained with both $\lambda/2$-thick aluminum transducers
with impedance matching layers and with $\lambda/40$ stainless-steel transducers with-
out impedance matching. The speed-of-sound analog output (C-DAC) provided a
convenient means of directly monitoring the average IF period. In the related
figures, the average period for "n" cycles is plotted versus the number of the
first cycle of those being monitored. In prior work, the periods of succes-
sive cycles were read with an oscilloscope having a readability of about $\pm$ 0.5
μs. The C-DAC output was not directly calibrated, but with an expanded re-
corder scale the readability was considerably improved (roughly 0.1% change in
C_O per division).

The tests again demonstrated the superiority of impedance matched aluminum
transducers. FIGURE 8-3 shows the period mode sensitivity to flow versus the
number of the initial IF cycle of the set monitored for sets of two, three,
and five IF cycles. The solid curves were obtained for $\lambda/2$ aluminum ("trans-
parent") thickness and $\lambda/4$-thick magnesium and Lucite impedance matching
layers, with f_O = 0.78 MHz. Variations in flow rate due to water main pressure
variations caused fluctuations in the flow rate, making the uncertainty in the
data at least as large as the variations in sensitivity shown for initial
cycles zero through three. The arrows on the solid curves indicate the data
time sequence. The lower points shown for all three curves at initial cycle
number 2 are indicative of the variations in actual flow rate due to water
main pressure changes. The theoretical period mode sensitivity is propor-
tional to the number of cycles monitored. The sensitivity ratios for the
three solid curves are 2:3:5, in agreement with the theory for uniform IF
cycles. The points for three cycles, for initial cycles 4 through 7, were
obtained in a preceding test. They indicate a gradual loss of sensitivity
for the later cycles.

The dashed curves of FIGURE 8-3 were obtained with f_O = 0.49 MHz. The trans-
ducer resonance in this region is believed to be a "compound" resonance, for
which the combined thicknesses of the crystal and aluminum are approximately
$\lambda/2$. For f_O = 0.5 MHz, the aluminum is approaching $\lambda/4$ thickness. The
impedance match is poor because the matching plates are approaching $\lambda/8$, for
which the phase shift is about 45 degrees. The effect on the uniformity of
the IF period-mode sensitivity is drastic. The initial cycles are too sensi-
tive, although the first two (actually, a total of six cycles) are uniformly
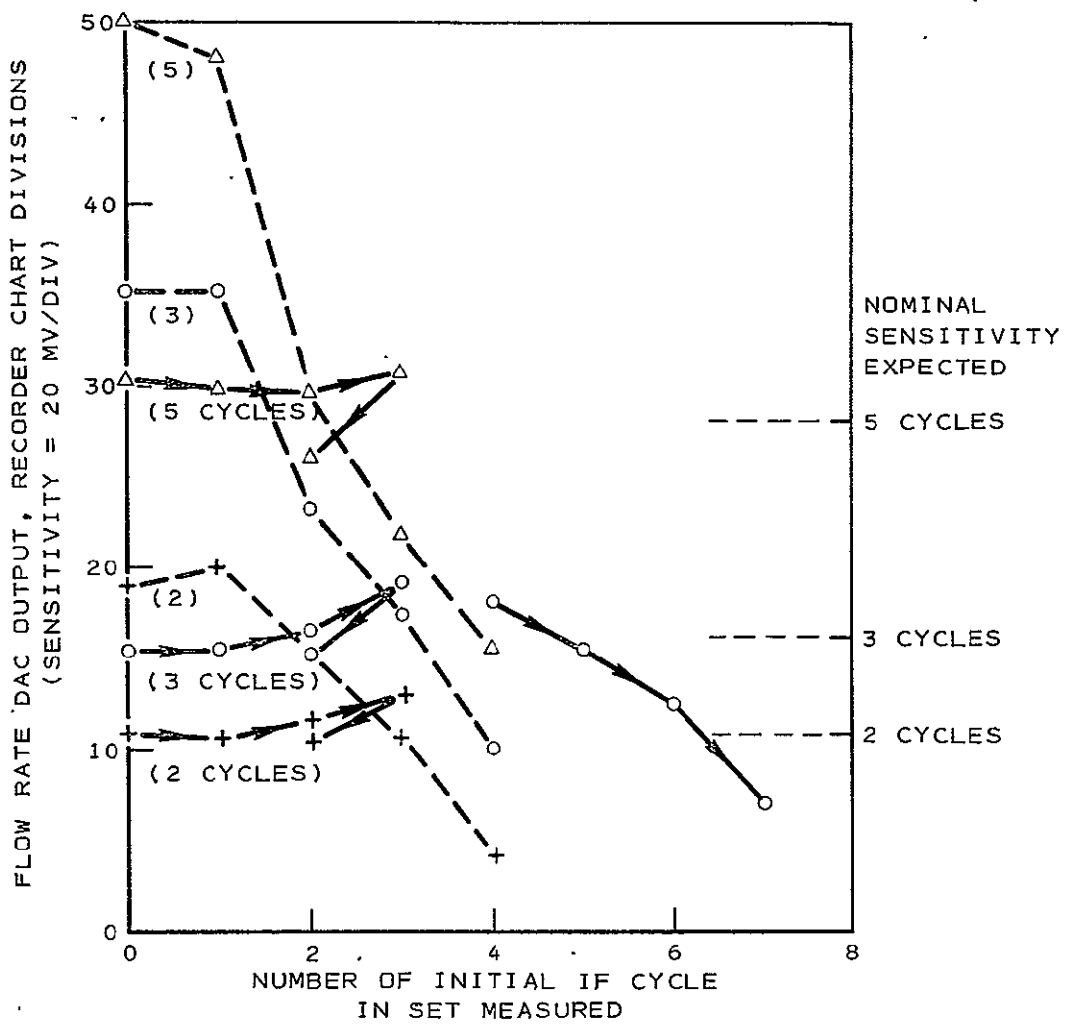
FLOW SENSITIVITY VERSUS NUMBER OF FIRST IF CYCLE
OF SET MEASURED.
FOR THREE AND FIVE CYCLES, ONE CYCLE TO THE LEFT
WAS ADDED TO THOSE MONITORED BY THE TWO CYCLE SCAN.
SOLID CURVES ARE FOR f_0 = 0.78 MHZ (IMPEDANCE
MATCHED AND ALUMINUM $\lambda/2$ THICK).
DASHED CURVES ARE FOR f_0 = 0.49 MHZ (MATCHING LAYERS
$\lambda/6.4$ AND ALUMINUM $\lambda/3,2$ THICK).

Figure 8-3. *Preliminary Test Data of 21 May, 1976, for Aluminum Transducers,*
Period-Mode, with Impedance Matching Facings.

8-11

sensitive to flow. For later cycles, the flow sensitivity decreases very rapidly toward zero. The sensitivity per IF cycle is not uniform for any set of cycles; that is, the ordinates for the three dashed curves do not stand in the ratio 2:3:5, as do those for the solid curves which were obtained at the design value of optimum f_0 for these transducers, 0.75 MHz.

The zero shift in output for cycle scan tests made at zero flow was negligible for both operating conditions. This demonstrated that the symmetry of the IF signal for successive T/R half cycles was excellent. The flow sensitivity nonuniformity must, therefore, be dependent on the rate of change of IF period with elapsed time (initial cycle number) and the degree to which flow effects dominate spurious effects in the IF signal (signal-to-noise ratio).

Unfortunately, the C-DAC output was not being recorded during the tests of the aluminum transducers described above. It is also unfortunate that the tests could not be repeated with the impedance matching plates removed. There is no direct evidence that the effect of impedance matching upon flow sensitivity at f_0 = 0.75 MHz (crystal resonance) is appreciable. The only direct evidence is that matching layers improve the IF cycle uniformity by a factor of two or more at zero flow. Since it was already decided that the thin stainless-steel transducers without impedance matching were to be used in the Final Design Feasibility Tests at NASA-JSC, and because of available test time limitations, the aluminum transducer tests were not repeated while recording the average period of the IF, or with the matching layers removed. The remaining time was devoted to testing of the stainless-steel transducers in the final test configuration.

The curves of FIGURE 8-4 were obtained with the thin stainless-steel transducers used in the Final Design Feasibility Tests in May, 1976. The solid curves were obtained with f_0 = 0.68 MHz, which provided good IF amplitude. The sensitivity was reversed for the initial cycles of the two cycle scan. The flow sensitivity was not uniform except in the 4th through 6th cycle region, and the sensitivity to flow was, according to notes taken at the time, only about half of the nominal value. The apparently low sensitivity was probably an erroneous result due to mis-reading the recorder range switch setting, because later tests performed at slightly different starting frequencies resulted in the expected flow sensitivity for cycles three through six.

The dashed curves of FIGURE 8-4 were obtained with f_0 = 0.38 MHz which is about one-half of the crystal fundamental resonance frequency. The stainless steel was only $\lambda/80$ thick at 0.38 kHz, which would make it more transparent. The reason a resonance existed at this frequency is not clear. It is probably a compound resonance involving the bonding layer, stainless steel, and crystal, and it may be dependent on cumulative phase shifts of multi-reflected signals. It is apparent from the shape of the dashed curves that no set of cycles provides either uniform flow sensitivity or the nominal flow sensitivity, except, perhaps, the five-cycle data for sets starting at cycles one and two. The corresponding two and three cycle data do not indicate

FLOW RATE OUTPUT,
DIVISIONS (20 MV/DIV)

NOMINAL
SENSITIVITY
EXPECTED

−5 CYCLES
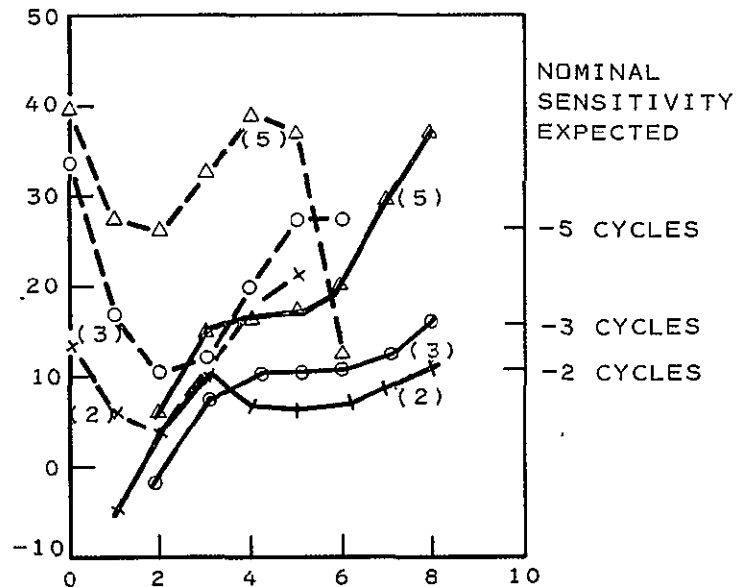
−3 CYCLES

−2 CYCLES

NUMBER OF INITIAL IF
CYCLE MEASURED FOR
2, 3, AND 5 CYCLE SCANS

A. PERIOD MODE FLOW SENSITIVITY

VARIATION OF C-DAC OUTPUT,
DIVISIONS (10 MV/DIV).
SENSITIVITY ROUGHLY 0.1%
CHANGE IN PERIOD/DIVISION
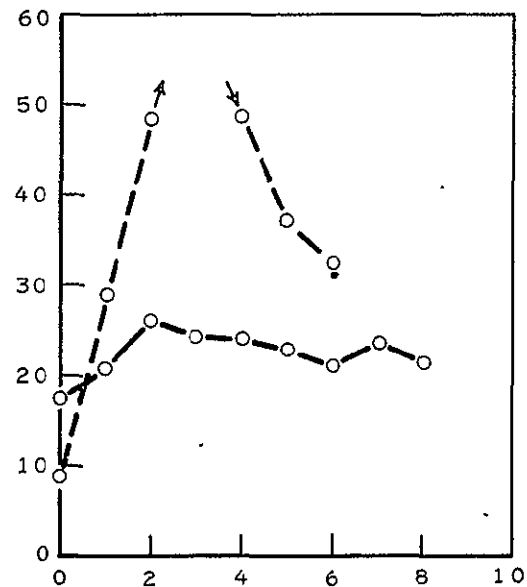
NUMBER OF INITIAL IF
CYCLE (3 CYCLE SCAN)

B. AVERAGE PERIOD FOR
THREE CYCLE SCAN

(A) PERIOD MODE FLOW SENSITIVITY AND (B) VARIATION OF AVERAGE PERIOD
(C-DAC OUTPUT) VS NUMBER OF FIRST IF CYCLE OF SET MEASURED. FOR THREE AND
FIVE CYCLE DATA OF PLOT (A), ONE CYCLE TO THE LEFT WAS ADDED TO THOSE
MONITORED BY THE TWO CYCLE SCAN. SOLID CURVES ARE FOR f_o = 0.68 MHz
(STEEL THICKNESS $\lambda/40$). DASHED CURVES ARE FOR f_o = 0.36 MHz (STEEL ·
THICKNESS $\lambda/80$) FOR WHICH THE CAUSE OF TRANSDUCER RESONANCE IS UNKNOWN.

Figure 8-4. Preliminary Test Data of 21 May, 1976, for "Thin" Stainless Steel
Transducers

uniformity of sensitivity, which means that the nominal sensitivity exhibited by the five cycle curve for cycles one and two is purely accidental. Even so, the results are better than for corresponding impedance matched (mismatched at 0.5 MHz) aluminum transducers at a roughly corresponding value of f_o, shown in the dashed curves of FIGURE 8-3. This implies that mismatched impedance matching layers were the major problem encountered with the aluminum transducers when operating at $f_o = 0.49$ MHz.

The average period variations versus initial cycle-number data, plot (b) of FIGURE 8-4, clearly indicate that operation at one-half of the fundamental frequency caused a large variation in the IF periods. However, the relatively small variation of average IF period for operation with $f_o = 0.68$ MHz (near the crystal fundamental resonance at 0.75 MHz) did not result in markedly improved flow sensitivity. Comparison of plots (a) and (b) of FIGURE 8-4 does not reveal any clear-cut correlation between IF period uniformity and flow sensitivity uniformity versus the initial IF cycle measured.

In a later series of tests f_o was shifted to 0.715 MHz (from 0.68 MHz) and data were taken for minor variations of f_o and f_m. Both uniform periods and uniform flow sensitivity were obtained for a portion of the total ramp time, but it was not possible to obtain a satisfactory alignment for measuring five cycles with a 5 ms ramp, because the uniform five cycles always extended beyond 5 ms. Since five cycles at 2 kHz IF is 2.5 ms, this means that more than 2.5 ms was required to obtain the first uniform IF cycle. Based upon prior data, a larger transmitted signal would have improved the response time of the IF filters, but time constraints did not permit such extensive rework. It was decided that the 10 ms ramp would be used for five cycle period mode data in the Final Design Feasibility Tests. This also assured that the minicomputer in the DCA would have adequate time to update the digital display.

The flow sensitivities by both the period mode and the phase mode were found to be essentially independent of the ramp time (5 ms or 10 ms). This was an important result, since the analytical work (see Appendix) had not included a comprehensive analysis of the possible effects of T/R cycle harmonics upon the IF signal for any case except that of constant amplitude transmitted and received RF signals, with a distortion-free IF filter.

The phase mode flow sensitivities for the two sets of transducers were found to be identical (within the limits of flow stability) when operating with f_o near crystal resonance. The phase mode sensitivity was not measured (inadvertantly) for the stainless-steel transducers with f_o at 0.38 MHz. The aluminum transducers provided only about 64% of the expected sensitivity when operated at 0.49 MHz. The phase shift was measured at a point corresponding to the first or second cycle of the dashed curves of FIGURE 8-3. Therefore, it was found that the phase shift sensitivity was low in this region for which the period mode sensitivity was high, but was decreasing rapidly.

The phase-mode linearity in the zero to 2.2 lb/s range was determined against the Fisher-Porter flowmeter. The plot was linear within the limits of readability of the average flow rate indication. This test verified that no detectable change in sensitivity occurs due to the transition from laminar to turbulent flow when measuring in the phase-mode. (See FIGURE 7-11 and the relevant discussion for comparable period-mode linearity data.)

9A   GENERAL COMMENTS AND SUMMARY OF TESTS PERFORMED

The NASA-JSC-ATT facility was only available for one week of final testing.
The first day was consumed in finding and repairing shipping damage to the
DCA. The master circuit board had been knocked out of its mounting slots
(no retaining screws) by either impact or vibration. The DCA did not operate
until bent (and electrically shorted) IC-socket pins were straightened. No
DAC components required replacement. The Flow Cell Electronics and Power
Supply Module suffered no shipping damage.

After repair of the DCA, the IF period uniformity at zero flow was determined
before making any readjustments. The rate of period increase with cycle
number was larger than it had been in the last test at Beckman, presumably
due to an increase of sample temperature from about 68° to $80^{\circ}F$. The ambient
temperature difference is unknown. The values of f_o and f_m were then adjusted
alternately to obtain the minimum variation in the C-DAC output versus cycle
number under zero flow conditions. The final setting of f_o was 0.733 MHz. It
had been 0.715 MHz when last set at Beckman, and measured 0.716 MHz as re-
ceived at JSC (using a different digital voltmeter). These frequencies (in
MHz) were obtained by dividing the measured voltage applied to the VFC input
by the f_o adjustment potentiometer by 2.00, which is the nominal transfer
characteristic for the VFC. Based on the results of the last test at Beck-
man, the system was expected to have the nominal (theoretical) period-mode
sensitivity using five IF cycles starting at the sixth cycle. It was left in
this configuration for testing the next day, 25 May.

For clarity of presentation, the following brief summary of the four-day May
test program is given below. The TTA facility rough log identified virtually
every test by "run number," including those for which no comparative data were
taken by the facility:

   25 May   Runs 51 through 55 were made at various flows to provide lin-
                earity data versus facility flowmeter FM 804 for the phase and
                period modes of operation. Nonlinearity above 150 gpm (66% of
                full scale) resulted in performance of the following test.

                Runs 56 through 70 were made at various flow rates to permit veri-
                fication of nonlinearity against the catch-weigh system. Non-
                linearity above about 150 gpm was confirmed. Furthermore, the
                flow sensitivity was only about one-half of the expected value.

   26 May   In the morning the system was realigned for operation at $f_o = 0.38$
                MHz (from 0.75 MHz) to reduce phase sensitivity and ensure linear-
                ity to the required full-scale flow. The C-DAC output was used to
                indicate the uniformity of the IF cycles (at zero flow). An oscil-
                loscope was employed to monitor the outputs of the mixer and IF

filter as guides in the adjustment of f_o and f_m to achieve the widest possible band of uniform IF cycle periods within the 10 ms transmitted ramp. When making this alignment, the amplitude of the IF was allowed to decrease in the interests of IF cycle uniformity.

Runs 71 through 74 were made after realignment of the NIGS for operation at f_o = 0.38 MHz in the manner described above. A steady flow of about 50 gpm was used to permit measurement of the flow sensitivity versus the IF cycles measured. Run 71 revealed that the alignment technique employed was not optimum. Specifically, as optimized for maximum uniformity at zero flow, there was essentially no sensitivity to flow. The next three runs permitted realignment to achieve uniform flow sensitivity. Basically, this involves obtaining near maximum IF amplitude for the value of f_o which provides the best uniformity of IF periods at zero flow.

Run 75 was either not logged, or an error in tabulation was made.

Runs 76 through 85 were made against the catch-weight system, and provided two sets of data each for 15, 50, 100, 150, and 200 gpm (nominal) flow rates. The sensitivity was approximately 160% of the nominal value, indicating that the selected region of uniform flow sensitivity was one of high signal distortion. The sensitivity also varied about 20% across the flow range and/or for replicate flow rate data. The poor stability is believed to have been the result of ambient temperature variations and poor circuit stability, which caused minor shifts of f_o, f_m, and the IF filter center frequency. Such minor changes can have large effects when operating in a region of the IF which has non-theoretical sensitivity.

27 May   Runs 86 through 95 were roughly a repeat of the test of runs 76 through 85 made on 26 May. No changes were made in the NIGS alignment, and in the first run (86) the sensitivity to flow was essentially as it had been the day before. The sensitivity decreased rapidly (pounds transferred per integrator output volt increased) in the first few runs. The digital circuitry failed at about 0930 hours, and it was necessary to shade the Flow Cell Electronics from the sunlight to keep the system running. (The sunlight came through a translucent plastic roof.) In addition, a large fan was positioned so that it created a draft past the NIGS system. The sensitivity to flow decreased to within 10% of the theoretical value soon after these changes in thermal environment were made.

Run 96 was aborted after about 87 pounds were transferred, due to a minor facility equipment failure. The data for this run should not be used because of uncertainty in the actual integration time.

Runs 97 through 114 were all made at a nominal flow rate of 16 gpm. Some were with steady flow and some were pulsed at 0.5, 1, 2, and 5 Hz. The 5 Hz pulses coincided with the natural resonance of the TTA system, resulting in large pressure variations. This caused about a 45% loss of sensitivity for the 5 Hz data, apparently due to pressure modulation of the path length. The 1 and 0.5 Hz data were unaffected. That is, the sensitivity was within the normal range for steady flow on 27 May. The 2 Hz data showed an apparent 17% change in sensitivity. The results of the pulsed flow tests are discussed further in paragraph 9C. In addition, a definite correlation between sensitivity and circuit temperature was demonstrated. This is also discussed in detail in paragraph 9B-3.

28 May In the morning the NIGS was switched into the phase mode and circuit alignment was visually checked using an oscilloscope.

Run 115 was made at a steady flow rate of 15 gpm to permit readjustment of f_O to ensure that the phase mode sensitivity was uniform for cycles adjacent to the one cycle monitored when in the phase mode. (Basically, f_O was shifted to move the uniform cycles used for the prior period mode test to the fixed-time Phase Mode IF Cycle Counter Reset Pulse.) This readjustment required a total time of about 12 minutes.

Runs 116 through 128 provided two steady 16 gpm flow rate references, followed by 0.5, 1, 2, and 5 Hz pulsed flows at the same flow control valve setting, plus two steady flow references at the end of the pulsed flow tests. The mean flow sensitivity for the beginning and ending steady flow reference tests decreased by about 7% (which is only 0.5% of full-scale flow), presumably due to temperature effects upon the circuitry. All pulsed flows caused loss of sensitivity in the period mode. The sensitivity loss varied from 16% for 0.5 Hz to about 60% for the 5 Hz pulses. These pulsed flow results are discussed in detail below, in paragraph 9C.

Runs 129 through 145 were made using various flow rates (usually with replicates) against the catch-weigh system for basic linearity data. There was a correlation between measured sensitivity and temperature. The results of these tests are discussed in paragraph 9B-4.

The above summary provides a chronological guide, and will assist in correlation of the raw data contained in the TTA Test Log with the detailed discussions which follow.

9-3

9B   DETAILED DISCUSSION OF FINAL DESIGN FEASIBILITY TESTING

9B-1   Details of 25 May Tests

The first test was a six-point flow rate scan against a TTA facility flow-
meter (FM-804) which had been calibrated against the catch-weigh system on
29 April. The linearity and reproducibility in the phase mode were excellent
below 150 gpm (60% of full scale). A retest in the period mode showed essen-
tially the same deviation from linearity. Later in the day a catch-weigh
test was performed to verify that the problem was not due to a change in the
calibration of FM-804. For two tests each at flow rates of 15, 50, and 100
gpm the mean sensitivity was 25.42 pounds per volt (integrator output) with
all six points within $\pm$ 2.5% of the mean value. Above 150 gpm the flow
sensitivity decreased by about 25%, and the noise increased markedly.

In reviewing the test results the following points became apparent:

- The nonlinearity above 150 gpm was due to excessive phase shift.
  There was a phase shift of 16% of the maximum allowable shift (π
  radians) due to increasing the system pressure from 100 to 250 psig
  after alignment of the C-DAC output feedback to f_0. (The pressure
  affected the path length.) In addition, the phase shift due to flow
  probably exceeded that anticipated. The combination resulted in a
  total phase shift for one direction of transmission greater than π
  radians. When this occurs the periods of five different cycles are
  measured for the two directions of sound transmission. No error would
  result if the periods were all uniform, but this was not the case for
  the test transducers.

- The sensitivity in the linear region was within about ten percent of
  that obtained in the final 30 April test using the same transducers
  (except with impedance matching facings). This sensitivity was also
  within about two percent of the theoretical sensitivity for the period
  mode with five cycles. The performance was, therefore, acceptable
  except for a design error which limited the useful flow response range
  too tightly for operation at the design value of f_0.

- For linear and stable operation to the required full-scale flow rate
  of 35 pounds per second (252.4 gpm) with any of the available trans-
  ducers, it was necessary to reduce the value of f_0 from 0.75 to 0.38
  MHz (nominal) to reduce the phase shift sensitivity by a factor of
  two.

It was concluded that the system would require alignment for operation at half
the crystal fundamental frequency. It was also reaffirmed that the thin
stainless-steel transducers without impedance matching facings would be used.
This means that the balance of the test data is directly comparable to that
obtained on 30 April. The only differences are summarized for convenient
reference below:

- Elimination of impedance matching layers. This reduced the quality of the IF obtained at f_O = 0.38 MHz. With new crystals having first resonance at this frequency, however, the lack of matching layers would not have mattered.

- Addition of phase mode measurement capability.

- Addition of C-DAC output, and feedback of this signal to the f_O input of the VFC to reduce phase shift due to C_O variations. This feedback also made the phase mode flow measurement independent of speed-of-sound changes.

- An increase of ramp time (T/R half-cycle) from 8.4 ms to 10 ms. This altered the integrator sensitivity expected by the ratio 10/8.4. The 30 April sensitivity of 19.31 pounds per volt would change to 22.99 pounds per volt as a result of this modification.

9B-2   Details of 26 May Tests

The data obtained on 26 May were an important part of the "learning curve," but they are not worth detailed reporting. The major points learned and/or confirmed were:

- Alignment for uniformity of IF periods at zero flow is a valid procedure only when f_m is set for very nearly maximum IF amplitude in the vicinity of the IF cycles which are to be monitored.

- Alignment of both f_O and f_m are effective in obtaining uniformity of IF cycles at zero flow but with the restriction on f_m noted above.

- Final alignment of f_O and f_m with flow is a necessary step because adjusting for uniform IF periods at zero flow is not a sufficient condition for uniform flow response.

- Alignment of f_O and f_m for operation of 0.75 MHz crystals (mounted on 0.017-inch-thick stainless steel and with no impedance matching to the load) for operation at 0.38 MHz is very critical. Thermal stability of the circuits is also much more critical than it is for operation at the design frequency of 0.75 MHz.

- There is no simple explanation for the test transducers having a resonance at about one-half of the nominal crystal resonance frequency. The superior RF resonance (and IF) obtained at 0.38 MHz on 30 April with impedance matching layers was probably due to a compound resonance of the crystal and magnesium facing, the sum of which is $\lambda/2$ thick at 0.38 MHz. The first resonance frequency is that for which the thickness is $\lambda/2$ when the load impedance is lower than that of the crystal and of the plate forming the compound structure.

● In light of the above points, the rather large variations in sensitivity observed on 26 May were believed to be about the best these transducers were capable of providing without either improved circuit stability, or restriction of the full-scale flow rate to about one-half that specified to permit operation at f_o = 0.75 MHz.

It was concluded that the best approach was to continue testing on 27 May without further adjustment, to further determine the thermal stability of the system and to determine the effect of pulsed flows. Up to this point in the tests it had not been recognized that thermal instability of the digital circuitry, as well as that of the analog circuitry, was a major source of sensitivity changes. This was discovered on 27 May, as described in the following paragraphs.

9B-3   Details of 27 May Tests

This was the last opportunity to obtain period-mode data, because the final day of facility availability was being reserved for phase-mode testing. The system was operated as on 26 May, with no readjustments. The first flow data obtained against the catch-weigh system verified that the sensitivity was about 150% of theoretical, as it had been on the previous afternoon. The sensitivity rapidly decreased with time as the ambient temperature increased. (The sensitivity in terms of pounds per integrator output volt increased.) The digital circuitry failed between runs 87 and 88, as noted on FIGURE 9-1. Shades were placed over the Flow Cell Electronics to bar direct sunlight, and a large fan was positioned to create a draft of air past the NIGS and to exhaust it through a test cell door. The sensitivity stabilized at about 19 pounds per volt, which was about 20% from theoretical (23 lb/volt) for period-mode measurement of five cycles with T_r = 10 ms. The water temperature stabilized at about the same time, but the evidence basically indicated that water temperature variations, per se, were not the major factor. The water temperature more-or-less followed the prevailing ambient temperature, which appeared to be the major cause of sensitivity variations.

The plots of FIGURE 9-1 show both the NIGS sensitivity and the water temperature versus run number. While the runs were sequential in time, the time between runs varied widely. There is an apparent correlation between water temperature and sensitivity for the first several runs but, as noted above, the temperature of the digital circuitry was approaching the "stall-point" during the time of this 4.5°C (10°F) water temperature change. The plot shows a period of good stability between runs 88 and 98, which covered the entire required flow range. (Run 96 was aborted and the data should not be used.) Runs 99 and 100, and runs 108 through 114 are omitted because they were for pulsed flows, and confuse the thermal-shift aspects of the data of FIGURE 9-1.

The feature of major interest of FIGURE 9-1 is shown by runs 97 through 107, all of which employed a nominal flow rate of about 16 gpm (7% of full scale, the specified minimum flow rate for the application). The NIGS zero offset
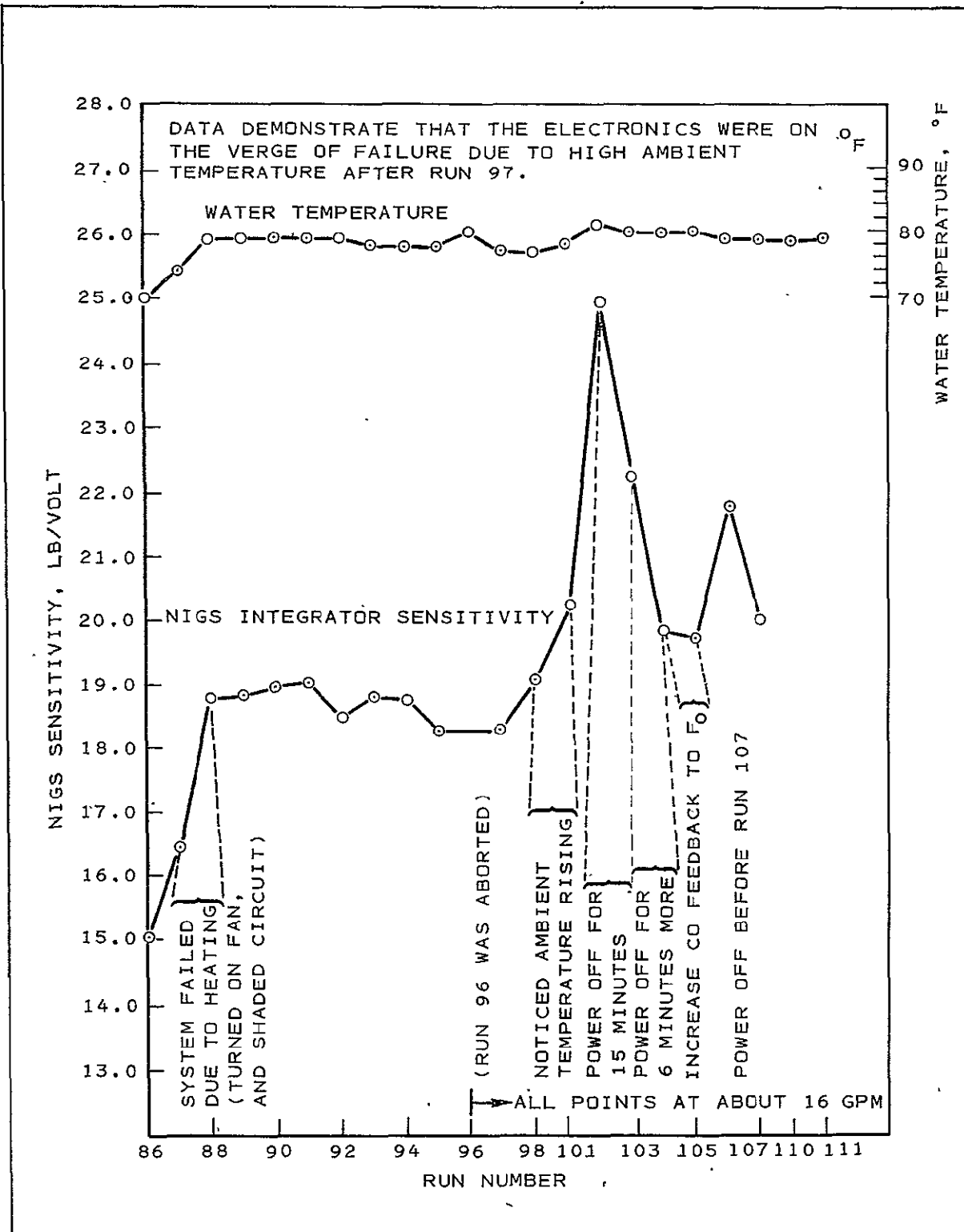
Figure 9-1. Data of 27 May, NIGS Integrator Sensitivity in the Period Mode and Measured Water Temperature Versus Run Number for All Steady State Flow Data.

becomes significant at this flow rate, and it appeared to be drifting both positive and negative, randomly, after run 94. The data plotted for runs 97 and 98 are the averages of the direct and "integrator drift corrected" values.

The very rapid drift in sensitivity between runs 101 and 102 led to a search for the cause. The power was turned off for about 15 minutes and back on for six minutes before run 103, resulting in an apparent 13% recovery of the sensitivity. Similarly, turning the power off for 6 minutes and back on for only 1.2 minutes before making run 104 resulted in an additional 12% recovery. These runs were of 3-minute duration, which would allow a significant amount of circuit component reheating.

Between runs 104 and 105 the amount of C-DAC output feedback to the f_0 input of the VFC was increased slightly to provide more complete stabilization of the nominal IF phase. (This was an open-loop feedback, requiring empirical adjustment. The initial adjustment had been made following a small thermal change on 26 May, to give approximate compensation.) The close agreement of sensitivities for runs 104 and 105 is not necessarily significant, since the random variations for repeat tests might well have been greater.

The power was off again briefly before run 107, and the sensitivity was restored as before. The evidence that circuit thermal coefficients were causing the shift of sensitivity is quite convincing. Incidentally, the average power dissipated in the transducers was less than 0.25 watts, even assuming a resistive load. As mounted and coupled to water, it is considered improbable that self-heating of the transducers was significant.

A correlation between period-mode flow sensitivity and water temperature, using all data of 27 May (except the flow pulse data), is shown in FIGURE 9-2. It should be noted that the effect of water temperature is not believed to be detectable, and that the correlation is actually with circuit temperature, which correlates roughly with water temperature. By reference to FIGURE 9-1 and the above discussion, the highest errors are due to circuit self-heating, which may be added to the basic ambient temperature effect upon capacitor values, etc. Nevertheless, there is a clear correlation between sensitivity and water temperature. The expected water density thermal effect would be less than 1/10%, which is clearly negligible compared to the roughly 30% variation shown in FIGURE 9-2.

Utilizing the data from runs 88 through 98 (except 96, which was aborted) provides an estimate of system performance in the absence of gross thermal effects. This performance approaches the best that could be expected from the 0.75 MHz crystals when operating with f_0 at 0.38 MHz, even if all circuit instabilities were to be eliminated by "closing loops" on f_0 and f_m, and by replacing the 20 MHz clock with one having adequate stability over the required temperature range. These ten sets of data cover the flow rate range of interest, and include roughly replicate tests for most of the flow
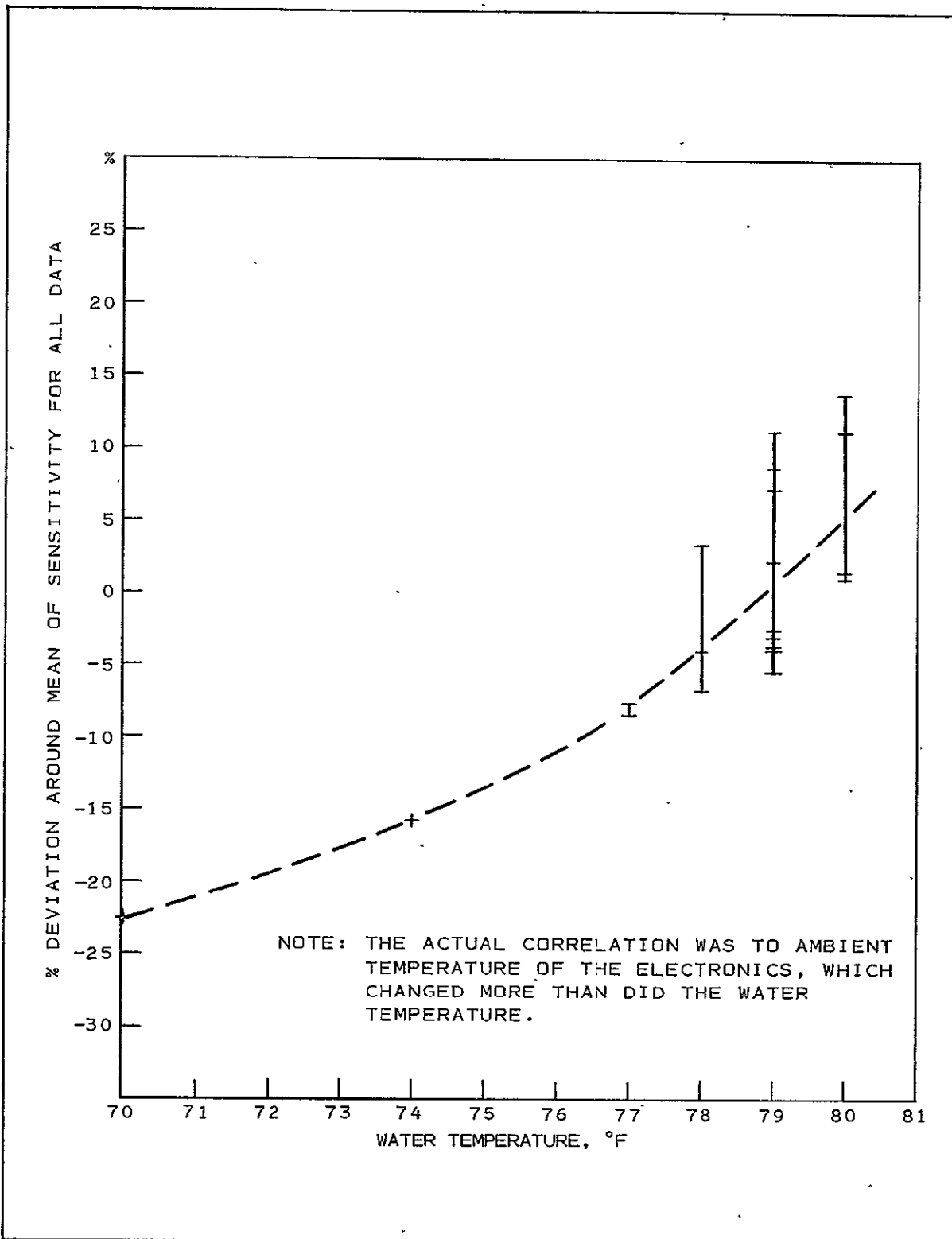
Figure 9-2.   Data of 27 May Showing Correlation Between Water Temperature and NIGS Integrator Sensitivity.

9-9

rates employed. The data from the original TTA Test Log plus the calculated results are presented in TABLE 9-1. The results are in basic agreement with those of TABLE 8-1, obtained on 30 April with the same basic operating parameters, except that the impedance matching facings had been removed. In the absence of circuit thermal instabilities, the NIGS integrator output would have shown a maximum transferred mass error of −28 pounds while emptying a 1725 kg (3800 pound) tank with the flow profile shown in TABLE 9-1. It would, therefore, have provided a knowledge of the remaining fuel mass to within 0.74% (28/3800). In fact, the pulsed flow data obtained for all but the 5-Hz pulses could also be included in the total mass transferred calculation without causing the error to exceed 1%.

The pulsed flow data obtained on 27 May are discussed in paragraph 9C, in relationship to corresponding data obtained on 30 April and 28 May. Briefly, the results indicated that the transducer must be stiffened (by rear potting, for example) to prevent significant modulation of the path length by pressure variations. The 0.178 cm (0.070 inch) thick magnesium and 0.076 cm (0.030 inch) thick Lucite matching layers used in April provided significant stiffening. There was also evidence that the period-mode output is less dependent on modulation of the path length than is the phase mode.

The output noise in the period mode was determined on 27 May, using a TTA Facility oscillograph. The output noise is discussed in paragraph 9D in connection with the phase-mode noise measured on 28 May. The relative noise for the two modes is of considerable theoretical interest, although the relatively noise-free integrator output is the one inherently required for the NIGS application.

9B-4   Details of 28 May Tests

This last day of Final Design Feasibility Testing was devoted to evaluation of the phase mode of operation. The C-DAC output (average IF period measurement) was fed back to the VFC input to make f_o vary with C_o to hold the ratio f_o/C_o constant. This, in turn, holds the nominal IF phase constant, which extends the operating temperature range of the system and makes it independent of the speed of sound. While this was an open-loop system, it reduced the phase mode dependence on the speed of sound to about one-tenth of what it would have been without the feedback. A closed-loop system would be required for a flight model to ensure that the system would lock in on the same IF cycle (i.e., the cycle generated by the same transmitted and received RF frequency), regardless of the temperature at the time the power came on. The open-loop system tested was adequate only for demonstrating the feasibility of the approach, and was potentially unstable for temperature changes greater than about ±3.3°C (±6°F) for which ± π radians phase shift would occur in the absence of such feedback.

FIGURE 9-3 presents all of the sensitivity data obtained on 28 May, compared to the catch-weigh system. Runs 118 through 125 were obtained for pulsed flows. Runs 118 and 119, 120 and 121, 122 and 123, 124 and 125 were replicate pairs for 0.5, 1, 2, and 5 Hz pulses, respectively. Each pair is joined by a line to indicate correspondence. These runs are not relevant to the steady flow

TABLE 9-1. *SUMMARY OF ALL STEADY-STATE FLOW DATA OBTAINED ON 27 MAY, USING PERIOD MODE, OMITTING DATA FOR WHICH LARGE CIRCUIT THERMAL ERRORS WERE DEMONSTRATED*

Run No.	Calculated Average Flow Rate Catch-Weigh		Transferred Mass		NIGS Integrator Voltage Change	Cumulative Mass Transferred (NIGS Means SENS. = 18.584 lb/volt)			
			By Catch-Weigh System	By NIGS Integrator Output, Calculated		Catch-Weigh System	NIGS Integrator Times Sensitivity	NIGS Integrator Error	NIGS Error, % of Total Mass
	(gpm)	(lb/s)	(lb)	(lb)	(volts dc)	(lb)	(lb)	(lb)	
88	241	33.5	335	331	17.81	335	331	− 4	−1.2
89	182	25.3	379	374.7	20.16	714	706	− 8	−1.2
90	182	25.3	377	370	19.91	1091	1076	−15	−1.4
91	225	31.2	340	331.7	17.85	1431	1408	−23	−1.6
92	132	18.3	367	368.3	19.82	1798	1776	−22	−1.2
93	134	18.6	372	368.3	19.82	2170	2144	−26	−1.2
94	79	11.0	330	326.5	17.57	2500	2472	−28	−1.2
95	81	11.2	448	456.6	24.57	2948	2929	−19	−0.6
96	−	−	aborted	−	−	−	−	−	−
97	26	3.6	430	446.2	24.01	3378	3375	− 3	−0.1
98	16	2.2	407	419.4	22.57	3785	3794	+ 9	+0.2

Figure 9-3. Data of 28 May. NIGS Integrator Sensitivity (in the Phase Mode) and Measured Water Temperature Versus Run Number for All Flow Data.

rate sensitivity, and are shown in FIGURE 9-3 only to illustrate the effect of modulation of the path length. The effect of pulsed flow is discussed below in paragraph 9C for the data of 30 April and 27 and 28 May.

The water temperature versus run number is also shown in FIGURE 9-3 for convenience of reference. The actual temperature dependence is almost certainly on ambient temperature in the locality of the electronics, as discussed in connection with the 27 May data. A correlation between the water temperature and the phase mode sensitivity is shown by FIGURE 9-4. Comparison to FIGURE 9-2, which is the corresponding figure for the period mode, indicates that the phase mode is less susceptible to circuit thermal effects by a factor of three to four. This might be a result of reading only one IF cycle in the phase mode, compared to five cycles in the period mode. The IF cycle distortion variations for the best cycle might well be less than that for the average of the best five cycles. On the other hand, all data were obtained in the morning of 28 May and uncontrolled factors effecting ambient temperature, such as cloud cover, may have caused the improvement in performance.

The sensitivity of the phase mode was not expected to be the same as for the period mode, but scaling by dividing the 20-MHz clock down to 4 MHz for the phase mode counting was expected to make the sensitivities of the two modes equal to within about 5%. The phase-mode data of 28 May were less sensitive by about 20% than was calculated for the idealized system, and less sensitive than the observed period-mode sensitivities for 30 April and 27 May (which were both too sensitive) by about 60%. Considering the non-uniformity of the IF cycles obtainable with the test transducers when operating at $f_0 = 0.38$ MHz, the agreement with simple theory was reasonably good.

TABLE 9-2 contains all non-pulsed flow data obtained on 28 May. Including the thermal errors with no correction whatsoever provides a direct indication of the performance obtained over a 3.9°C (7°F) range of water temperature. The improvement that could be expected with more stable circuitry is admittedly speculative, but it is reasonable to assume that the errors in cumulative mass shown in TABLE 9-2 would have all been less than ±1% if the thermal effect shown in FIGURE 9-4 had been eliminated. It is also apparent that the major errors occurred for the runs at low flow rate (16 gpm, or 7% of full scale) for which a 7% integrator error is equivalent to an error of only 0.5% of full-scale flow. Since the first five runs tabulated accounted for 21% of the total mass transferred, 831.7 kg/3975 kg (1832 lb/8757 lb), the most severe test conditions were accentuated by this presentation. For example, if run 132 (at 123 gpm) had been the first in the sequence, the error for run 116 would have been reduced by about a factor of two. (This point is valid, of course, only if the pulsed flows are measured without systematic error.) It is also apparent that if a 4090.9 kg (9000 lb) tank had been the water supply, the remaining water would have been known to within 0.8% (31.7 kg [70 lb] is the maximum cumulative error) after each and every run. Therefore, the system met the requirements of the NIGS specifications over the 22.2° to 26.1°C (72° to 79°F) range, at least, for various steady flow rates, without requiring any improvement, in thermal stability. Since the specified

DEVIATION AROUND MEAN OF
SENSITIVITY FOR ALL DATA

THE ACTUAL CORRELATION WAS TO AMBIENT TEMPERATURE OF THE
ELECTRONICS, WHICH CHANGED MORE THAN DID THE WATER
TEMPERATURE.

WATER TEMPERATURE °F
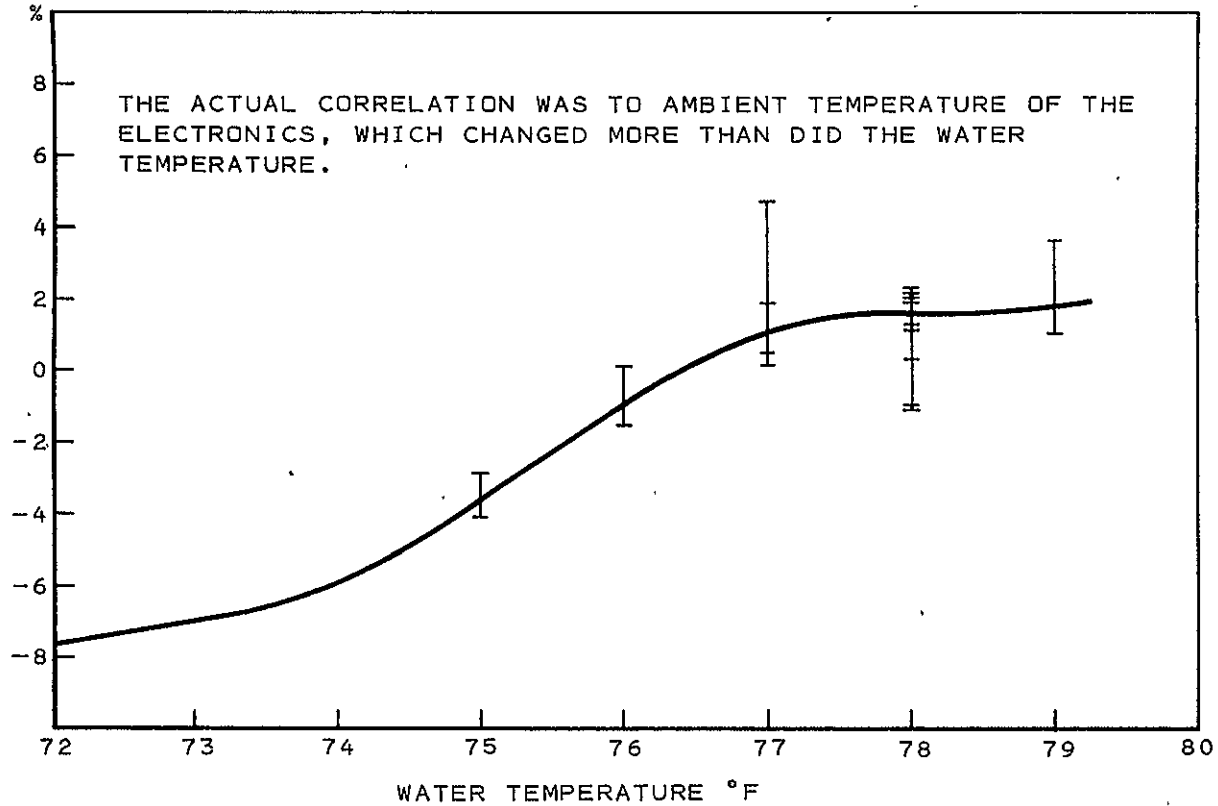
Figure 9-4.   Data of 28 May Showing Correlation Between Water Temperature and
NIGS Phase Mode Integrator Sensitivity.

TABLE 9-2. SUMMARY OF ALL STEADY-STATE FLOW DATA OBTAINED ON 28 MAY, USING THE PHASE MODE. These runs were completed before the ambient temperature increased to the point causing failure of the electronics.

Run No.	Calculated Average Flow Rate Catch-Weigh (gpm)	(lb/s)	Transferred Mass By Catch-Weigh System (lb)	By NIGS Integrator Output, Calculated (lb)	NIGS Integrator Voltage Chabge (volts dc)	Cumulative Mass Transferred (NIGS Means SENS. = 31.50 lb/volt) Catch-Weigh System (lb)	NIGS Integrator Times Sensitivity (lb)	NIGS Integrator Error (lb)	NIGS Error, % of Total Mass
116	16	2.2	399	427	13.56	399	427	+28	+7.0
117	16	2.2	398	428	13.60	797	855	+58	+7.3
126	16	2.2	399	411	13.04	1196	1266	+70	+5.9
127	14	1.9	358	343	10.90	1554	1609	+55	+3.5
128	11	1.5	278	265	8.42	1832	1874	+42	+2.3
129	51	7.1	427	412	13.08	2259	2286	+27	+1.2
130	52	7.2	431	427	13.54	2690	2713	+23	+0.9
131	123	17.1	342	338	10.74	3032	3051	+19	+0.6
132	123	17.1	428	427	13.56	3460	3478	+18	+0.5
133	108	15.0	452	459	14.57	3912	3937	+25	+0.6
134	70	9.7	327	327	10.37	4239	4264	+25	+0.6
135	80	11.1	223	219	6.95	4462	4483	+21	+0.5
136	12	1.7	308	306	9.73	4770	4789	+19	+0.4
137	154	21.4	536	530	16.83	5306	5319	+13	+0.2
138	157	21.8	436	440	13.98	5742	5759	+17	+0.3
139	206	28.6	418	409	12.99	6160	6168	+ 8	+0.1
140	203	28.2	423	415	13.18	6583	6583	0	0
141	240	33.3	499	497	15.79	7082	7080	- 2	-0.03
142	252	35.0	524	530	16.81	7606	7610	+ 4	-0.05
143	214	29.7	386	381	12.10	7992	7991	- 1	0
144	224	31.1	373	365	11.59	8365	8356	- 9	-0.1
145	71	9.9	392	384	12.20	8757	8740	-17	-0.2

range is 21.1° ±16.7°C (70° ±30°F), a factor of five or more improvement in the thermal stability of the electronics is required for a flight model. The sensitivity of the NIGS to pulsed flow is considered further in the following paragraph.

9C   SENSITIVITY OF THE NIGS TO PULSED FLOW

All pulsed flow data (except run 31, which was aborted) are summarized in TABLE 9-3. The April pulsed flow tests were performed with impedance matching plates on the transducers. The plates were 0.178 cm (0.070 inch) magnesium and 0.076 cm (0.030 inch) Lucite, bonded with thin layers of epoxy cement. The cement was also applied in a heavy layer around the edges to prevent water from attacking the magnesium. Lucite, which has an acoustic impedance equal to that of Teflon, was used in the interest of economy. Comparison of the pulsed flow tests performed in April and in May (without impedance matching) reveals that the matching plates contributed significant stiffening to the crystal mounts. The mounts were approximately 1.9 cm (0.75 inch) in diameter, with 0.127 cm (0.050 inch) thickness, counter-bored with 1.01 cm (0.40 inch) diameter to 0.043 cm (0.017 inch) thickness from the inside. The crystals were 0.64 cm (0.25 inch) diameter and were cemented in the center of the 1.01 cm (0.40 inch) diameter section with conductive silver/epoxy. The rear cavities could have been filled with tungsten powder/epoxy mixture to further improve the crystal backloading and to stiffen the crystal mounts. This was not done for two reasons: the effect that thermal expansion and contraction might have on the crystal/aluminum alloy cone structure was unknown; and the transducers would be more difficult to repair or modify if they were potted before testing. For a flight model, rear potting would ensure stiffening at least comparable to that provided by the magnesium and Lucite impedance matching plates.

The 30 April test showed an apparent increase in sensitivity (decrease in pounds per volt integrator output) of about 7% at 5 Hz compared to the mean value of the data for steady flow, 0.5, and 1 Hz pulses. This is within the allowable range of the NIGS specifications, since the 7% error at 7% of scale is only 0.5% of full scale.

The 27 May data, also obtained with the period mode of operation but without impedance matching faces, showed little effect due to 0.5 and 1 Hz pulses, but a 17% loss of sensitivity at 2 Hz (only one test) and an average loss of 51% at 5 Hz (four sets of data). Both shifts were increases in terms of pounds per volt sensitivity. The effect was also opposite to that at 5 Hz (7%) seen in April with the impedance matching layers in place.

The phase-mode data indicated large (possibly linear with frequency) effects for pulses at 0.5, 1, 2, and 5 Hz. The maximum effect, 61% average at 5 Hz, is not significantly larger than the 51% average error seen for the period mode on 27 May. The phase mode errors at all other frequencies were, however, larger than for the period mode. The reason for this is not immediately apparent, but it may be related to the fact that the phase mode basically utilized less than one-half of an IF cycle for measurement, while the period mode utilized five full cycles.

TABLE 9-3. SUMMARY OF ALL PULSED FLOW DATA (SHEET 1 OF 2)

Run No.	Frequency of Flow Pulses, Hz	NIGS Integrator Sensitivity, lb/volt	Sensitivity Error, % of Mean for Steady Flow	Calculated Average Flow Rate at Peak gpm	lb/s	Remarks
22	0	18.25	mean=	15.3	2.1	29 April Data
23	0	17.72	17.985 lb/volt	15.3	2.1	
24	1	18.55	+3.1%	15.0	2.1	Period mode, five IF
25	1	18.56	+3.2%	15.0	2.1	cycles. Impedance matched
26	0.5	17.95	-0.2%	14.3	2.0	for 0.75 MHz, operated at
27	0.5	17.71	-1.6%	14.3	2.0	0.75 MHz. Nonlinear above
28	0.5	18.85	+4.8%	14.3	2.0	about 150 lb/s.
29	5.0	17.13	-5.0%	6.8	0.9	
30	5.0	16.74	-7.4%	6.8	0.9	
98	0	18.03	(used)	16.3	2.3	27 May Data.
99	5.0	33.00	+66.0%	15.8	2.2	
100	5.0	29.09	+46.0%	15.4	2.1	Period mode, five IF
101	0	20.23	(used)	16.2	2.2	cycles. No impedance
102	0	24.95	(not used)	16.1	2.2	matching layers. Oper-
103	0	22.22	(not used)	16.4	2.3	ating 0.75 MHz crystals
104	0	19.84	mean of six	16.3	2.3	at 0.38 MHz. Runs 102
105	0	19.75	data used =	16.2	2.2	and 103 not used in ob-
106	0	21.76	19.935	16.2	2.2	taining steady state mean
107	0	20.00	lb/volt	16.3	2.3	value because they dis-
108	5.0	27.59	+38.0%	15.4	2.1	played a thermal error
109	5.0	30.48	+53.0%	15.4	2.1	not applicable to pulsed
110	0.5	21.25	+6.6%	16.3	2.3	flow data.
111	0.5	20.96	+5.1%	16.1	2.2	
112	1	20.00	+0.3%	16.3	2.3	
113	1	20.99	+5.3%	16.3	2.3	
114	2	23.33	+17.0%	16.8	2.3	

TABLE 9-3. *SUMMARY OF ALL PULSED FLOW DATA (SHEET 2 OF 2)*

Run No.	Frequency of Flow Pulses, Hz	NIGS Integrator Sensitivity, lb/volt	Sensitivity Error, % of Mean for Steady Flow	Calculated Average Flow Rate at Peak gpm	lb/s	Remarks
116	0	29.42	mean for three	16.0	2.2	28 May Data
117	0	29.26	data=29.76 lb/V	15.9	2.2	
118	0.5	35.00	+17.6%	11.2	1.6	Phase Mode, no impedance
119	0.5	33.13	+11.3%	11.1	1.6	matching layers. Oper-
120	1.0	42.22	+42.0%	11.4	1.6	ating 0.75 MHz crystals
121	1.0	39.24	+32.0%	11.3	1.6	at 0.38 MHz.
122	2.0	40.43	+36.0%	11.2	1.6	
123	2.0	40.94	+36.0%	11.3	1.6	
124	5.0	46.70	+57.0%	10.6	1.5	
125	5.0	49.53	+66.0%	10.6	1.5	
126	0	30.6	(used)	16.0	2.2	

The pulsed flows caused errors because the TTA system rings at 5 Hz. This is apparent from the oscillograph records made during the May tests, portions of which are reproduced as FIGURES 9-5 through 9-15. Some of the oscillograph records also indicate that the phase-mode flow rate DAC output of the NIGS had a negative transient error at each valve closure. (These figures are discussed further below.) Logically, the flow will stop faster than it can rise, which creates the potential of a systematic error due to a higher rate of increase of flow cell pressure due to valve closure than the compensating rate of decrease of pressure when the valve opens. Recalling that the relative error due to pressure modulation of the path length (Equation 8D) is amplified by C/v, which is $130/0.07 = 1857$ for a flow of 15 gpm = 7% of full scale, an effective modulation (dL/L) of about 0.027% would cause a 50% of reading error at 7% of full scale. For a 100 psi difference in the pressure rise and fall rates, and a 10 ms ramp time, this corresponds to a change in the nominal 8-cm (3.15 inch) path length of only about 10^{-4} cm/psi (40 microinches/psi). The error from this source should also increase with the frequency of the flow pulses, as was observed to be the case.

The assumed asymmetry of the rate of change of pressure being reasonable, it is probable that the major portion of the pulsed flow errors is accounted for by this mechanism. Ringing of the system at 5 Hz would cause the amplitude of the pressure transients to build up for flow pulses of this frequency. The test was conducted in a worst-case manner from this standpoint, since the normal RCS firing will be random rather than periodic. Some ringing should be expected for every flow pulse. The oscillograph records confirm that ringing occurred at every valve closure.

In connection with the above discussion, it should be noted that the T/R cycle frequency (50 Hz) used in the May tests was an even harmonic of all pulsed flow tests except the 2-Hz test, for which it was the twenty-fifth harmonic. Modulation of L at odd harmonics would be expected to introduce a systematic error proportional to the amplitude of the pressure modulation, while an equal amplitude modulation at even harmonics should not. The 2-Hz data for the phase mode test of 28 May shows a smaller error than does the 1-Hz data, suggesting that an odd harmonic modulation effect was also present. The sign of the odd harmonic modulation error would depend on the phase relationship between the T/R cycle and the flow pulse train, meaning that the error could be either positive or negative. A positive error of this type for the 2-Hz pulses may have occurred on 27 May, and a comparable negative error may have occurred on 28 May.

In a flight model it will be necessary to reduce the sensitivity to such pressure variations by stiffening the transducer mounts. Rear-potting is an obviously beneficial step. The use of crystals with 0.38 MHz first resonance (instead of 0.75 m Hz crystals operating at 0.38 MHz) will permit a trade-off between markedly improved IF quality with the same steel thickness, or moderate improvement with twice the steel thickness. Doubling the mount thickness will increase the rigidity by a factor of eight, which is probably more than is required. It is concluded that minor, and otherwise desirable, design changes will make the performance of a flight model NIGS essentially independent of the pressure transients associated with pulsed flow.

FIGURES 9-5 through 9-8 are reproductions of sections of oscillograph charts taken during the period mode pulsed flow tests on 27 May. The recorder chart speed was four inches per second. Each flow rate DAC output update, which lasted 20 ms, can be seen in the records. The flow rate DAC output was very noisy when these oscillograph records were made. Comparison to other period mode runs made the same day suggests that there may have been a faulty electrical connection at the time of these tests. It is also possible that the digital circuitry was too hot, since the power was being cycled manually at the time of these test runs. (Output noise is discussed further in the following section.) The integrator output shows essentially no noise, and only a small change in output during the elapsed time shown in the illustrations. The sensitivity was about 3.6 kg (8 lb) per small (vertical) chart division.

FIGURE 9-6 indicates that FM-1 also responded to the system pressure variations. The reason for this is not clear, but it is probable that air was trapped between the on-off valve and both flowmeters in this test (run 112).

FIGURES 9-9 through 9-13 are copies of oscillograph data obtained during phase mode pulsed flow tests on 28 May. All sensitivities are comparable to those in FIGURES 9-5 through 9-8, but the recorder chart speed was only one inch per second for all of these figures. The flow rate DAC output updates (20 ms duration) are not as easily distinguished as they are in FIGURES 9-5 through 9-8, for which the chart speed was four times as fast. The noise level is also much lower than it was in FIGURES 9-5 through 9-8, which is at least partly due to the lower noise in the phase mode of operation. However, as noted above and discussed further in Section 9-D, it is probable that either a faulty oscillograph connection or circuit thermal instability caused a major part of the noise in the records shown in FIGURES 9-5 through 9-8. At any rate, the lower noise of FIGURES 9-9 through 9-13 makes it possible to discern negative transients in the flow rate DAC output for each valve closure.

FIGURES 9-9 and 9-10 indicate that FM-1 was following the 5-Hz pressure ringing during the 0.5 and 1.0 Hz flow pulses (runs 119 and 121). It is probable that an air bubble was trapped between the on-off valve and the two flowmeters, resulting in an oscillatory flow superimposed upon the steady flow.

FIGURES 9-12 and 9-13 show the beginning and end, respectively, of two different phase mode, 5-Hz, flow pulse runs. The negative transients in the flow rate DAC output started as soon as the flow pulses started and ceased as soon as the pulses stopped. There is no correlation, therefore, between the amplitude of the pressure ringing and amplitude of the negative output transients. This strongly suggests that electromagnetic coupling of either the FM-1 output or the valve drive circuit introduced the negative spikes in the flow rate DAC output. It is not clear whether the system, or simply the oscillograph, was affected.

Figure 9-5. *End of Run 110. Period mode test with 0.5 Hz flow pulses. Peak flow rate was about 2.2 pounds per second.*

NIGS INTEGRATOR
DAC OUTPUT, 8 LB/DIV

0.25
SECOND

TIME

NIGS PERIOD MODE
FLOW RATE DAC OUTPUT,
0.18V/DIV.

PRESSURE, P801, 33.3 PSIG/DIV.

FLOW

ZERO FLOW

FACILITY FLOW METER,
FM-1, 0.15 LB S^{-1} (DIV)$^{-1}$

Figure 9-6.   Middle of Run 112.   Period mode test with 1.0 Hz flow pulses.   Peak
flow rate was about 2.2 pounds per second.

9-22

0.25
SECOND

TIME

NIGS INTEGRATOR
DAC OUTPUT, 8 LB/DIV

NIGS PERIOD MODE
FLOW RATE DAC OUTPUT,
0.18V/DIV.

PRESSURE, 'P801, 33.3 PSIG/DIV.

FLOW

ZERO FLOW

FACILITY FLOW METER,
'FM-1, 0.15 LB S^{-1} (DIV)$^{-1}$

Figure 9-7. Middle of Run 114. Period mode test with 2 Hz flow pulses. Peak
flow rate was about 2.2 pounds per second.

9-23

NIGS INTEGRATOR
DAC OUTPUT, 8 LB/DIV

0.25
SECOND

TIME

NIGS PERIOD MODE
FLOW RATE DAC OUTPUT,
0.18V/DIV.

PRESSURE, P801, 33.3 PSIG/DIV.

FLOW

ZERO FLOW

FACILITY FLOW METER,
FM-1, 0.15 LB S^{-1} (DIV)$^{-1}$

Figure 9-8.   End of Run 108.   Period mode test with 5 Hz flow pulses. Peak
flow rate was about 2.2 pounds per second.

Figure 9-9. *Start of Run 119. Phase mode test with 0.5 Hz flow pulses. Peak flow rate was about 2.2 pounds per second.*

Figure 9-10. Start of Run 121. Phase mode test with 1.0 Hz flow pulses. Peak flow rate was about 2.2 pounds per second.

NIGS INTEGRATOR
DAC OUTPUT, 8 LB/DIV

1.0
SECOND

NIGS PHASE MODE
FLOW RATE OUTPUT,
0.18V/DIV.

PRESSURE, P801, 33.3 PSIG/DIV.

FLOW

ZERO FLOW

FACILITY FLOW METER,
FM-1, 0.15 LB S^{-1} (DIV)$^{-1}$

Figure 9-11. Start of Run 123. Phase mode test with 2 Hz flow pulses. Peak
flow rate was about 2.2 pounds per second.

9-27

NIGS INTEGRATOR
DAC OUTPUT, 8 LB/DIV

1.0
SECOND

NIGS PHASE MODE
FLOW RATE OUTPUT,
0.18V/DIV

PRESSURE, P801, 33.3 PSIG/DIV

FLOW

ZERO FLOW

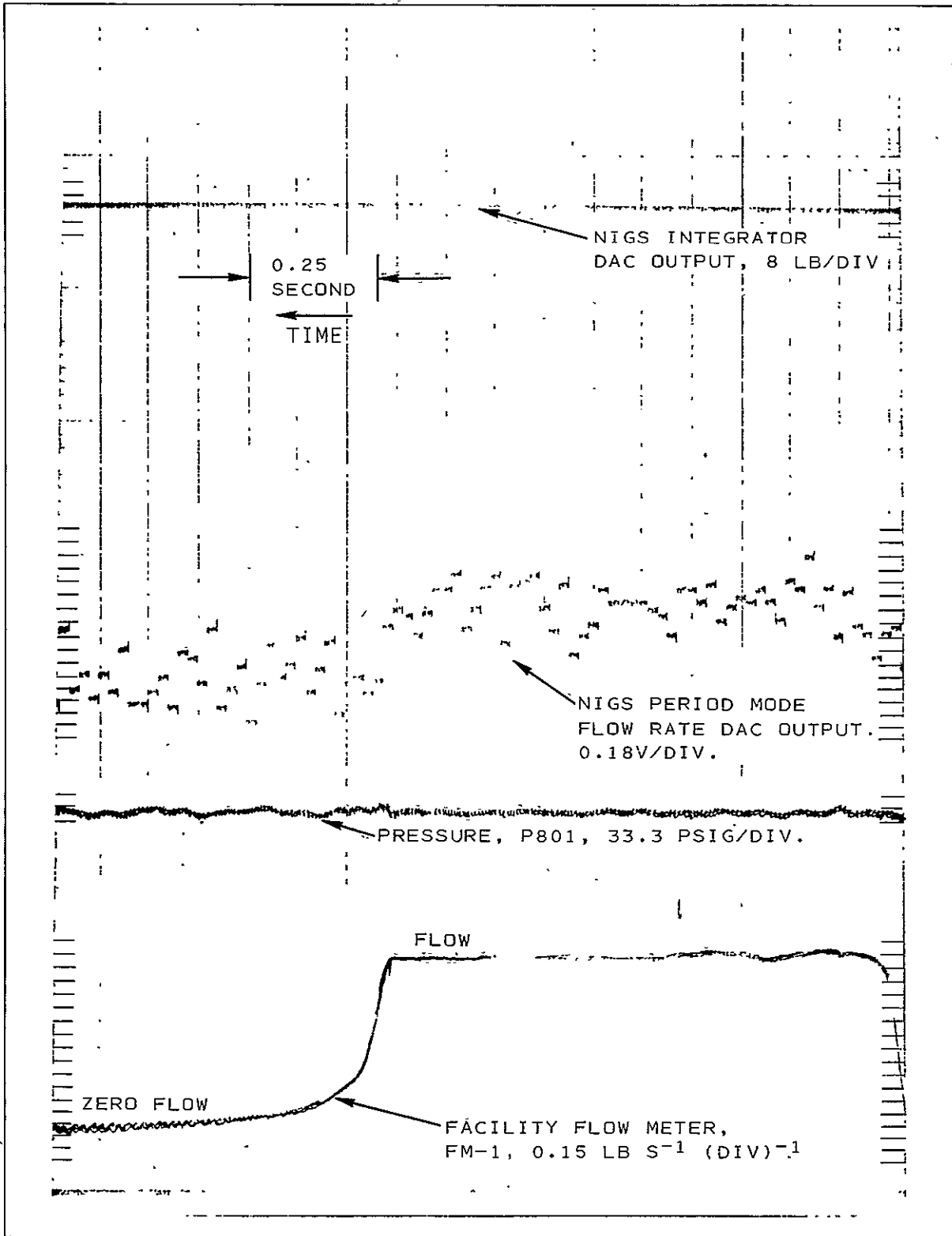FACILITY FLOW METER,
FM-1, 0.15 LB S^{-1} (DIV)$^{-1}$

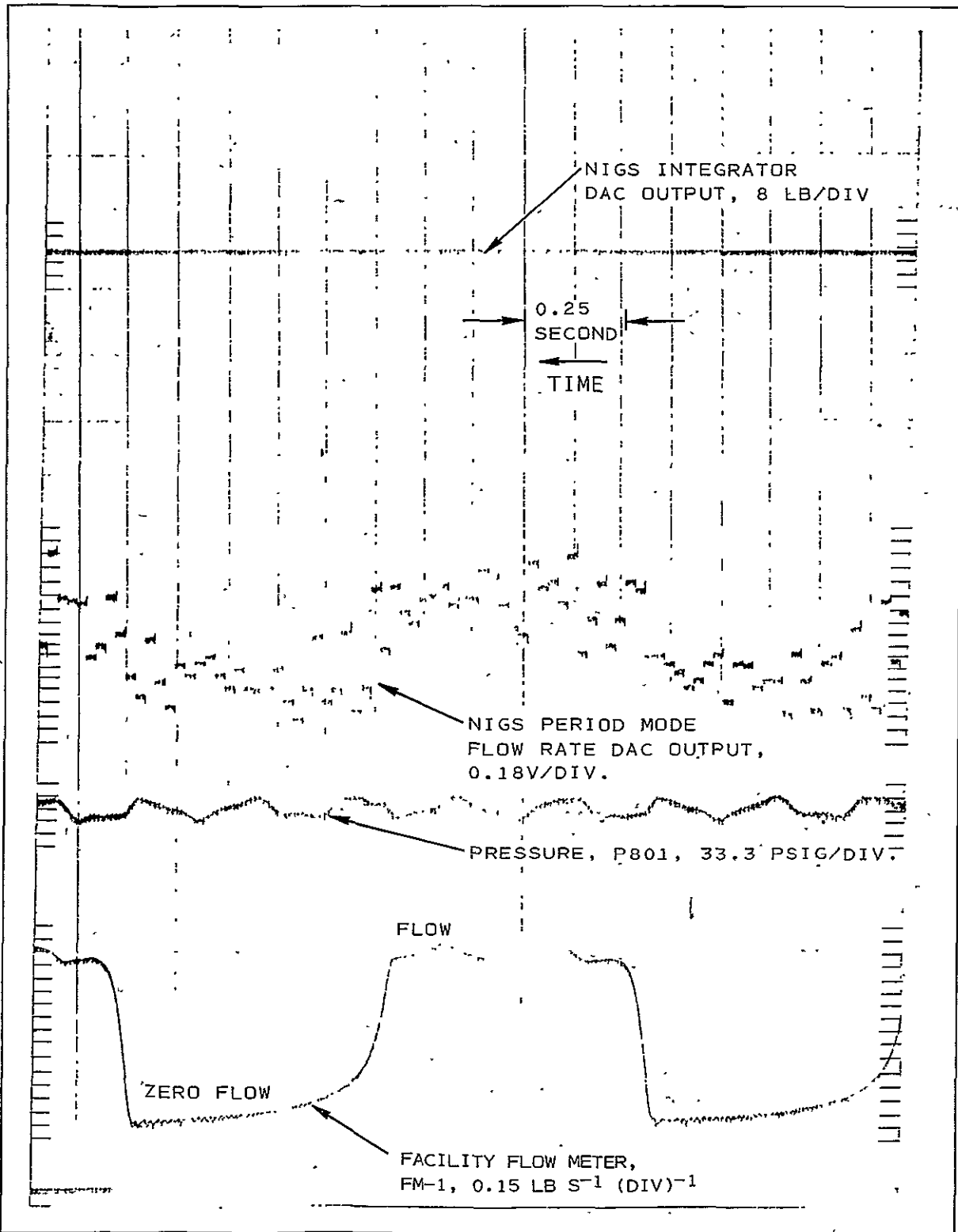*Figure 9-12.   Start of Run 124.   Phase mode test with 5 Hz flow pulses.   Peak
flow rate was about 2.2 pounds per second.*

Figure 9-13. End of Run 125. Phase mode test with 5 Hz flow pulses. Peak
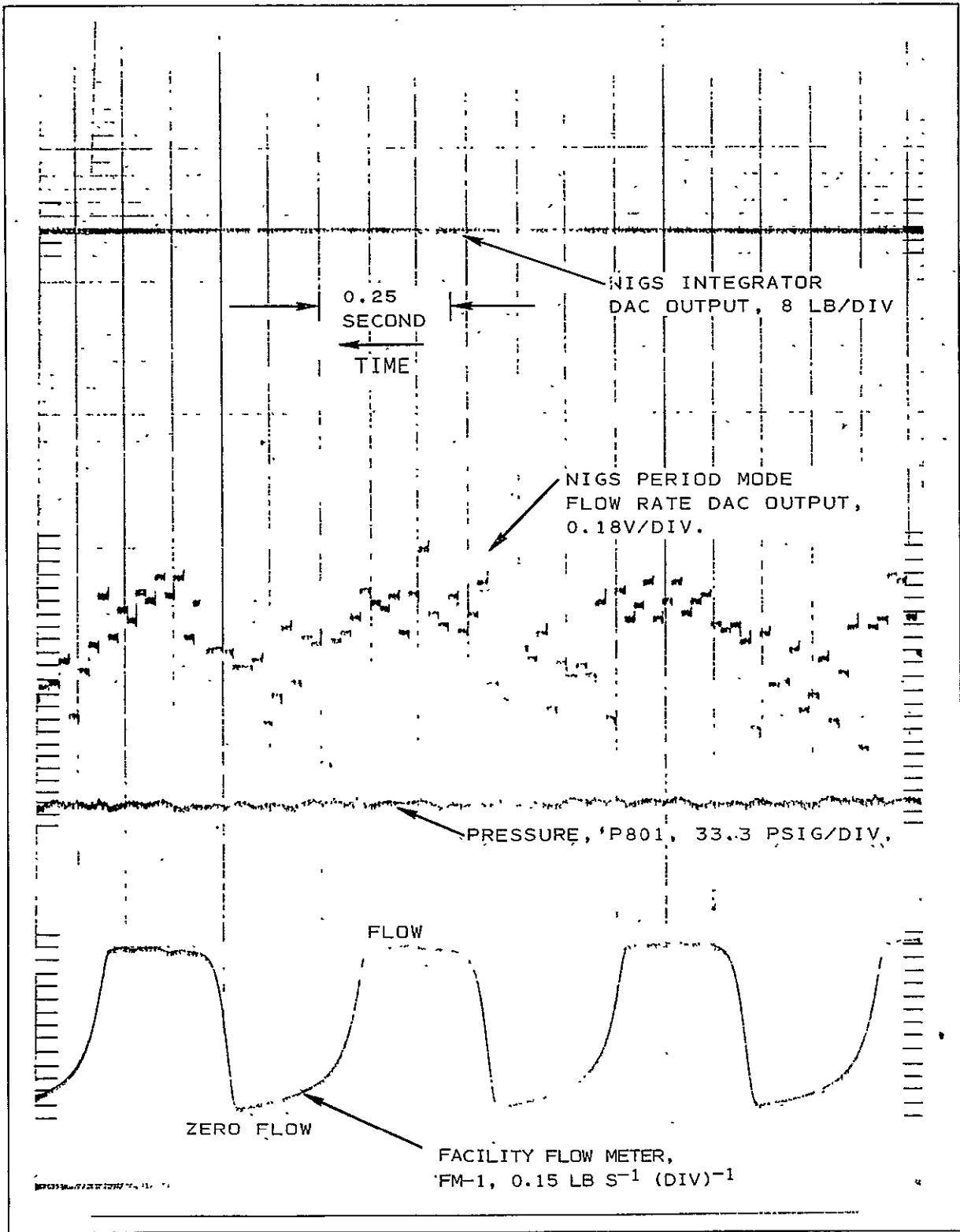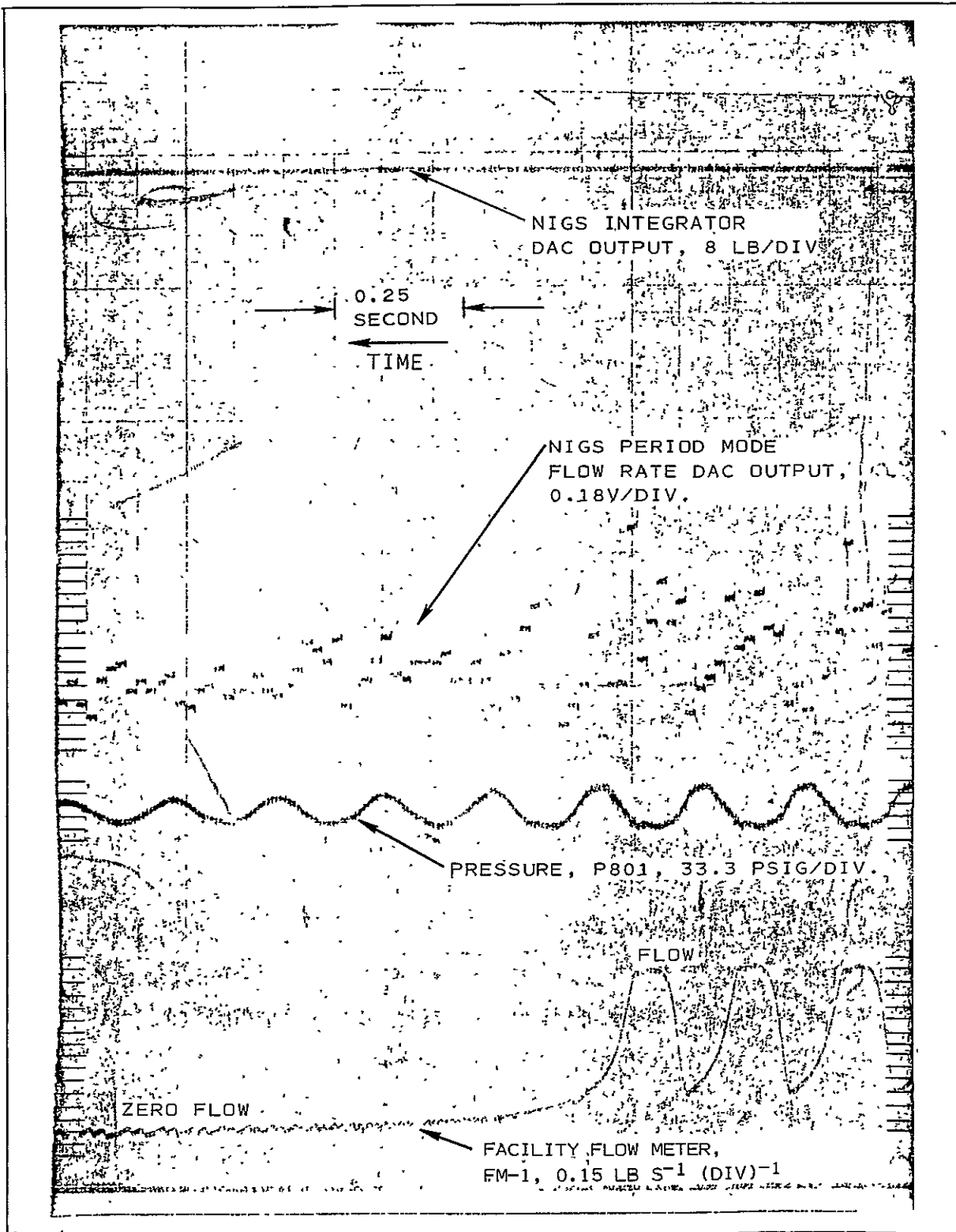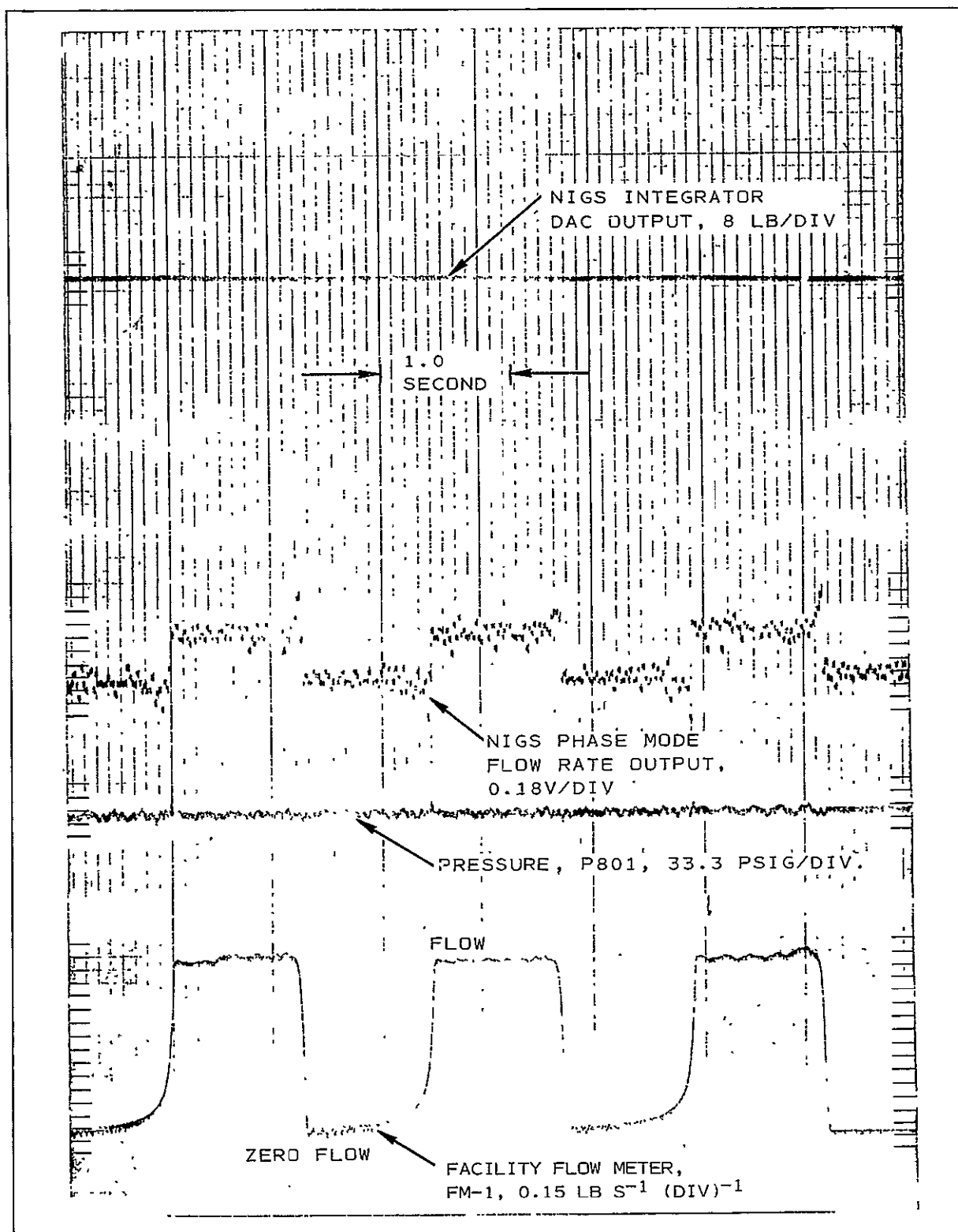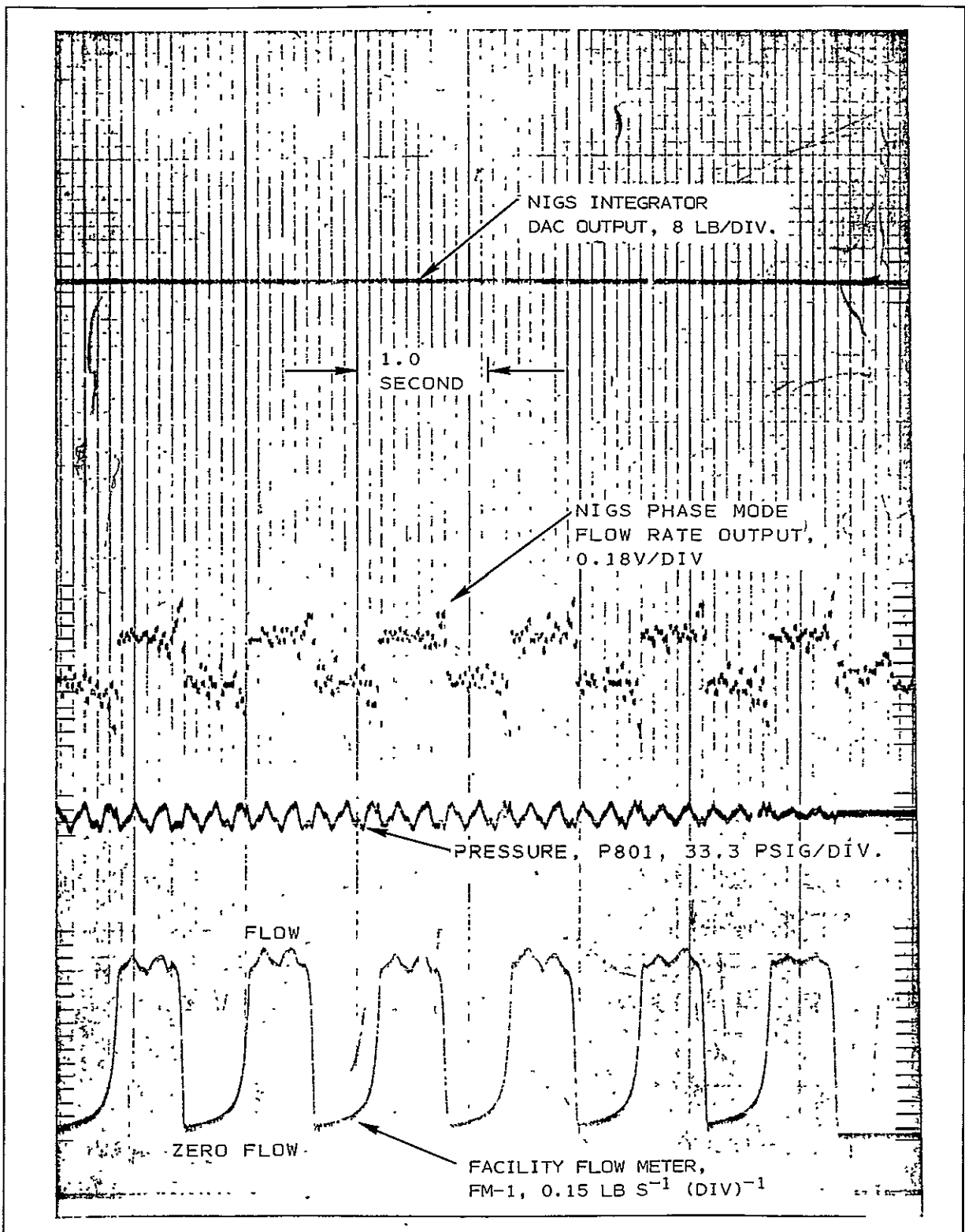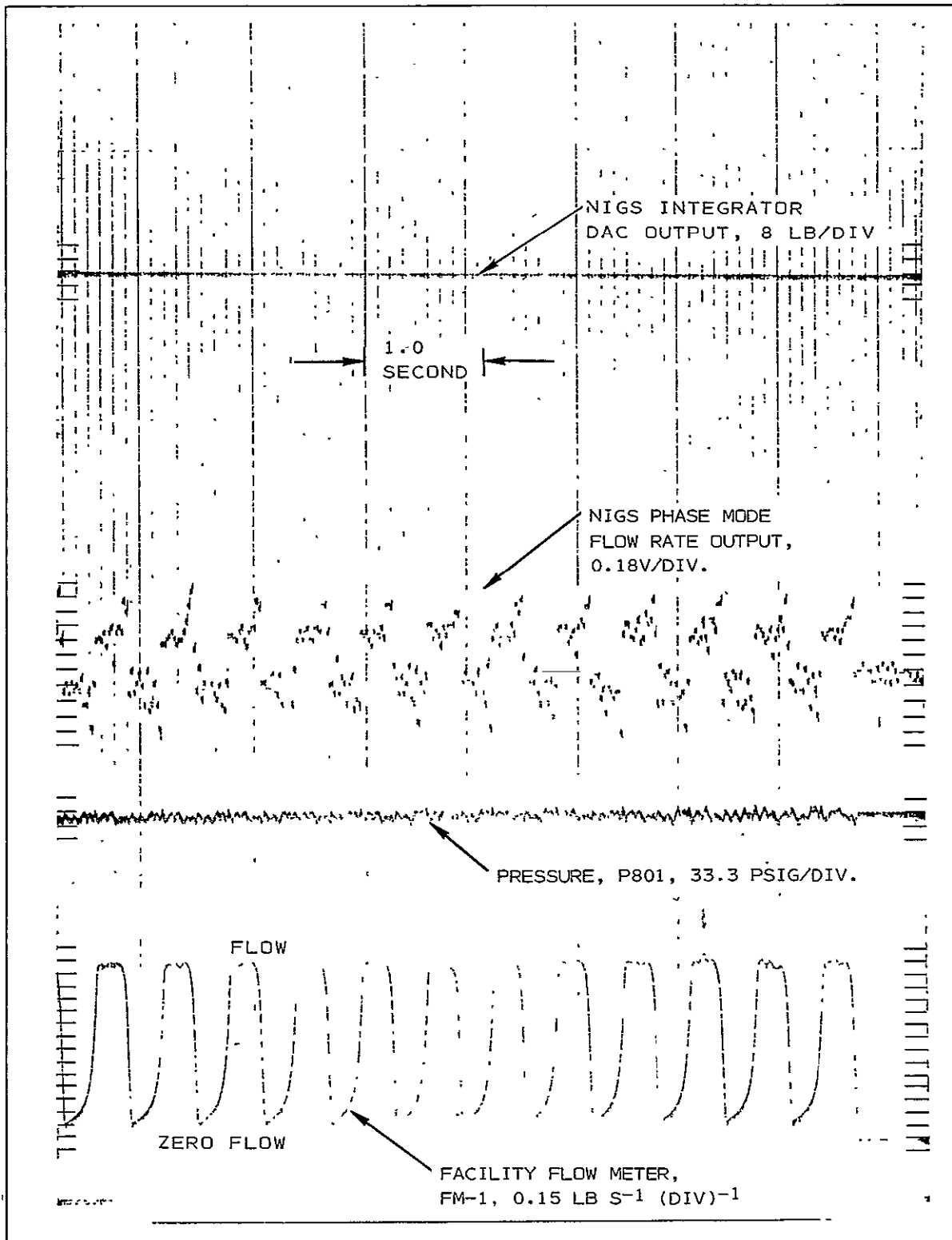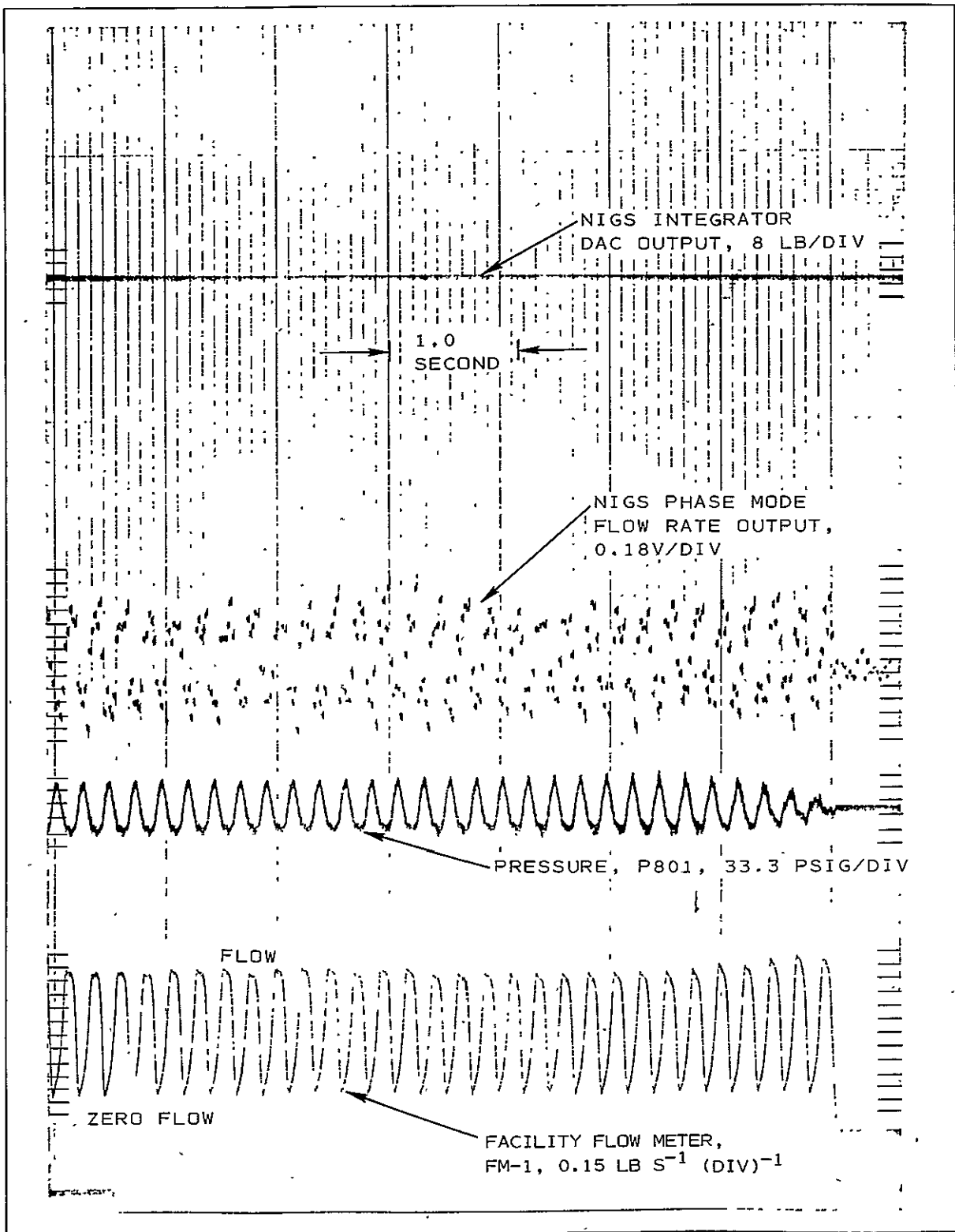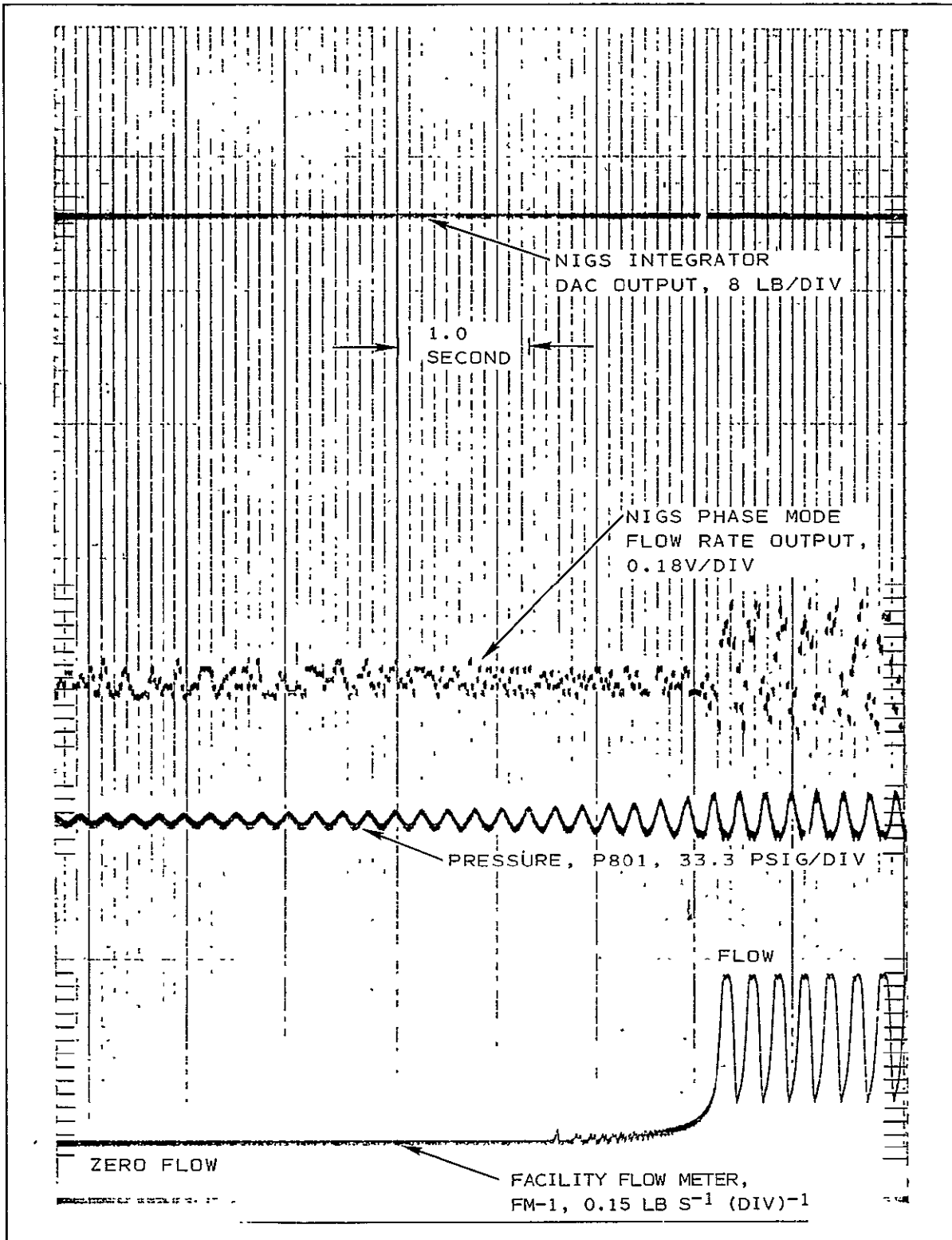flow rate was about 2.2 pounds per second.

9D   NOISE IN THE FLOW RATE DAC OUTPUT

The random noise in the flow velocity measurement is of considerable theoretical interest, although the basic requirement for monitoring the RCS fuel and oxidant consumption permits cancellation of random noise by integration. The noise is best shown in FIGURES 9-14 and 9-15 for the period- and phase-mode of operation, respectively. The period-mode noise shown in FIGURE 9-14 is believed to be essentially correct. The higher noise shown in FIGURES 9-5 through 9-8 is believed to have been due to an oscillograph interconnection problem, and/or due to a thermal problem with the digital electronics which were being turned on and off during those runs to prevent over-heating.

FIGURE 9-14 is a composite of the end-flow transients obtained for the runs indicated. The system pressure ring at 5 Hz, which occurred for every valve closure, is apparent. The NIGS integrator output is noise free, although the flow rate DAC output shows about 20% of reading peak noise at the higher flow rates. At zero flow, the peak noise is 5% of full-scale flow output, which is in remarkable agreement with the theoretical noise for the period mode output calculated from Equation (7D). Specifically, the noise estimate for an IF signal-to-noise ratio of 100 for the parameters employed in the subject test is 3% peak. This error stems from jitter in the IF signal zero crossing when the SNR ratio is only 100.

FIGURE 9-15 is a composite of the end-flow transients for phase-mode data obtained in the test runs indicated, plus one start-flow transient. The system rang when flow was started in run 133. This was not the normal response, and it is believed that a large air bubble was trapped between the shut-off valve and the NIGS flow cell. Both the facility flowmeter (FM-804) and the NIGS flow rate DAC outputs rang when the flow started, and it is believed that an oscillatory flow actually occurred.

The phase-mode noise is shown to be no more than $\pm 3\%$ of full scale in the records of FIGURE 9-15. An estimate of the peak noise, based on an expression derived in the Appendix, is 0.7% for the phase mode, using the assumptions used in estimating the period-mode noise discussed above. Randomly varying noise in the zero flow output in both modes of operation strongly suggests that there was about 2% of scale noise due to a faulty output DAC. In particular, the noise at zero flow was often much larger than it was when the zero was deliberately offset. While the phase-mode noise at full-scale flow is noticeably different from that at zero flow, the peak noise is not twice as large. It is not obvious why the phase-mode noise is less affected by flow rate than the period-mode noise, since the digital measurement techniques are quite similar. The major differences in the measurements made are due to the use of different clock frequencies, and the difference in duration of the counting times. The phase-mode circuit counted a 4-MHz clock for a nominal time of 0.25 ms for each T/R half cycle. The period-mode circuit counted a 20 MHz clock for a nominal time of 2.5 ms for each T/R half cycle. It seems possible that there was a problem in one of the DCA registers that resulted in degraded digital difference capability for the larger nominal period-mode count. The difference counts were made roughly equal for the two modes by using different clock
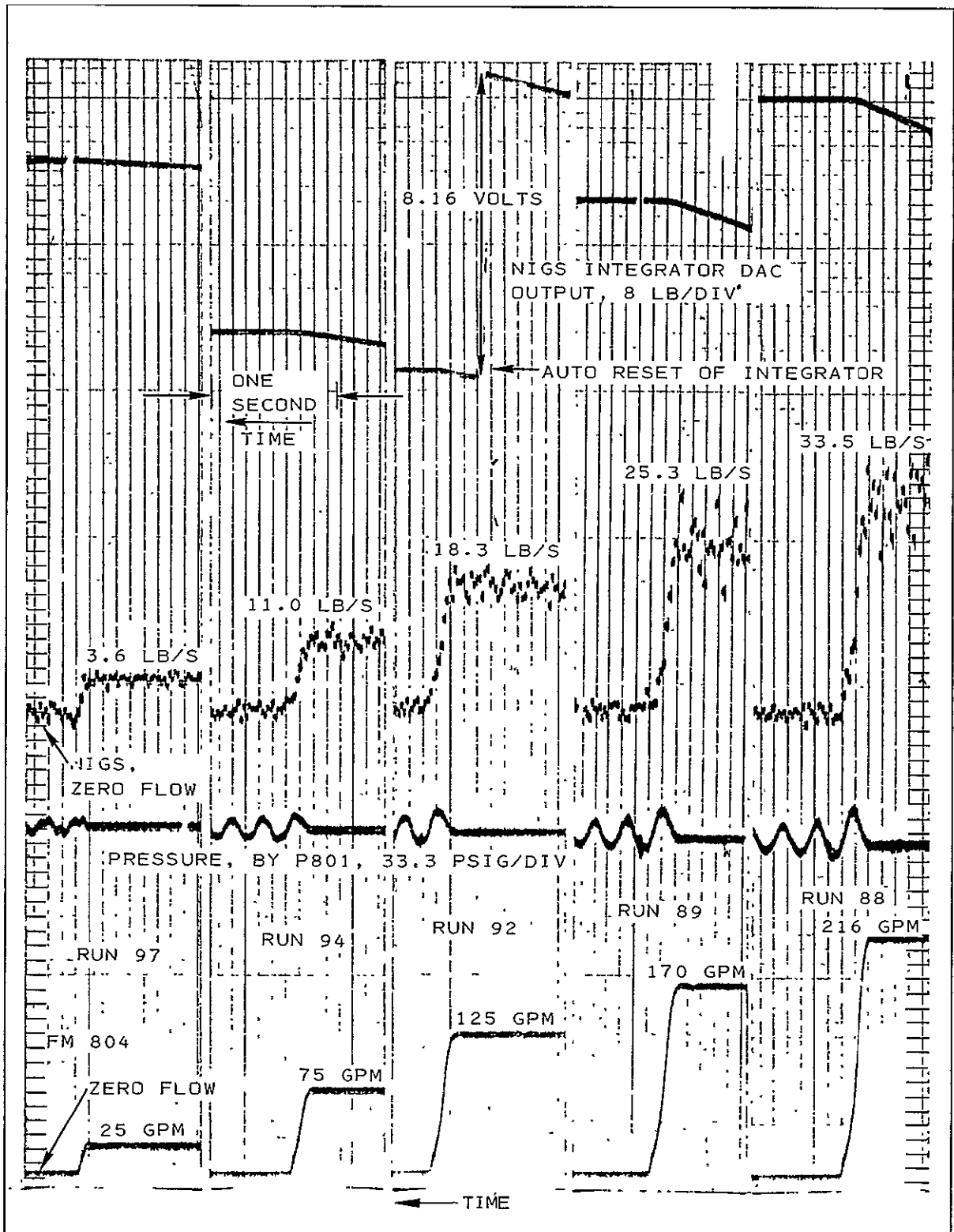
Figure 9-14. *Ends of Runs (Noted) in Linearity and Noise Tests for Period Mode on 27 May.*
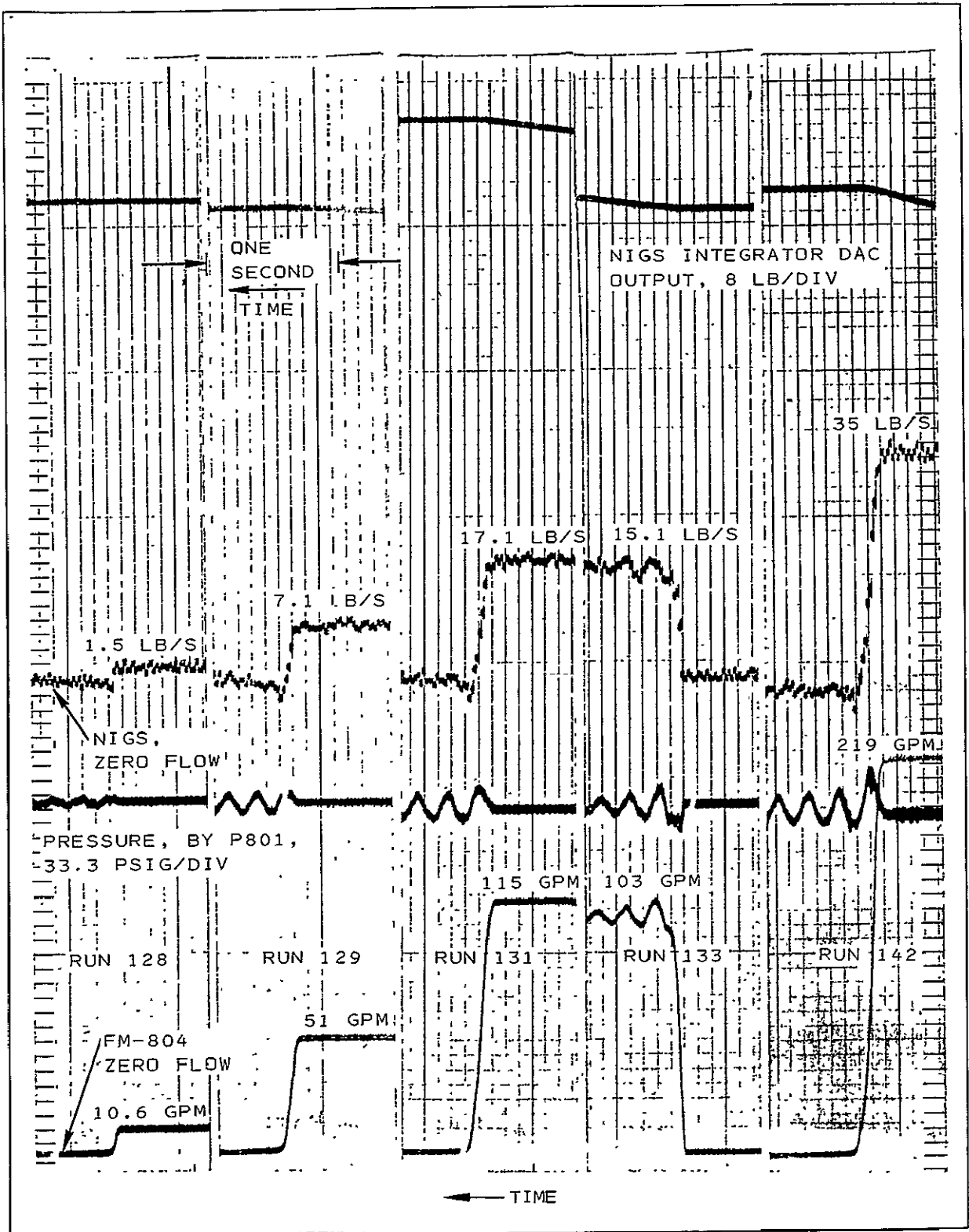
Figure 9-15. Ends of Runs (Noted) in Linearity and Noise Tests for Phase Mode on 28 May, Plus Start of One Run.

9-32

periods, but the nominal count for the period mode was fifty times greater than for the phase mode. The details shown by FIGURE 9-14 support this hypothesis. Specifically, the noise levels at 11 and 15 kg/s (25 and 33 lb/s) are almost identical, and they are both more than twice as large as the noise level at 6.03 kg/s (13.3 lb/s).

It is concluded from consideration of all test results that the noise of the frequency chirp system is significantly lower than that for other ultrasonic systems. The discrimination against flow-generated noise shown by the phase mode was especially gratifying. It is also concluded that the parameters that affect the noise are well understood, and that optimization of design parameters can be made for any given set of operational requirements. It appears that the phase mode will provide optimum performance for applications requiring minimum output noise. Specifically, the 28 May tests demonstrated that an rms noise of 2% of full scale with 50-Hz output bandpass (20 ms DAC updates) had been achieved by the prototype, and that two-thirds of this noise was probably due to a faulty output DAC. Furthermore, the tests were performed with a 20-ms data rate only to provide data directly comparable to that previously obtained in the period mode of operation, and to assure that the digital display was also updated. The phase readings for each ramp were actually obtained in about 3 ms, meaning that the output bandpass could have been at least 167 Hz (6 ms data updates) without significantly increasing the noise.

9E   TEST WITH SLUG OF HOT WATER IN LINE (29 APRIL)

The TTA flow system included a section of large diameter pipe about 0.91 meter (3 feet) long which could be heated. Test time constraints permitted only one test to be performed. Run 32 was made on the afternoon of 29 April, about one hour after the pulsed flow tests (runs 22 through 30 plus run 31, which was aborted) were completed.

Two thermocouples were used to monitor the temperature of the water. One was located in the heated pipe section (T800) and the other between the heated section and the NIGS flow cell (T801). The water temperature in the previous tests had been 21.7°C (71°F). The heater was left on until T800 indicated 27.8°C (100°F) and T801 indicated 32.2°C (90°F). The pneumatically operated valve was opened into the catch-weigh system with the throttle valve still set as it was in the previous runs. The calculated average flow rate was 0.93 kg/s (14.8 gpm) for a total mass transfer of 167.5 kg (368.5 lb, or 44.4 gal) in three minutes. The two temperatures were T800 = 23.3°C (74°F) and T801 = 22.2°C (72°F) at the time the flow was stopped.

It is unfortunate that this test could not be repeated in May when the speed of sound (C-DAC) output was available. This would have provided directly comparable records of the effect of temperature on both the C-DAC and flow rate DAC outputs. For the test conducted, the best indication of any effect is the slope of the integrator output.

In the period mode of operation the variations in the speed of sound should not affect the sensitivity. This, however, is true only for the ideal system,

having perfectly uniform IF cycle periods and having no change in the speed of sound between successive T/R half cycles. A 16.7°C (30°F) change in steady-state water temperature would cause a dc/c change of about 4%. Operating at $f_o = 0.75$ MHz as it was in this test, the IF may have shifted through up to three full cycles. It is known that there would be no appreciable effect at zero flow, but at 7% of full-scale flow the sensitivity might be expected to shift several percent of reading (either positive or negative) at each temperature corresponding to multiples of π radians phase shift. Actually, it is estimated that the maximum temperature within the flow cell was less than 37.8°C (100°F) due to mixing at pipe diameter changes ahead of the flow cell and due to heating of the cool pipes ahead of the flow cell. The average for the total mass transferred was probably less than 26.1°C (79°F) since the slug heated to 37.8°C (100°F) was probably less than one-fourth of the volume transferred. This combination of factors might even have prevented phase shifts beyond that for which the system was capable of providing uniform sensitivity, but changes in slope of the integrator output suggest that steps in sensitivity did occur. A step could be expected for roughly each 3.3°C (6°C) thermal change, and an actual temperature variation between 22.2° and 28.9°C (72° and 84°F), and back, during the three-minute run does not seem improbable.

The rate of change of the water temperature with time is also a potential source of error, in accordance with Equation (8C). If the temperature of the water in the flow cell increased more rapidly than it decreased, the indicated flow rate would be high.

The integrator output slope (proportional to flow rate) was determined by segments. The plot of FIGURE 9-16 shows ten regions of approximately constant slope of varying duration, in bar-graph form. Large air bubbles passed through the flow cell between 62 and 66 seconds after the flow started. These bubbles were confirmed visually at the catch-weigh tank. Large bubbles decrease the received RF and the IF signals to the point where the IF comparator randomly makes square waves out of the residual noise. The effect due to the bubbles was a large negative flow rate indication and a corresponding offset in the integrator output during the four-second bubble-passage time.

The flow rate DAC output (and the actual flow rate) of the TTA system decreased with time in every run made due to a drop in gas pressure as the water was delivered. It is not known what portion of the decline in mean flow rate (integrator slope) should be assigned to this factor, but the dashed-line curve suggests a plausible rate of actual flow decrease, starting with the mean of the first three measured slopes (0 to 43 seconds). The effect of the hot water is apparently discernible. Specifically, the gas bubbles would have been liberated from the stagnant water as it was heated. Logically, the rapid thermal gradient would have reached the flow cell either just before or with the bubbles. Recalling that the water was 32.2°C (90°F) at T801, between the heater and the flow cell, the large drop in apparent flow rate that occurred at about 43 seconds was probably due to IF cycle "skipping" caused by increasing temperature. An additional output offset due to the rate of increase of flow cell temperature may account for part of the rise in output after 43
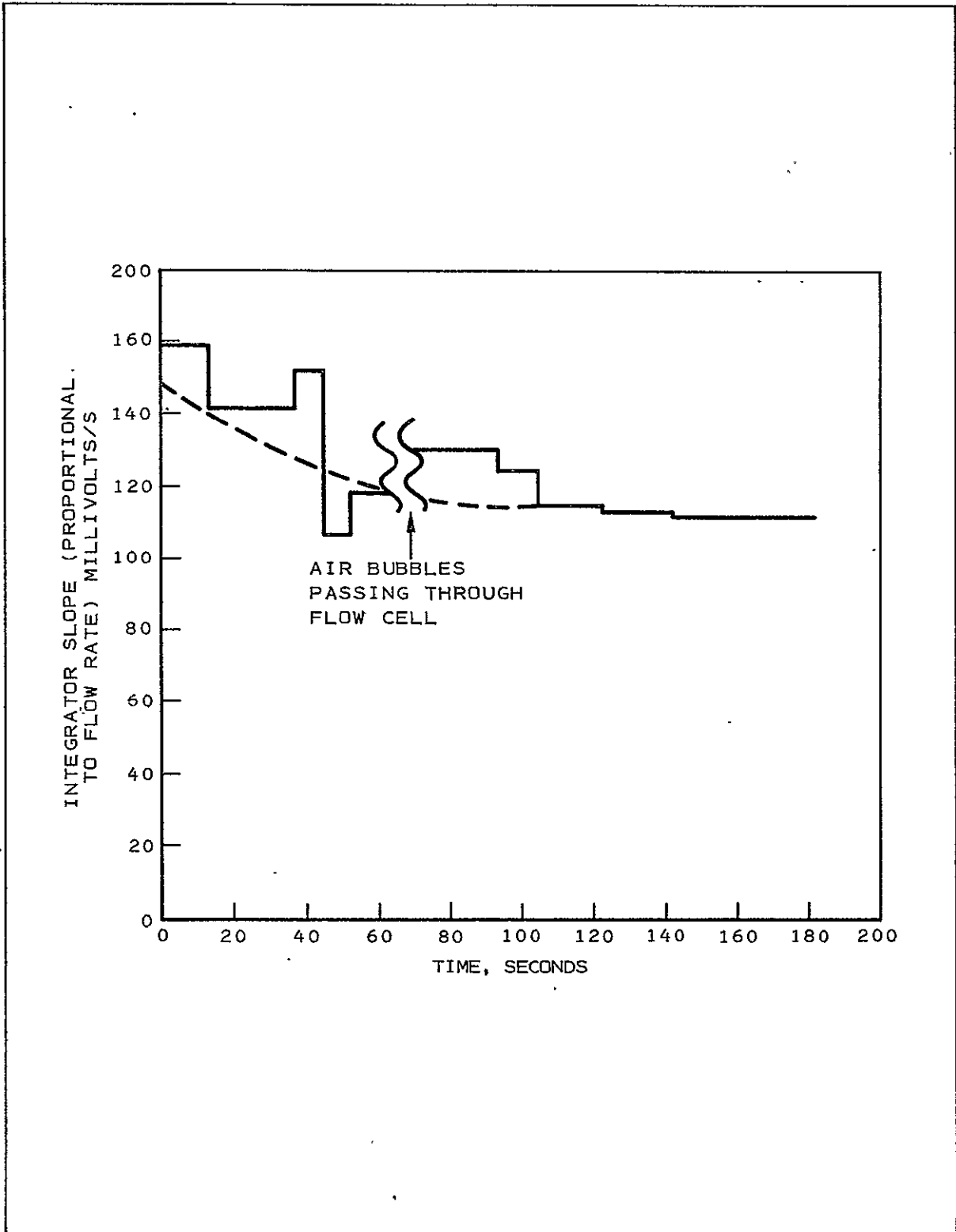
Figure 9-16. Changes of Integrator Output Slope (Proportional to Flow Rate). A "slug" of water at 100°F passed through the NIGS flow cell.

seconds. The time of slowly varying peak temperature was probably between about 65 seconds (including some air bubbles) and about 90 seconds. The two major step decreases that occurred at 92 and 103 seconds may be indicative of skipping of IF cycles as the nominal phase shifted through multiples of π radians as the temperature decreased. The steps at 12 and 36 seconds may have been due to small air bubbles that formed in the stagnant water near T801, which was at 32.2°C (90°F) at the start of the test.

The mass transfer indicated by the NIGS integrator in run 32 was 180.7 kg (397.6 lb), using the mean sensitivity for runs 22 and 23. This is 7.9% larger than the actual weight transferred, measured by the catch-weigh system. (This is equivalent to only 0.6% of full-scale flow rate error.) It seems probable that part of the error was due to cycle skipping, but the deviation for replicate runs (22 and 23) at this low flow rate was itself 3%. It is possible, therefore, that the hot slug of water had no significant direct effect.

Finally, it should be noted that the density change for water in the 21.1° to 37.8°C (70° to 100°F) range is very slight. The maximum error due to ignoring the density variation in converting from flow velocity to mass flow rate would be 0.3% for a 16.6°C (30°F) change. A thermal change of density, therefore, cannot account for the effect observed.

BIBLIOGRAPHY

Rozenberg, L.D., "Physical Principles of Ultrasonic Technology," Volume 1, Plenum Press, New York-London.

El'piner, Isaak Efimovich, "Ultrasound — Physical, Chemical, and Biological Effects," Consultants Bureau, New York, 1964.

Mason, Warren P., "Physical Acoustics — Principles and Methods," Volume 1, Part A, Academic Press, New York-London, 1964.

Pajewski, W., "Piezoelectric Transducers with a Face Plate," *Ultrasonics International,* pp 303-308, London, March 1973.

Keramos, Inc., "Kezite — Lead Metaniobate Ceramic K-81," Bulletin 7001, 104 North Church Street, Lizton, Indiana.

Goll, Jeffrey H. and Bertram A. Auld, "Multilayer Impedance Matching Schemes for Broadbanding of Water Loaded Piezoelectric Transducers and High Q Electric Resonators," *IEEE Transactions on Sonics and Ultrasonics,* Volume SU-22, 1, January 1975.

Kossoff, George, "The Effects of Backing and Matching on the Performance of Piezoelectric Ceramic Transducers," *"IEEE Transactions on Sonics and Ultrasonics,* Volume SU-13, 1, pp 20, March 1966.

Frederick, J.R., *Ultrasonic Engineering,* pp 363, John Wiley & Sons, Inc., New York, 1965.

Goldman, Richard, *Ultrasonic Technology,* Reinhold Publishing Corporation, New York; Chapman & Hall, Ltd., London.

APPENDIX

DERIVATION OF DESCRIPTIVE EQUATIONS

A1   IDEALIZED FREQUENCY CHIRP SYSTEM

Two transducers are assumed to be positioned on opposite sides of a flow conduit (FIGURE A-1A) with the line connecting their centers (the sonic path) at an angle, α, with respect to the axis of flow through the conduit. It is assumed that the transducers are alternately switched into transmit and receive modes by the T/R switches shown in the illustration. The frequencies of the transmitted and received signals are as indicated in FIGURE A-1B for zero flow, and as indicated (in exaggerated proportions) in FIGURE A-1C when flow from transducer A toward transducer B óccurs. The sonic velocity for transmission between the two transducers is the vector sum of the speed of sound in the medium and the flow velocity component resolved along the sonic path. The symbols to be employed in the derivations are defined as follows:

     L = sonic path length between transducers

     C_o = speed of sound in the flowing medium

     F = flow velocity. A uniform velocity will be assumed for the idealized system. This assumption was justified by test results.

     $v = F \cos \alpha$ = vector flow velocity component along the sonic path

     $C = C_o + v$ = vector flow velocity

     τ = sonic transit time = L/C. In the interests of clarity, it will be assumed that the total path, L, is affected by flow for the idealized system. (The effect of "inactive" portions of the path is to reduce the sensitivity slightly.)

     T_r = time duration of each transmit/receive (T/R) half cycle

     T_p = time duration of flow pulse, assumed to be rectangular. The minimum value of T_p is 40 ms for current NIGS specifications.

The transmitted signal frequency (for either direction) is expressed as follows:

$$f(t) = f_o + f_m t$$

The instantaneous phase of the signal is as follows:

$$\theta = 2\pi \int_o^t f(t)dt = 2\pi \left(f_o + \frac{f_m t}{2}\right)t$$

A. *Illustration of Ultrasonic Flow Meter Cell and T/R Switches for Alternate T/R Cycles*
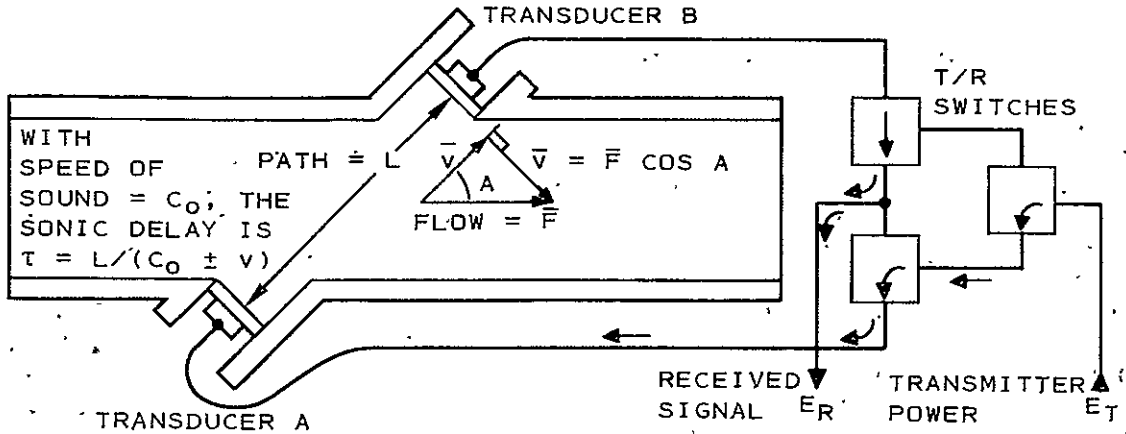
TRANSDUCER B

T/R SWITCHES

WITH SPEED OF SOUND = c_O; THE SONIC DELAY IS $\tau = L/(c_O \pm v)$

PATH = L $\bar{v}$ $\bar{v} = \bar{F} \cos A$

FLOW = $\bar{F}$

RECEIVED SIGNAL E_R

TRANSMITTER POWER E_T

TRANSDUCER A

B. *Transmitted and Received Signals vs Time for Zero Flow*

SIGNAL, E_T (AB), TRANSMITTED BY A TO B

SIGNAL, E_T (BA), TRANSMITTED BY B TO A

SIGNAL, E_T (AB), TRANSMITTED BY A TO B

SLOPE = f_m

f_{IF} (AB)

f_{IF} (BA)

f_{IF} (AB)

FREQUENCY

f_o

τ_{AB}

τ_{BA}

τ_{AB}

SIGNAL, E_R (B), RECEIVED BY B

SIGNAL, E_R (A), RECEIVED BY A

$\tau_{AB} = L/c_O$

$\tau_{BA} = L/c_O$

0   T_R 2 T_R 3 T_R

TIME

C. *Transmitted and Received Signals vs Time With Flow (Exaggerated) from A Toward B*

E_T (AB)

E_T (BA)

SLOPE = f_m

$f_{IF(AB)}$

$f_{IF(BA)}$

$f_{IF(AB)}$

τ_{AB}

τ_{BA}

τ_{AB}

E_R (B)

E_R (A)

$\tau_{AB} = \dfrac{L}{c_O + v}$

$\tau_{BA} = \dfrac{L}{c_O - v}$

T_R 2 T_R 3 T_R
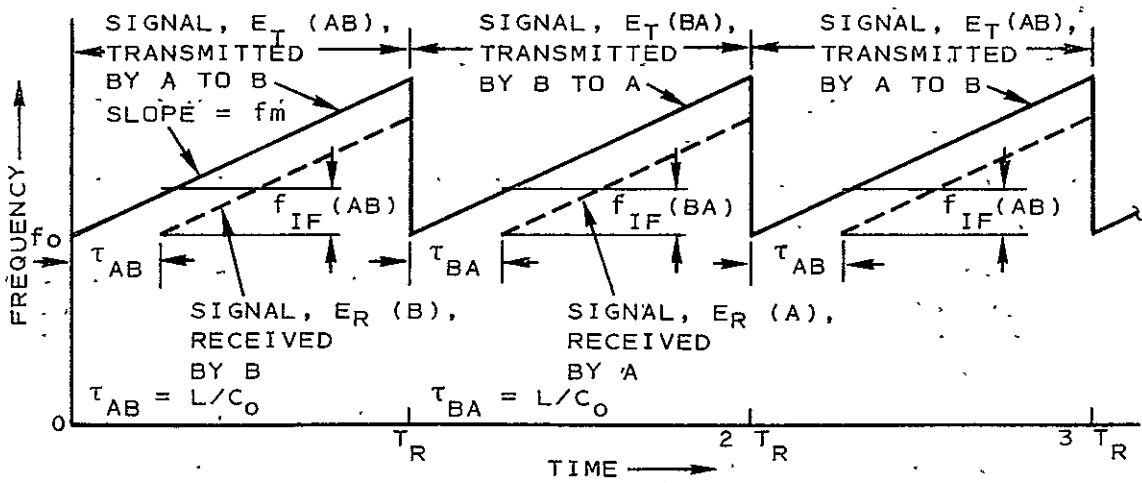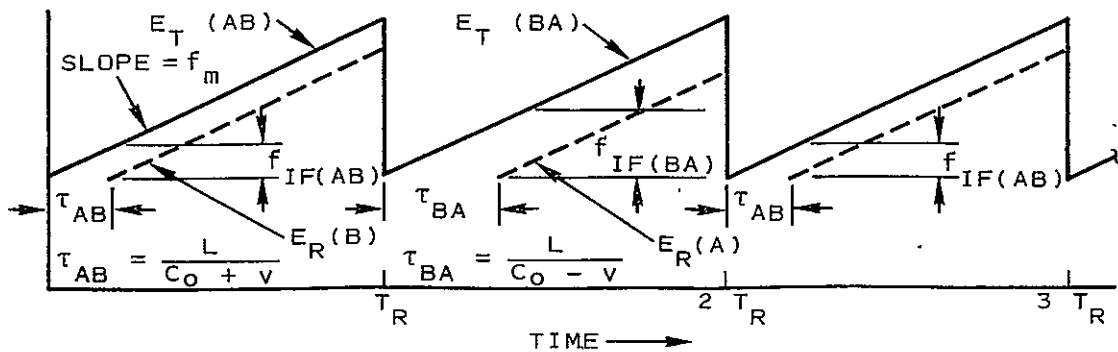
TIME

Figure A-1. Typical Flow Cell Design and Frequency versus Time Plots for the Frequency Chirp System.

The transmitted signal, assuming constant amplitude, is as follows:

$$e_t = E_t \cos 2\pi\left(f_o + \frac{f_m t}{2}\right)t \qquad (1C)$$

The received signal is that transmitted, time-shifted by the transit time, τ, and attenuated in amplitude as follows:

$$e_r = E_r \cos 2\pi\left[f_o + \frac{f_m}{2}(t-\tau)\right](t-\tau) \qquad (1D)$$

Constant amplitude is assumed for simplicity. The actual case was considered only when and as necessary to obtain a better understanding of test results.

If a fraction of the transmitted voltage is multiplied by the received signal and filtered to pass the low side band only, the resulting signal is a function of the cosine of the difference of the instantaneous phase angles of the two multiplied signals (by trigonometric identities). This intermediate frequency (IF) may be expressed as follows:

$$e_m = E_m \cos 2\pi\left[f_m \tau t + \left(f_o - \frac{f_m}{2}\tau\right)\tau\right] \qquad (1E)$$

It follows from Equation (1E) that the IF signal has both frequency and phase which are functions of the sonic transit time, τ. The frequency of the IF signal is as follows:

$$f_{IF} = f_m \tau = f_m L/C \qquad (1F)$$

The phase of the IF signal is as follows:

$$\phi = 2\pi\left(f_o - \frac{f_m}{2}\tau\right)\tau = 2\pi\left(f_o - \frac{f_m L}{2C}\right)\frac{L}{C} \qquad (1G)$$

A2   THE CHARACTERISTICS OF THE IF PERIOD

A2-1   Measurement of Flow by Difference of IF Periods

The difference in sonic transit times for the two directions is measured by taking the difference of the IF periods, which are the reciprocals of the corresponding frequencies:

$$\Delta P = \frac{1}{f_m \tau_{ab}} - \frac{1}{f_m \tau_{ba}} = \frac{C_o + v}{f_m L} - \frac{C_o - v}{f_m L} = \frac{2v}{f_m L} \qquad (2A)$$

The quantity, v, can be measured independent of C_0 by this approach. If the difference of frequencies is taken, the measured ΔP depends on C_0^2. The period may be measured by digitally counting a clock of frequency f_c between successive zero crossings of the IF signal to obtain a number of counts proportional to the period. If the clock is counted between zero crossings which define n IF cycles, then the clock counts for transmission from transducer A to B and _vice versa_ are as follows:

$$N_{ab} = \frac{f_c n}{f_m \tau_{ab}} = \frac{f_c n}{f_m L} (C_0 + v) \text{ and } N_{ba} = \frac{f_c n}{f_m L} (C_0 - v) \qquad (2B)$$

The difference in counts, corresponding to the difference in IF periods for the two directions of transmission, is as follows:

$$\Delta N_p = \frac{2f_c n}{f_m L} (v) = \frac{2f_c n}{f_m L} \frac{\cos\alpha}{\rho A} (M) \qquad (2C)$$

Where A is the cross-sectional area of the conduit, ρ is the density, and M is the mass flow rate of the medium.

A2-2   <u>Period Mode Errors and Signal-to-Noise Ratio</u>

The idealized IF period, as measured, is given by Equations (2B). Using standard differential calculus techniques, the change in counts due to variations in all parameters is as follows:

$$dN = \frac{\delta N}{\delta f_c} df_c + \frac{\delta N}{\delta f_m} df_m + \frac{\delta N}{\delta L} dL + \frac{\delta N}{\delta C_0} dC_0 + \frac{\delta N}{\delta v} dv \qquad (3A)$$

$$= \frac{n}{f_m L} (C) df_c - \frac{f_c n}{f_m^2 L} (C) df_m - \frac{f_c n}{f_m L^2} (C) dL + \frac{f_c n}{f_m L} dC_0 + \frac{f_c n}{f_m L} dv$$

The desired signal is that due to changes in v, and the difference in counts for the two directions of sound transmission is twice that for one direction. Equation (2C), for the signal, is obtained from Equation (3A) when terms not involving v are neglected and dv is replaced by $2v$, which is valid for values of v which are small compared to C_0. In view of Equation (2C), replacement of dv by $2v$ is valid for all values of v which are less than C_0. The peak noise and/or error of the measurement is due to twice all terms of Equation (3A) except that involving v. The signal-to-noise ratio for the period mode of measurement is, therefore:

$$SNR_p = \frac{\dfrac{f_c n}{f_m L} v}{\dfrac{n}{f_m L}(C)\, df_c - \dfrac{f_c n}{f_m^2 L}(C)\, df_m - \dfrac{f_c n}{f_m L^2}(C)\, dL + \dfrac{f_c n}{f_m L}\, dC_o} \qquad (3B)$$

$$= \frac{v}{C} \frac{1}{df_c/f_c - df_m/f_m - dL/L + dC_o/C}$$

This relationship indicates that the sum of all of the relative noises (or errors) in the parameters f_c, f_m, L, and C_o must be small compared to v/C_o if SNR_p is to be large. This interpretation of Equation (3B) is the absolute worst case, in that peak values of noise (or error) from all parameters are considered to be additive, and that the errors (or noise) are modulated at the T/R switching rate so that they are doubled by taking the difference of IF periods for successive T/R half cycles. Random noise (or errors) would contribute to the rms noise by the square root of the sum of their squares, and they would also tend to cancel when a flow rate is ·integrated over a period of time to obtain the total volume (or mass) transferred. The total mass transferred is the output of primary interest in the RCS application. However, modulation of f_m by EMI coupling from the T/R switch drive circuitry, for example, could cause systematic errors in the total flow (integrated output), which would be "amplified" by taking the difference of periods. Similarly, modulation of L by pressure variations at harmonics of the T/R cycle frequency would result in amplified, systematic errors. Transient variations in C might also be systematic if, for example, a systematic thermal transient occurred for each flow pulse. Steady-state (or very slow) thermal changes in C_o would not affect the period mode output, but significant changes of C_o that occur during a T/R cycle contribute to error (or noise) in accordance with Equation (3B). Using T_r for the time duration of each T/R half cycle, the relative error in dC/C arising from thermal transients is as follows:

$$\frac{dC}{C} = \frac{1}{C} \frac{dC}{dT} \frac{dT}{dt} T_r \qquad (3C)$$

If the fluid temperature is rising rapidly (increasing) it causes high period-mode readings.

For N_2O_4, the effect of temperature on the speed of sound is roughly 4×10^{-3} per degree Celsius. For $T_r = 0.01$ second, and C/v = 130 (maximum value at full-scale flow), the maximum allowable value of dT/dt for $SNR_p = 20$ may be calculated as follows:

$$\frac{dT}{dt} < \frac{v_{max}}{C} \times \frac{1}{\dfrac{1}{C}\dfrac{dC}{dT} \times T_r} \times \frac{1}{20} = 10°C/s, \text{ for } SNR_p > 20 \qquad (3D)$$

All other error (or noise) sources are neglected in arriving at ·inequality (3D). It is apparent that thermal gradients can be a problem unless the

gaging system is located in a position that makes systematic thermal transients smaller than 10°C/s. A ramp time of less than 10 ms will also be beneficial.

Variations in flow cell pressure will cause variations in L which might introduce significant errors. In particular, pulsed flow results in large "water hammer" transient pressures, and results in pressure "ringing" at the system resonant frequency. These pressure effects on L result in a relative path length error (or noise) given by the following:

$$\frac{dL}{L} = \frac{1}{L}\frac{dL}{dP}\frac{dP}{dt}T_r \qquad (3E)$$

If the flow cell pressure systematically rises more rapidly than it falls, the system provides low period-mode readings.

Equation (3E) may be used to calculate the spring constant of the flow cell and/or transducer mounts in terms of the maximum specified pressure transients, the parameter T_r, and the allowable error due to such modulation of dL/L.

Equation (3A) may be rearranged to reflect the errors as an additive term, which is a convenient expression for some purposes. By factoring the term of Equation (3A) involving v from all terms, and doubling all errors as well as the signal for a period difference measurement for the worst-case situation, one obtains the following:

$$\Delta N_p = 2\ dN_p = \frac{2vf_c n}{f_m L}\left[1 + \frac{C}{v}\left(\frac{dC_o}{C} - \frac{dL}{L} - \frac{df_m}{f_m} + \frac{df_c}{f_c}\right)\right] \qquad (3F)$$

This expression clearly illustrates that all errors in measurement of each period can be amplified by C_o/v in their effect on the difference of periods, which is the desired signal. Such amplification occurs in the worst-case situation for which the errors are synchronous, having maximum value and opposite sign for successive T/R half cycles and for thermal and pressure transients. It is also applicable to peak noise considerations, although random noise rms values are of greater significance. The total rms noise would be the square root of the sum of the squares of the individual relative rms noise values, which is significantly smaller than the peak, worst case, value.

It is now convenient to consider the complete expression for the mass flow output, which is the output required for the RCS system. From the second form of Equation (2C), and by analogy to Equation (3F), the mass flow rate expression is as follows:

$$\Delta N_p \text{ (mass)} = 2dN_p \text{ (mass)} \tag{3G}$$

$$= \frac{2f_c n \cos\alpha}{f_m LA\rho} \text{ (M)} \left[1 + \frac{C}{v}\left(\frac{dC_o}{C} - \frac{dL}{L} - \frac{df_m}{f_m} - \frac{df_c}{f_c} - \frac{dA}{A} - \frac{d\alpha}{\cot\alpha}\right) - \frac{d\rho}{\rho} \right]$$

The ratio of the vector sound velocity, C, to the flow velocity component, v, is used as the error multiplier as a matter of convenience, but C/v may be replaced by C $A\rho$/M cos α if desired. This expression is complete, in that variations of all parameters are included. The relative errors in cross-sectional area, A, and in angle, α, are also multiplied by C/v to cover the worst case of modulation at the T/R cycle frequency (and its odd harmonics). Variations in A and α which are synchronous with the T/R cycle could be amplified, since they will affect the apparent value of v measured at a constant M. In a flight system the correction for density variations will be made by measuring the speed of sound, independent of flow velocity, as the average of two successive IF periods for the two directions of transmission. The relative error (or noise) in density, $d\rho/\rho$, used in conversion of the average flow velocity component, v, to mass flow rate, M, would not be amplified by C/v if this approach is utilized. The major source of density variation and errors in its measurement will be thermal transients. The residual errors in M after correction for density in the proposed manner is discussed in the following paragraphs.

A2-3   Measurement of Density by Average IF Period

From Equation (2B), it is apparent that measurement of the average IF period for successive T/R half cycles will provide an output proportional to the speed of sound in the medium independent of the flow velocity. The expression may be written as follows:

$$\overline{N} = \frac{N_{ab} + N_{ba}}{2} = \frac{f_c n}{f_m L} (C_o) \tag{4A}$$

Since the sum, rather than the difference, of large numbers is taken, there is no error amplification as there was for the flow velocity output. The errors (or noise) are 130 times smaller, making them negligible for this measurement if they are made acceptable for the difference measurement. By application of principles of the differential calculus, the relative variations in average period counts is equal to that of the speed of sound in the medium as follows:

$$\frac{d\overline{N}}{\overline{N}} = \frac{dC}{\overline{C}} + \frac{df_c}{f_c} - \frac{df_m}{f_m} - \frac{dL}{L} \approx \frac{dC_o}{\overline{C}} \tag{4B}$$

where $\overline{C}$ is the constant nominal speed of sound for a given medium at the nominal temperature. As noted above, the variations in the parameters f_c, f_m, and L are negligible in a practical system capable of making the period mode flow velocity measurement.

Both the density and the speed of sound of a liquid may be described by polynomials of the temperature variation, T, about the nominal temperature. Using general functional notation, convenient expressions are as follows:

$$C = \bar{C}\left[1 + g(T)\right] \tag{4C}$$

$$\rho = \bar{\rho}\left[1 + h(T)\right] \tag{4D}$$

The bar-values are the constant values at a convenient nominal temperature, and T is the variation from this nominal temperature. The order of the functions $g(T)$ and $h(T)$ depends on the liquid properties, the temperature range, and the required precision of the approximation. Equation (4C) is solved for T, in a general sense, as follows:

$$T = g^{-1}\left(\frac{C}{\bar{C}} - 1\right) = g^{-1}\left(\frac{\Delta C}{\bar{C}}\right) \tag{4E}$$

where g^{-1} symbolizes solution of the polynomial for T as a function of the measured relative change in the speed of sound. From Equations (4B) and (4E),

$$T = g^{-1}\left(\frac{d\bar{N}}{\bar{N}_0}\right) \tag{4F}$$

where $\bar{N}_0$ is the constant nominal average period count. Substitution of Equation (4F) in (4D) yields the density as a function of the measured variable, $d\bar{N}/\bar{N}_0$, and constants as follows:

$$\rho = \bar{\rho}\left[1 + h\left\{g^{-1}\left(\frac{d\bar{N}}{\bar{N}_0}\right)\right\}\right] \tag{4G}$$

The average mass flow rate, M, may be computed for each successive pair of T/R half cycles using Equation (3G), and substituting the density, ρ, computed from Equation (4G). The two computed quantities are obtained as the sum and difference of the directly measured IF periods for each half cycle. The density correction, therefore, should be excellent.

The final expression for M for the period mode of flow measurement may be obtained from Equations (3F) and (4G), and by solving for M as follows:

$$M_p = \Delta N_p \frac{f_m L A \bar{\rho}}{2 f_c n \cos\alpha} \cdot \frac{1 + h\left[g^{-1}\left(\frac{d\bar{N}}{\bar{N}_0}\right)\right]}{1 + \frac{C}{v}\left[\frac{dC_0}{C} - \frac{dL}{L} - \frac{df_m}{f_m} + \frac{df_c}{f_c} - \frac{dA}{A} - \frac{d\alpha}{\cot\alpha}\right] - \frac{d\rho}{\rho}} \tag{4H}$$

The expression in the denominator involving C/v is the noise (or error) contribution from the various parameters which must be made negligible. The error

due to $d\rho/\rho$ is not amplified by C/v, and must also be made negligible. The function $h(g^{-1})$ in the numerator is the density correction that must be calculated from the single variable $d\bar{N}$, which is the variation of the average IF period about its nominal (constant) value, $\bar{N}_o$. The only other variable is ΔN_p, which is the number of clock counts obtained as the difference of the measured IF periods for successive T/R half cycles.

A2-4   Inherent Resolution for the Period-Mode

A2-4-1   Digital Resolution Error

An inherent uncertainty in the period difference measurement arises from the fact that one clock pulse may be missed per interval timed, or two pulses for the difference of periods. The digital resolution error (relative) is the ratio of the time for two clock counts to the time corresponding to the measured difference of IF periods. From Equation (3E), the relative error for each T/R cycle due to digital resolution limitations is as follows:

$$_p\varepsilon_r = \frac{2}{\Delta N_p} = \frac{f_m L}{v f_c n} = \left(\frac{C_o}{v}\right) \frac{f_m L}{C_o f_c n} = \left(\frac{C_o}{v}\right) \frac{f_{if}}{n f_c} = \left(\frac{C_o}{v}\right) \frac{P_c}{n P_{if}} \tag{5A}$$

This noise is minimized by reducing the clock period, P_c, and by increasing the time of counting for each T/R half cycle, $n P_{if}$. The ratio C_o/v has a minimum value of 130 for the RCS application, corresponding to the maximum flow rate for water. Defining n_o to be the ratio of the T/R half-cycle time, T_R, to the IF period, P_{if}, and $k T_R$ to be the active measurement time, Equation (5A) becomes:

$$_p\varepsilon_r = \frac{C_o}{v} \frac{1}{k T_r f_c} \tag{5B}$$

A2-4-2 · Sampling Rate (Inactive/Active Time Ratio) Error

The system cannot respond accurately to flow changes that start or stop when the IF period is not being measured. Assuming a square-wave flow pulse of time duration, T_p, which is large compared to T_r, the uncertainty in measured flow (relative) is given by the ratio of the inactive time of one T/R half cycle to the time of the flow pulse. If the period is measured for a fraction k of the T/R half-cycle time, T_r, then the inactive time is $(1-k) T_r$. The relative error is as follows:

$$_p\varepsilon_s = (1-k) \, T_r/T_p \tag{5C}$$

The noise in measurement of a single flow pulse is reduced by reducing T_r and by increasing k, the fraction of the time during which the IF period measurement is actually being made. From Equation (5B) it is apparent that reducing T_r increases the digital resolution error, $_p\varepsilon_r$. An engineering trade-off is required, therefore, to achieve optimum net errors unless one of the components can be made negligible by choice of parameters other than T_r.

A2-4-3   IF Zero-Crossing Uncertainty (Jitter)

Noise in the IF signal results in noise in the measured period. Assuming a sine wave IF signal, then near zero amplitude the signal may be approximated by a linear function, as follows:

$$e_m = E_m \sin (2\pi f_{if} t) \approx E_m (2\pi f_{if})\Delta t \tag{5D}$$

If noise of peak amplitude E_n is present, then the peak uncertainty in IF zero crossing may be estimated by equating e_m of Equation (5D) to E_n and solving for Δt as follows:

$$\Delta t = \frac{E_n}{E_m(2\pi f_{if}} = \frac{E_n}{E_m} \cdot \frac{C}{2\pi f_m L} \tag{5E}$$

The relative noise in ΔN_p due to the uncertainty in zero crossing time is the ratio of twice $\Delta t f_c$ (the double uncertainty, converted to counts), to the number of counts due to the difference in periods, ΔN_p:

$$_p\varepsilon_z = \left(\frac{C}{v}\right) \frac{1}{2\pi k T_r f_{if} E_m/E_n} \tag{5F}$$

The noise from zero-crossing "jitter" can be minimized by increasing T_r and by increasing $f_{if} E_m/E_n$, which is the product of the IF frequency and its amplitude signal-to-noise ratio. Increasing k also reduces the noise from this source.

A2-4-4   Estimate of Inherent Period-Mode Noise per Flow Pulse

Provided the T/R cycle time is short compared to the minimum flow pulse duration, T_p, the errors $_p\varepsilon_r$ and $_p\varepsilon_z$ per flow pulse are smaller than the peak errors per T/R cycle estimated above. By statistical considerations, the noise in the mean value of N data points per flow pulse approaches the noise of a single measurement divided by the square root of the number of data points as N increases. The number of data points per flow pulse is $T_p/2T_r$. Combining Equations (5B), (5C), and (5F), and dividing by the square root of $T_p/2T_r$, the expected noise (or error) per flow pulse is as follows:

$$\sum \bar\varepsilon_p = \left(\frac{C}{v}\right)\sqrt{\frac{2}{T_r T_p}} \left(\frac{1}{k}\right)\left(\frac{1}{f_c} + \frac{1}{2\pi f_{if} E_m/E_n}\right) + (1-k)\frac{T_r}{T_p}$$

The bar over $\bar\varepsilon$ signifies that this equation applies to a flow pulse of duration greater than the T/R cycle time. It is apparent that increasing the percentage of time for which measurements are made, k, reduces all of these errors. Increasing f_c can make the digital resolution component negligible. Increasing the product $f_{if} E_m/E_n$ reduces the noise due to zero-crossing "jitter." Reducing T_r reduces the sampling rate error but increases the other two. Therefore, T_r

may have an optimum value once the other parameters are optimized. C_0/v and T_p have minimum values of 130 (for water) and 40 ms, respectively, in the RCS application.

A3   CHARACTERISTICS OF THE IF PHASE

A3-1   Measurement of Flow Velocity by IF Phase Difference

From Equation (1G) the phase of the IF signal is given by the following:

$$\phi = 2\pi\left(f_o - \frac{f_m}{2}\tau\right)\tau = 2\pi\left(f_o - \frac{f_m L}{2C}\right)\frac{L}{C} \tag{6A}$$

The difference in phase shift due to flow for the two directions of sonic transmission may be obtained by doubling the effect on phase due to variations in C, in a manner similar to that used in paragraph A2-2 for the period measurement. The complete differential of ϕ is as follows:

$$d\phi = 2\pi\frac{L}{C}\left(f_o - \frac{f_m L}{C}\right)\left[\frac{df_o}{f_o - f_m L/C} - \frac{L}{2C}\frac{df_m}{f_o - f_m L/C} - \frac{dL}{L} - \frac{dC}{C} - \frac{dv}{C}\right] \tag{6B}$$

The desired signal is given by twice the term involving v. The peak, absolute worst case, noise (or error) is given by twice the sum of all other terms. Factoring dv/C and replacing dv with v, the difference in phase for successive T/R half cycles is as follows:

$$\Delta\phi = 4\pi L\left(\frac{v}{C^2}\right)\left(f_o - \frac{f_m L}{C}\right)\left\{1 - \frac{C}{v}\left[\frac{df_o}{f_o - f_m L/C} + \frac{L}{2C}\frac{df_m}{f_o - f_m L/C} - \frac{dL}{L} - \frac{dC}{C}\right]\right\} \tag{6C}$$

The phase (relative) may be measured by counting clock pulses between a fixed time and a specific zero crossing of the IF. The difference in counts for the phase of two successive T/R half cycles will be proportional to $\Delta\phi$. The proportional relationship is as follows:

$$\frac{\Delta\phi}{2\pi} = \frac{\Delta N_o}{P_{if}/P_c} = \frac{f_{if}}{f_c}\Delta N_\phi = \frac{f_m L}{C f_c}\Delta N_\phi \tag{6D}$$

The ratio P_{if}/P_c is the number of counts obtained in one IF cycle, which is 2π radians. Therefore, the relationship between clock counts and phase difference is as follows:

$$\Delta N_\phi = \frac{C f_c}{2\pi f_m L}\Delta\phi \tag{6E}$$

Combining Equations (6C) and (6E), the phase difference signal in clock counts is as follows:

$$\Delta N_\phi = \frac{2f_c}{f_m}\left(\frac{v}{C}\right)\left(f_o - \frac{f_m L}{C}\right)\left\{1 - \frac{C}{v}\left[\frac{df_o}{f_o - f_m L/C} + \frac{L}{2C}\frac{df_m}{f_o - f_m L/C} + \frac{df_c}{f_c} - \frac{dL}{L} - \frac{dC}{C}\right]\right\} \quad (6F)$$

Note that df_c/f_c has been added to the error expression to include the clock error. Also note that while $\Delta\phi$ is proportional to both L and to v/C^2, the digital difference of counts, ΔN_ϕ, is not directly proportional to L, and is proportional to v/C rather than to v/C^2. Furthermore, $f_m L/C$ is negligible compared to f_o in a practical system, which simplifies the expression considerably. The second order term is retained in this discussion, except as noted, to assure that no errors are overlooked.

The signal-to-noise ratio for the phase difference measurement is the reciprocal of the noise term (having C/v as a factor) in Equation (6F). The phase-mode SNR is as follows:

$$SNR = \frac{v}{C}\left[\frac{1}{\dfrac{df_o}{f_o - f_m L/C} + \dfrac{df_m}{f_m} \cdot \dfrac{f_m L}{2C(f_o - f_m L/C)} - \dfrac{dL}{L} - \dfrac{dC}{C} + \dfrac{df_c}{f_c}}\right] \quad (6G)$$

Comparison of Equation (6G) to the SNR for the period difference measurement given by Equation (3B) indicates that the phase mode has additional noise due to variations of f_o, but the contribution of noise from f_m is attenuated. Specifically, the noise due to f_m for the phase mode divided by that for the period mode is as follows:

$$\left.\frac{dN_\phi}{dN_p}\right|_{f_m} = \frac{f_m L}{2C(f_o - f_m L/C)} = \frac{f_{if}}{2(f_o - f_{if})} \approx \frac{f_{if}}{2f_o}$$

The approximate form applies to the practical case for which f_{if} is much less than f_o. The effect of noise (or errors) in f_m on the phase mode output is, therefore, much less than it is for the period-mode output. The additional phase noise due to noise in f_o may be relatively negligible when using a voltage-to-frequency converter (VFC) for generating the frequency ramp. In this case, f_o arises from a fixed dc input, which may be heavily filtered. The dc ramp used to generate the frequency ramp, at rate f_m, must necessarily have a broad band-pass to achieve linearity of the ramp. It is reasonable to assume, therefore, that the phase-mode noise may be significantly lower than the period-mode noise due to its reduced sensitivity to noise in f_m. This has been found to be the case experimentally for both the Beckman respiratory flowmeter and for the prototype NIGS.

From Equation (6F) the difference of counts, ΔN_ϕ, which is the measure of the difference of IF signal phases for successive T/R half cycles, is inversely proportional to the speed of sound in the medium, C. From Equation (4A), the speed of sound may be measured as the average IF period, $\bar{N}$. Rearranging Equation (4A), the following is obtained:

$$C_O = \frac{f_m L}{f_c n} \bar{N} \quad .$$

(7A)

Substituting Equation (7A) for C_O into Equation (6F), the speed of sound dependence may be eliminated. The resulting expression, neglecting $f_m L/C$ compared to f_O in the error term to simplify the equation, is as follows:

$$\Delta N_\phi = \frac{2f_c^2 n}{f_m^2 L \bar{N}} \left(f_O - \frac{f_m L}{C} \right) v \left\{ 1 - \frac{C}{v} \left[\frac{df_O}{f_O} + \frac{f_m L}{2Cf_O} \cdot \frac{df_m}{f_m} - \frac{dL}{L} - \frac{dC}{C} + \frac{df_c}{f_c} \right] \right\}$$

(7B)

Equation (7B) contains C only in second order terms, which are negligible for practical systems. The average period measurement being relatively noise-free, there is no significant increase in output noise (or error) when the compensation for C_O is made. This point is discussed fully in paragraph A2-3, above.

Conversion of flow velocity to mass flow rate can be accomplished as for the period-mode, discussed in paragraph A2-2. The density would be calculated as explained in paragraph A2-3. By analogy to Equation (4H) (the mass flow rate for the period-mode measurement), the mass flow rate measured in the phase mode, corrected for both the speed of sound and density variations, is as follows:

$$M_\phi = \Delta N_\phi \frac{f_m^2 L \bar{N} A \bar{\rho}}{2f_c^2 n(f_O - f_m L/C) \cos\alpha} \quad x$$

(7C)

$$\frac{1 + h \left[g^{-1} \left(\frac{d\bar{N}}{\bar{N}_O} \right) \right]}{1 - \frac{C}{v} \left[\frac{df_O}{f_O} + \frac{f_m L}{2Cf_O} \frac{df_m}{f_m} - \frac{dL}{L} - \frac{dC_O}{C} + \frac{dA}{A} - \frac{d\alpha}{\cot\alpha} + \frac{df_c}{f_c} \right] - \frac{d\rho}{\rho}}$$

The expression in the denominator having C/v as a factor is the noise (or error) contribution of the various parameters that must be made negligible. The speed of sound variation, dC_O/C, is included in the "amplified" error term to allow for the possibility of systematic thermal transient effects on the speed of sound, which are imperfectly cancelled by the measured average period. The density error term, $d\rho/\rho$, is not multiplied by C/v because ρ is not

obtained by a difference measurement. The function $h(g^{-1})$ in the numerator is the density correction that must be calculated from the single variable $d\bar{N}$, which is the variation of the average IF period about its constant nominal value, $\bar{N}_O$. The only other variables are ΔN_ϕ and $\bar{N}$, where ΔN_ϕ is the number of measured counts corresponding to the difference of IF phase for successive T/R half cycles, and $\bar{N}$ is the average number of counts measured for the IF periods for successive T/R half cycles.

A3-3   Inherent Resolution for the IF Phase Mode

A3-3-1   Digital Resolution

Following the approach used in paragraph A-2-4-1, the digital resolution error for the phase mode is as follows:

$$\phi \varepsilon_r = \frac{2}{\Delta N_\phi} = \frac{f_m}{f_c} \frac{C}{v} \frac{1}{f_o - f_m L/C} \approx \frac{f_m}{f_c f_o} \frac{C}{v} \tag{8A}$$

The second order term of ΔN_ϕ is neglected in the approximate expression, which causes less than a 1% effect in the predicted error for a practical system.

A3-3-2   Sampling Rate (Inactive/Active Time Ratio) Error

In the phase-shift mode the active measurement time is less than one IF period (unless more elaborate circuitry is employed to permit multi-cycle, phase-shift measurement). Using the approach of paragraph A2-4-2, k becomes P_{if}/T_r. Substituting this expression for k in Equation (5C) yields the following:

$$\phi \varepsilon_s = \frac{T_r - P_{if}}{T_p} = \frac{T_r}{T_p} - \frac{P_{if}}{T_p} \approx \frac{T_r}{T_p} \tag{8B}$$

The approximation is justified for rough error estimation since a number (5 or more) of IF cycles per T/R half cycle appears to be necessary. Further, the approximation is worst case, corresponding to k = o.

A3-3-3   IF Zero-Crossing Uncertainty (Jitter)

Following the approach used in paragraph A2-4-3, the zero-crossing noise for the phase-mode measurement is as follows:

$$\phi \varepsilon_z = \left(\frac{C}{v}\right) \frac{C}{2\pi f_o L E_m/E_n} = \left(\frac{C}{v}\right) \frac{f_m}{2\pi f_o f_{if} E_m/E_n} \tag{8C}$$

A3-3-4   Estimate of Inherent Phase-Mode Noise per Flow Pulse

Following the approach of paragraph A2-4-4, the sum of the relative errors per flow pulse expected for the phase mode of operation is as follows:

$$\sum \bar{\epsilon}_\phi = \left(\frac{C}{v}\right)\sqrt{\frac{2}{T_r T_p}}\left(\frac{f_m T_r}{f_o}\right)\left[\frac{1}{f_c} + \frac{1}{2\pi f_{if}E_m/E_n}\right] + \left(1 - \frac{1}{T_r f_{if}}\right)\frac{T_r}{T_p} \qquad (8D)$$

Equation (8D) is deliberately arranged for direct comparison to Equation (5G), which is the corresponding expression for the period mode. The first terms are identical except for the factor $f_m T_r/f_o$ in Equation (8D), which replaces $1/k$ in Equation (5G). Since $k < 1$ by definition, $1/k$ must always be greater than unity. On the other hand, $f_m T_r$ is the frequency swept each T/R half cycle, and $f_m T_r/f_o \leq 1$ is a possible (perhaps necessary) condition. The inherent resolution of the phase mode (both digital resolution and zero-crossing jitter) may, therefore, be superior to that of the period mode. The sampling rate error (the second term) is smaller for the period mode since the period of several cycles of IF can be measured. In the phase mode, barring complicated circuitry required to measure phase shifts greater than $\pm \pi$ radians, a time corresponding to only one-half of an IF cycle can be measured. For short flow pulses the period mode may be preferred, therefore, depending on the relative magnitudes of the two corresponding terms of Equations (5G) and (8D).

A3-3-5   Limitation of Phase-Shift Sensitivity

Since the IF signal phase shift is dependent on the speed of sound in the media as well as on the flow velocity, it is necessary to consider the effect of changes in the speed of sound on the signal processing circuitry. The required geometry and range of the RCS application dictate that the full-scale value of v/C is about $\pm 0.77\%$. The value of dC/C for MMH and N_2O_4 may be about $\pm 8\%$ over the required temperature range of 21.1° ± 16.7°C (70° ± 30°F). The nominal phase may shift, therefore, about ten times the full-scale, flow-induced, phase shift. Measurement of the phase as it shifts through $\pm n\pi$ radians is not a straight-forward problem.

The simple phase measurement scheme discussed above in connection with the phase mode analysis is illustrated in FIGURE A-2. The squared IF signal nominal phase is shown in curve A for zero flow. The phase of successive T/R half cycles is identical. The nominal phase shifts with C, L, and f_o, but both half cycles shift identically. A fixed-time pulse is indicated at time "0" in curve B. This pulse initiates a Flow Counter Enable signal, curve C, which continues until the next negative transition of the IF. The times measured for the successive T/R half cycles, t_{AB} and t_{BA}, are equal at zero flow, and the difference in clock counts is zero.

Curve D illustrates the IF phase for sound transmission from A to B for one flow which shifts the phase just under π radians, indicated by trace X' and Y'. For less than π radians phase shift (just below full-scale flow) the counter is enabled (curve E) for just under 2π radians, corresponding to time

t_{AB}. For just over full-scale flow, the next negative transition of the IF will occur very shortly after the fixed-time pulse at 0 occurs, at the time indicated by Y". The time t_{AB}, for which the counter is enabled, jumps from 2π to zero as the flow passes through full scale. By analogy, it is apparent from curves F and G that the opposite phase shift for transmission from B to A will display similar characteristics. The phase difference measured as $(t_{AB}-t_{BA})$, therefore, reverses sign when full-scale flow is exceeded. This fact is indicated in curve H of FIGURE A-2.

When a random shift of the nominal phase of both T/R half cycles is superimposed upon the timing diagrams of FIGURE A-2, it is apparent that ambiguous results are obtained at a lower flow rate than for the optimum alignment discussed above. When the nominal phase shifts $\pm\ \pi/2$ radians, for example, the output becomes ambiguous at half the maximum permissible flow rate. The optimum setting of the fixed-time pulse for a system operating in this manner is, therefore, in coincidence with a positive transition of the squared IF signal, as illustrated in FIGURE A-2.

Complicated circuitry that would reverse the sign of the signal for successive shifts of π radians is not inconceivable, but minor noise in the measurements would result in successive zero and twice full-scale outputs, causing a SNR of only 0.5. This would occur at each flow (or value of C_0) for which the fixed-time pulse for either direction of transmission coincides with a negative transition of the IF signal. It would definitely be preferred to operate with limited phase-shift sensitivity if the performance goals can be achieved.

A3-3-6   Limitation of Phase Shift by Choice of f_0

Examination of Equation (6C) reveals that the only design parameter that may be freely varied to control the phase shift sensitivity is f_0 (neglecting $f_m L/C$). Neglecting all sources of phase shift except v and C in Equation (6C), and making $\Delta\phi<2\pi$, results in the following inequality:

$$f_0 < \frac{C}{v} \cdot \frac{C}{L} \cdot \frac{v}{2(dC+v)} = \frac{C}{v} \cdot \frac{1}{2\tau} \cdot \frac{v}{dC+v} \tag{9A}$$

Since the variation in C with temperature, dC, is expected to be about $10 \cdot v$ for MMH and N_2O_4, it follows that:

$$f_0 < \frac{1}{22\tau} \frac{C}{v} \tag{9B}$$

if the maximum phase shift is to be less than π radians.

It is important to note that all parameters of Equation (9A) are fixed by the RCS system requirements. The minimum value of τ is about 50 µs and the maximum value of C/v is about 130 for water, under the RCS constraints. The value of C/v is about 100 for MMH and N_2O_4, and the minimum value of τ is about 70 µs.
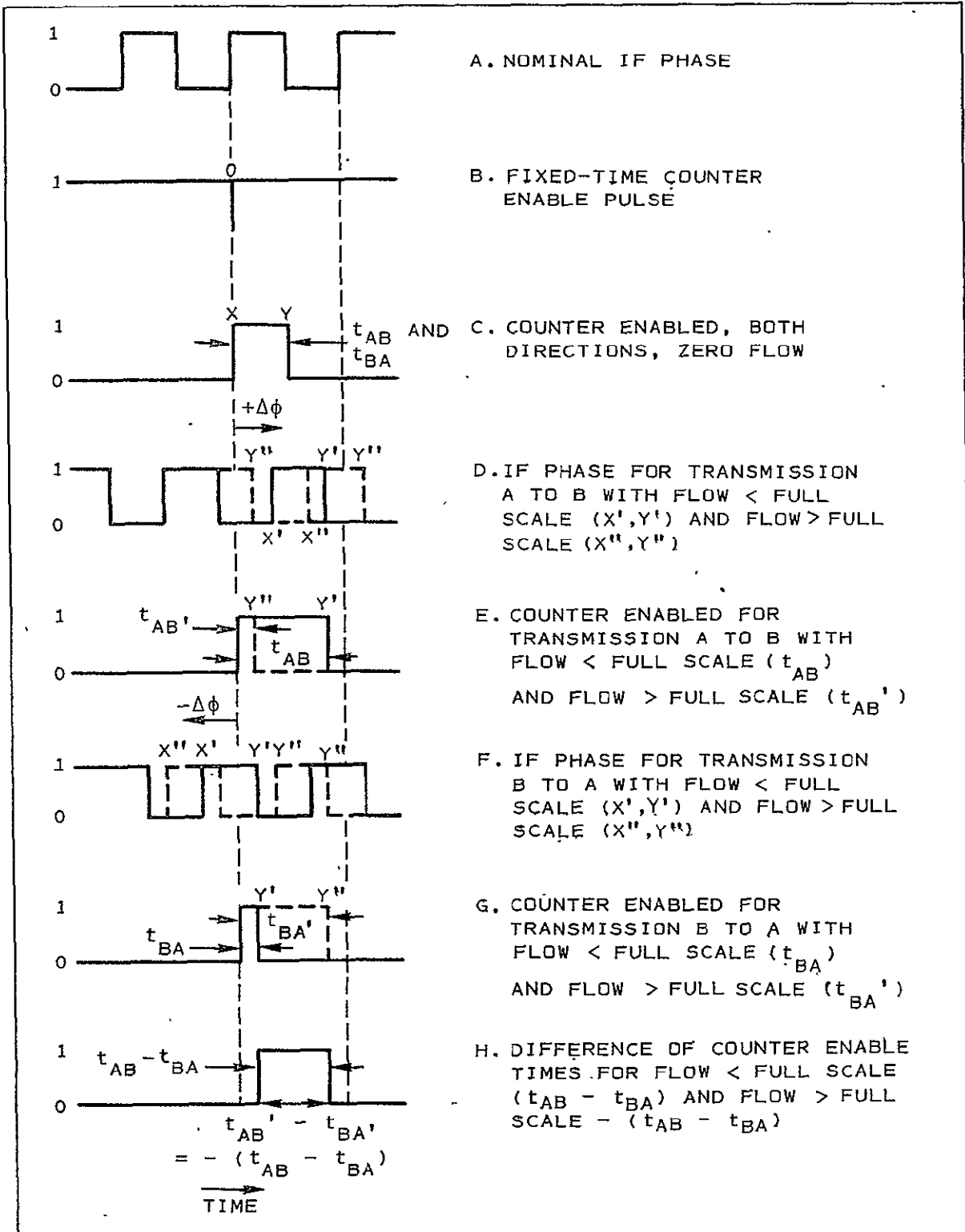
Figure A-2. *Phase Shift Due to Zero Flow and Flow Just Below and Above Full Scale, Showing Reversal of Output at Full Scale*

Using the approximate values for water, $f_o < 127$ kHz may be calculated from Inequality (9B). Under this condition it may be calculated from Equation (6F) that the full-scale flow provides about 5000 counts when using a 20-MHz clock, an IF frequency of about 400 Hz, and $T_t = 10$ ms. The corresponding value of f_m is about 6×10^6 Hz/s, and the frequency is swept to about 150% of f_o. This would require a broadband transducer, which may not be feasible. Furthermore, only 4 IF cycles (400 Hz) would be obtained per 10 ms T/R half cycle. A different approach to limiting the phase shift sensitivity, considered below, is probably preferable.

A3-3-7   Reduction of Phase Sensitivity by Dividing IF Frequency

If the frequency of the squared IF signal, shown in FIGURE A-2, is digitally divided by a constant factor, D, the resultant signal phase would shift only π radians when the basic IF signal phase shifted $D\pi$ radians. The zero-crossing detection would still be done at the basic IF frequency (higher) which would help reduce zero-crossing noise. With this approach, Inequality (9B) becomes:

$$f_o < \frac{D}{22\tau} \frac{C}{v} \tag{10A}$$

A practical limitation on the maximum value of D arises from the necessity of having at least one full cycle of frequency f_{if}/D within each T/R half cycle. This condition may be expressed as follows:

$$D < T_r f_{if} \tag{10B}$$

Division of the IF signal frequency by D to reduce the phase shift sensitivity has the net effect of leaving ΔN_ϕ unaltered, while increasing the nominal count for each T/R cycle by the factor D. The same difference of larger numbers is, therefore, being measured. This has negligible effect on the signal-to-noise ratio, however, since the digital technique has a fixed resolution error. The counter simply requires a larger capacity, such as four more bits.

On the positive side, the "sampling rate" error described in paragraph A3-3-2 and A3-3-4 would be reduced by virtue of counting for a larger percentage of the time. (As long as a rectangular flow pulse starts or stops while the clock is being counted, it will correctly affect the differential count obtained at the end of a T/R cycle.) As D approaches half of the limit defined by inequality (10B), the value of k approaches one-half, and the error is reduced by a factor of about two. Specifically, Equation (8D) becomes:

$$\sum \bar{\varepsilon}_\phi = \frac{C}{v} \cdot \sqrt{\frac{2}{T_r T_p}} \cdot \frac{f_m T_r}{f_o} \left[\frac{1}{f_c} + \frac{1}{2\pi f_{if} E_m/E_n} \right] + \left(1 - \frac{D}{T_r f_{if}} \right) \frac{T_r}{T_p} \tag{10C}$$

This is the summation of relative errors. The error as a fraction of full-scale flow is obtained by using the full-scale value of v in the first term,

and by multiplying the second term by the fraction of full-scale flow attained for a flow pulse of duration T_p. The assertion that the peak flow rate is less than full scale for small values of T_p is obviously contradictory to the assumption of rectangular flow pulses. The rectangular flow pulse assumption simplifies the analysis, and indicates a larger error than would be calculated for either a triangular or a saw-tooth waveform. It is retained, therefore, for the worst-case analysis. The best estimate currently available is that the peak flow rate is about 1 kg/s (2.2 lb/s) which is 7% of full scale when the RCS valve opens for 40 ms. Therefore, the specification for the prototype gaging system was made 1.0 kg/s (2.2 lb/s) maximum (7% of full scale) for the minimum flow pulse duration of 40 ms.

A4 SUMMARY OF POSSIBLE IMPROVEMENTS

A4-1 Modification of Transducers

The final Design Feasibility Test results make it clear that the transducers must be modified to reduce $(1/L) \, dL/dP$, the relative change in path length per unit pressure. This can be done in the following way without loss of performance for other reasons:

- Pot the rear cavity with tungsten powder/epoxy mixture.

- Replace the 0.75 MHz crystals with 0.30 to 0.40 MHz crystals and increase the stainless steel thickness from 0.043 cm (0.017 inch) to about 0.086 cm (0.034 inch). As an option offering better performance at higher development cost, relatively thick aluminum could be fused or welded inside of a very thin stainless shell.

The second change will improve the quality of the received RF significantly, and will decrease the response to pressure by a factor of eight. The first change will also improve the signal quality, and can "stiffen" the transducers by a factor of 5 or more. A factor of at least five is required.

Further consideration should be given to a concept that arose late in the contract work. It appears possible to utilize a second crystal in each transducer for the purpose of cancelling transmitter phase shifts. In this scheme, the transmitted signal input to the mixer comes from the second (receiver only) crystal that receives the sound at a time close to that at which the sound entered the flowing medium. In principle, at least, the sonic transmission is timed between two similar receivers along the path, cancelling IF signal distortions due to phase shift of the signal actually transmitted relative to the phase of the driving voltage.

A4-2 Modification of the Electronics

There was direct evidence of both analog and digital circuit instabilities with moderate temperature changes. These deficiencies must obviously be corrected for a flight model. The DCA was a no-cost breadboard of a laboratory instrument, designed to operate in an air-conditioned room. No problems are foreseen

in flight model design, since suitable components are available and similar circuits are known to have been qualified for aerospace use.

The major recommended electronic improvements are along the lines of closing loops that were open in the prototype. The most critical parameters that can be stabilized in this manner, and the recommended approaches, are as follows:

- The starting frequency, f_o, should be measured during the first ten or so cycles of RF transmitted. The measured value of f_o should be compared to the average IF period (measured in the preceding T/R cycle), and the error signal of this comparison should be fed back to shift f_o to maintain the ratio f_o/C_o constant. This circuit assures that the phase (and period) of the same IF cycle is always measured. It also automatically eliminates the speed-of-sound dependence of the phase-mode measurement. (More IF cycles of good uniformity are necessary for optimal performance of this circuit.)

- The frequency rate of change, f_m, should be measured directly (by counting the RF zero crossings over a fixed time interval) during each ramp. The deviation from normal should be fed back to the ramp rate determining input of the VFC. This approach automatically corrects f_m for capacitor and resistor variations with temperature, aging, etc.

- All timing functions should be derived from a thermally stable system clock (oscillator). Too many one-shot circuits were used in the prototype.

- More stable IF filters are desirable.

In addition, consideration should be given to the possible benefits of closing the f_m loop described above to hold a constant number of IF cycles within a fixed time. This is equivalent to holding the product $f_m\tau = f_{if}$ constant by varying f_m as τ varies. Assuming that this can be done with sufficient speed and accuracy, the measured parameter will be the difference in the feedback voltage determining f_m for successive T/R half cycles, instead of the IF period differences. In this scheme, the IF frequency remains constant, permitting use of relatively very narrow band IF filters, possibly at higher IF frequencies, for high noise rejection over a relatively wide range of C_o. A thorough analytical evaluation of this approach appears to be warranted if an order of magnitude improvement in performance for critical applications is of interest.

An Inexpensive Economical Solar Heating System for Homes
N76-27671/PAT 59 p PC$4.50/MF$3.00

Viking I: Early Results
N76-28296/PAT 76 p PC$2.00/MF$3.00

Energy Fact Book 1976, Chapters 1 through 21
ADA-028 284/PAT 432 p PC$11.75/MF$3.00

Security Analysis and Enhancements of Computer Operating Systems
PB-257 087/PAT 70 p PC$4.50/MF $3.00

Evaluation of the Air-to-Air Heat Pump for Residential Space Conditioning
PB-255 652/PAT 293 p PC$9.25/MF$3.00

Monitoring Groundwater Quality: Monitoring Methodology
PB-256 068/PAT 169 p PC$6.75/MF$3.00

An Air Force Guide to Software Documentation Requirements
ADA-027 051/PAT 178 p PC$7.50/MF$3.00

The Production of Oil from Intermountain West Tar Sands Deposits
PB-256 516/PAT 98 p PC$5.00/MF$3.00

Analysis of Large Scale Non-Coal Underground Mining Methods
PB-234 555/PAT 581 p PC$13.75/MF$3.00

Who's Who in the Interagency Energy/Environment R and D Program
PB-256 977/PAT 35 p PC$4.00/MF$3.00

Local Area Personal Income, 1969-1974. Volume 2: Central and Northeastern States
PB-254 056/PAT 578 p PC$13.75/MF$3.00

Feasibility of Considerably Expanded Use of Western Coal by Midwestern and Eastern Utilities in the Period 1978 and Beyond
PB-256 048/PAT 61 p PC$4.50/MF$3.00

Availability of Potential Coal Supply Through 1985 by Quality Characteristics
PB-256 680/PAT 121 p PC$5.50/MF$3.00

Flat-Plate Solar Collector Handbook: A Survey of Principles, Technical Data and Evaluation Results
UCID-17086/PAT 96 p PC$5 00/MF$3.00

HOW TO ORDER

When you indicate the method of payment, please note if a purchase order is not accompanied by payment, you will be billed an additional $5.00 *ship and bill* charge. And please include the card expiration date when using American Express.

Normal delivery time takes three to five weeks. It is vital that you order by number or your order will be manually filled, insuring a delay. You can opt for *airmail delivery* for $2.00 North American continent; $3.00 outside North American continent charge per item. Just check the *Airmail Service* box. If you're really pressed for time, call the NTIS Rush Handling Service (703)557-4700. For a $10.00 charge per item, your order will be airmailed within 48 hours. Or, you can pick up your order in the Washington Information Center & Bookstore or at our Springfield Operations Center within 24 hours for a $6.00 per item charge.

You may also place your order by telephone or if you have an NTIS Deposit Account or an American Express card order through TELEX. The order desk number is (703) 557-4650 and the TELEX number is 89-9405.

Thank you for your interest in NTIS. We appreciate your order.

METHOD OF PAYMENT

☐ Charge my NTIS deposit account no. _____

☐ Purchase order no. _____

☐ Check enclosed for $_____

☐ Bill me. Add $5.00 per order and sign below. (Not available outside North American continent.)

☐ Charge to my American Express Card account number

☐☐☐☐☐☐☐☐☐☐☐☐☐☐☐☐☐

NAME_____

ADDRESS_____

CITY. STATE. ZIP_____

Card expiration date_____

Signature _____

☐ Airmail Services requested

Clip and mail to.

NTIS

National Technical Information Service
U.S. DEPARTMENT OF COMMERCE
Springfield, Va. 22161
(703) 557-4650 TELEX 89-9405

Item Number	Quantity		Unit Price*	Total Price"
	Paper Copy (PC)	Microfiche (MF)		

All prices subject to change The prices above are accurate as of 3/77 .

Foreign Prices on Request.

Sub Total ▢
Additional Charge ▢
Enter Grand Total ▢

A-21